Department of Pure and Applied Chemistry

Searching for Mechanistic Insights in Complex Reaction Pathways

By

Allan Young

September 2019

A report submitted to the Department of Pure and Applied Chemistry, University of Strathclyde, in part fulfilment of the regulations for the degree of Doctor of Philosophy.

Declaration of Ownership

This thesis is the result of the author's original research. It has been composed by the author and has not been previously submitted for examination which has led to the award of a degree.

The copyright of this thesis belongs to the author under the terms of the United Kingdom Copyright Acts as qualified by University of Strathclyde Regulation 3.50. Due acknowledgement must always be made of the use of any material contained in, or derived from, this thesis.

I certify that the report has been written by me. Any help I have received in my research work and the preparation of the report itself has been acknowledged. In addition, I certify that all information sources and literature used are indicated in the report.

The data associated with the results presented within this thesis can be found on the University of Strathclyde data repository, Pure:

https://doi.org/10.15129/5b238091-c903-4506-9d62-7557a1db5cf8

Signed: A. Young   Date: 31/7/19

I

"You can mark my words,

I'll make changes to earth

While I'm alive, I'll make tiny changes to earth"

Frightened Rabbit

Acknowledgments

Publications

---

1. Andrew J. Smith, **Allan Young**, Simon Rohrbach, Erin F. O'Connor, Mark Allison, Hong-Shuang Wang, Dr. Darren L. Poole, Tell Tuttle, John A. Murphy, *Angew. Chem. Int. Ed.*, 2017, **56**, 13747 – 13751. "Electron-Transfer and Hydride-Transfer Pathways in the Stoltz–Grubbs Reducing System (KO^tBu/Et_3SiH)"
(Chapter 5)

2. Florimond Cumine, **Allan Young**, Hans-Ulrich Reissig, Tell Tuttle, John A. Murphy, *Eur. J. Org. Chem.*, 2017, **46**, 6867 – 6871. "A Computational Study of Anionic Alkoxide–Allene and Amide–Allene Cyclizations"

3. Katie J. Emery, **Allan Young**, J. Norman Arokianathar, Tell Tuttle, John A. Murphy, *Molecules*, 2018, **23**, 1055. "KO^tBu as a Single Electron Donor? Revisiting the Halogenation of Alkanes with CBr_4 and CCl_4"

4. Giuseppe Nocera,[¥] **Allan Young**,[¥] Fabrizio Palumbo, Katie J. Emery, Graeme Coulthard, Thomas McGuire, Tell Tuttle, John A. Murphy, *J. Am. Chem. Soc.*, 2018, **140**, 9751 – 9757. "Electron Transfer Reactions: KO^tBu (but not NaO^tBu) Photoreduces Benzophenone under Activation by Visible Light"
(Chapter 6)

5. Josh Barham, Samuel Dalton, Mark Allison, Giuseppe Nocera, **Allan Young**, Matthew John, Thomas McGuire, Sebastien Campos, Tell Tuttle, John A. Murphy, *J. Am. Chem. Soc.*, 2018, **140**, 11510 – 11518. "Dual Roles for Potassium Hydride in Haloarene Reduction: CS_NAr and SET Reduction via Organic Electron Donors Formed in Benzene"

[¥] These authors contributed equally.

Abbreviations

(B)HAS	(Base-Promoted) Homolytic Aromatic Substitution
°C	Degree(s) Celsius
CDFT	Constrained Density Functional Theory
CFL	Compact Fluorescent Lamp
CPCM	Conductor-Like Polarisable Continuum Model
CS_NAr	Concerted Nucleophilic Aromatic Substitution
CT	Charge Transfer
CV	Cyclic Voltammetry
DFT	Density Functional Theory
ΔG^*	Predicted Gibbs Free Energy of Activation
$\Delta G^{\ddagger}$	Gibbs Free Energy for the transition state
ΔG_{rel}	Gibbs Free Energy for the relative energies
DMEDA	1,2-dimethylethylenediamine
DMF	N,N-dimethylformamide
DMSO	Dimethylsulfoxide
E	Electrophile
e^-	Electron
E1cB	Elimination Unimolecular conjugate Base
EPR	Electron Paramagnetic Resonance
equiv.	Equivalents
Et_3SiH	Triethylsilane
Fc	Ferrocene
GCMS	Gas Chromatography - Mass Spectrometry
GGA	Generalised Gradient Approximation
GTOs	Gaussian Type Orbitals
h	Hour(s)
H-F	Hartree-Fock
H-K	Hohenberg-Kohn
HOMO	Highest Occupied Molecular Orbital
ISET	Inner-sphere electron transfer
kcal/mol	Kilocalories per mole
KH	Potassium Hydride

KOH	Potassium Hydroxide
KO^{t}Bu	Potassium *tert*-butoxide
LDA	Local Density Approximation
LED	Light Emitting Diode
LiO^{t}Bu	Lithium *tert*-butoxide
LSDA	Local Spin-Density Approximation
LUMO	Lowest Unoccupied Molecular Orbital
MeCN	Acetonitrile
mg	Milligrams
mol%	Molar percentage
NaH	Sodium Hydride
NaK	Sodium-Potassium alloy
NaO^{t}Bu	Sodium *tert*-butoxide
^{n}BuLi	*n*-Butyllithium
NMR	Nuclear Magnetic Resonance
OSET	Outer-sphere electron transfer
PAH	Polycyclic Aromatic Hydrocarbon
PCM	Polarisable Continuum Model
PES	Potential Energy Surface
ppb	Parts per billion
ppm	Parts per million
r.t.	Room temperature
SCE	Saturated Calomel Electrode
SCF	Self-Consistent Field
SET	Single Electron Transfer
SOMO	Singly Occupied Molecular Orbital
S$_{RN}$1	Unimolecular Radical Nucleophilic Substitution
STOs	Slater Type Orbitals
TDDFT	Time-Dependent Density Functional Theory
TEMPO	2,2,6,6-Tetramethyl-1-piperidine-1-oxyl
THF	Tetrahydrofuran
TMS	Trimethylsilyl
UV-vis	Ultraviolet-visible
V	Volt(s)
vdW	van der Waals
VIP	Vertical Ionisation Potential

vs	Versus
W	Watt(s)
XC	Exchange-Correlation

Table of Contents

Abstract

In order to further advance chemical reactions, understanding the mechanism underpinning complex reaction pathways is key. This is the overarching aim of the work contained in this thesis, and through the application of density functional theory calculations four different systems are studied.

Investigation of the mechanism of 1,2,4-triarylbenzene formation from 1,3-diaryl-2-propen-1-ols as proposed by Ghorai *et al*.[1] demonstrates that the phenyl anion can be a competent leaving group. The implications of this study are that simply considering the pK$_a$ of the leaving group's conjugate acid does not afford a reliable prediction, for when the choice of leaving group is hydride or phenyl anion - the phenyl anion wins. Such a leaving group would not be predicted to be competent by the simple consultation of a pK$_a$ table, and this opens further possibilities of bad leaving groups made good.

Competing reaction pathways are an inherent part of complex reaction systems; as such it is no surprise that in order to gain mechanistic insights into the reducing abilities of the Stoltz-Grubbs reducing system two competing reduction mechanisms were investigated. Through calculations it was possible to determine that the hydride and single electron transfer mechanisms were indeed not competing but were individually active for different types of substrate. Hydride reduction was applicable to the polyaromatic hydrocarbons naphthalene, phenanthrene and anthracene, whilst single electron transfer was deemed responsible for the reduction of N-benzylindole and N-phenyl-N-methylaniline.

Time is often key in achieving mechanistic insights for some complex reactions, one such reaction has been shown to be the reduction of benzophenone by KO^{t}Bu. Studied initially by Ashby *et al*.[2] in the 1980s this reduction was predicted to occur by electron transfer from KO^{t}Bu to benzophenone resulting in the blue coloured benzophenone ketyl. The mechanism behind this reaction has now been uncovered and shown to involve the visible light excitation of a complex between KO^{t}Bu and benzophenone resulting in a charge transfer from KO^{t}Bu to benzophenone.

The homocoupling of benzene under the action of potassium metal and an alkali metal salt was recently disclosed by experimental colleagues in the Murphy Group. A preliminary study of this complex reaction has shown that a further understanding of the

composite structures formed upon mixing potassium metal and alkali metal salt is required in order to facilitate meaningful computational studies.

1. Introduction

1.1 Motivation for the Thesis

Many reactions in chemistry are composed of a myriad of solvents, reactants, catalysts, ligands and other additives and as such can often present equally complex mechanistic problems. On the other hand, there are often reactions consisting of a solvent and two reactants which form distinct products, *via* a relatively simple mechanism. However, one cannot simply propose a linear relationship between the number of reaction components and the complexity of the reaction mechanism.

Each of the chapters herein seeks to explore the mechanistic landscape of what, at first glance, seem to be relatively simple chemical systems. However, through observing their experimental outcomes it was quite clear that these did not present simple mechanistic problems. The motivation for this thesis was thus to find mechanistic insights for each of the chemical systems studied and show the clear path to further understanding each mechanism. Upon finding mechanistic insights, it should be possible for the potential, of each chemical system studied here, to be fully realised and exploited.

1.2 Layout of the Thesis

The thesis opens with a discussion of the relevant literature in Chapter 2, this includes the initiation of base-promoted homolytic aromatic substitution reactions by *in-situ* generated electron donor species. The majority of the review centres on formation of electron donor species from small organic molecules and potassium *tert*-butoxide (KO^{t}Bu), and how experimental and computational tools were able to help elucidate mechanistic details. The review expands to the more recent case where the combination of triethylsilane and KO^{t}Bu together, perform remarkable reductive chemistry. Potassium *tert*-butoxide's ability to act as a standalone electron donor is also reviewed in depth.

The computational nature of this thesis necessitates a discussion of the methods utilised within, and the theoretical underpinnings of these methods. Chapter 3 begins with a fundamental discussion of quantum mechanics, leading to the Hartree-Fock Theory and the method applied in this work, density functional theory (DFT). The applications of DFT within this work, namely transition state theory and Marcus theory will be discussed to conclude the chapter.

The results of this research will be presented across four chapters, with Chapter 4 exploring the formation of 1,2,4-triarylbenzenes from 1,3-diaryl-2-propen-1-ols. Results of DFT-based mechanistic investigation of this intriguing reaction will be presented, with a keen focus on the aryl anion as a leaving group. Chapter 5 will probe the conflicting reactivity observed for the KO^{t}Bu and triethylsilane reducing system, utilising DFT calculations. With unexpected reactions determined experimentally, computational results will be presented here in order to more fully understand the mechanisms in play. Chapter 6 will again visit KO^{t}Bu, this time investigating the ability of this base to act as an electron donor towards benzophenone or to form *in-situ* electron donor species through reactions with benzophenone. Chapter 7 will further expand the scope of curious reactivities presented within this thesis, with the mechanism of benzene homocoupling under the action of potassium metal and an alkali metal salt being investigated.

Chapter 8 will present conclusions from the work discussed throughout the thesis and discuss whether mechanistic insights have indeed been reached for the seemingly simple reactions studied.

2. Literature Review

Within this literature review, the idea of competing mechanistic proposals should remain at the fore of your thoughts, despite in many cases the reactions involving quite simple combinations of reagents. The underlying theme of the research conducted for this thesis has been that of exploring the seemingly obvious reaction mechanism, based on current chemistry knowledge, only to be confronted with data and observations to the contrary. This has proven to push the research into uncharted territory, following unknown paths in search of mechanistic insights.

A case in point from the Murphy and Tuttle research groups has been the area of base-promoted homolytic aromatic substitution (BHAS) reactions, affording coupling of haloarenes with arenes in the presence of a strong base (in most cases potassium *tert*-butoxide, KO*t*Bu) and commonly a small organic additive. This review begins with this topic as it underlines the mechanistic paths which have been trod by our groups and other researchers in search of mechanistic insights.

The previous decade has seen an explosion in publications within the area of carbon-carbon bond formations afforded without the need for transition metals. A recent review paper by Sun and Shi[3] neatly summarises the various facets of this evolving field of research, one such reaction type was BHAS. The first report of transition metal-free Suzuki-type coupling reactions by Leadbeater and Marco in 2003[4] initiated a vast array of research into transition metal-free coupling reactions, base-promoted homolytic aromatic substitution and organic electron donors. Following on from their initial publication, Leadbeater and Marco published the scope and limitations of their transition metal-free coupling reactions with elemental analysis data presented as proof the reaction was indeed transition metal-free.[5] However, the following year the authors published a reassessment of their work in which they stated low parts per million (ppm) or even parts per billion (ppb) of palladium contaminants present in their reagents were capable of catalysing the observed Suzuki-type coupling reaction. Nevertheless, the publication undoubtedly sparked interest into the possibility of conducting carbon-carbon coupling reactions under transition metal-free reaction conditions.

Indeed, 5 years later Itami *et al.*[6] discovered that the coupling of pyridine (**2.1**) and iodobenzene (**2.2**) in the presence of potassium *tert*-butoxide (KO*t*Bu) occurred with a similar yield in the presence or absence of a transition metal catalyst, Scheme 2.1.
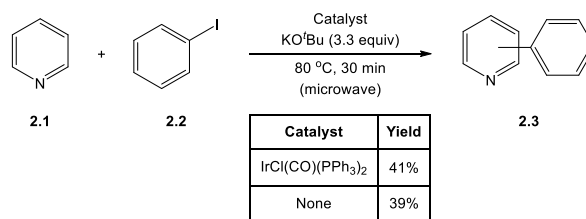
Scheme 2.1: Coupling of pyridine and iodobenzene in the presence and absence of an iridium catalyst by Itami *et al.*.[6]

Itami *et al.*[6] also demonstrated that the coupling reaction worked not only between iodobenzene and pyridine, but also for other nitrogen heterocycles (pyrazine, pyridazine, pyrimidine and quinoxaline). Interestingly, in a control experiment they observed that the addition of radical scavengers, 2,2,6,6-Tetramethylpiperidine-1-oxyl (TEMPO), galvinoxyl or acrylonitrile, shut down the reaction between pyrazine and iodobenzene, indicating that the reaction may involve radical intermediates. Lei *et al.*[7] tested a range of small organic molecules, in combination with KO*t*Bu, to catalyse the transition metal-free coupling between iodotoluene and benzene. It was found that molecules with free -NH or -OH groups were most effective in catalysing the coupling reaction, with 1,2-dimethylethylenediamine (DMEDA) producing the highest yield. Using DMEDA as the catalyst in the presence of TEMPO, Lei *et al.* observed no coupled product and proposed that aryl radical anions were being formed in the reaction by activation from DMEDA radical anions, previously reported to form by reaction of DMEDA with *n*BuLi.[8] In 2010, two further reports of transition metal-free carbon-carbon coupling were made; the first by Hayashi *et al.*[9] who published results of coupling between 4-iodotoluene and benzene in the presence of phenanthroline and sodium *tert*-butoxide (NaO*t*Bu, Scheme 2.2a). Shi *et al.*[10] published soon after with a similar report of coupling between halobenzenes and anisole in the presence of phenanthroline and KO*t*Bu (Scheme 2.2b).
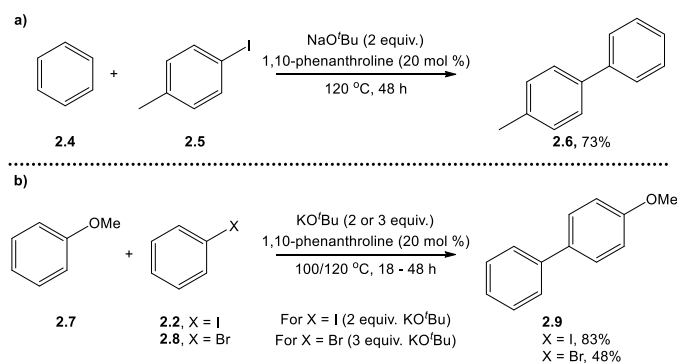
**Scheme 2.2: a)** Coupling reaction of iodobenzene and benzene in the presence of NaO*t*Bu and 1,10-phenanthroline reported by Hayashi *et al.*[9] **b)** Coupling reaction of anisole and aryl halides in the presence of KO*t*Bu and 1,10-phenanthroline reported by Shi *et al.*[10]

These initial reports of transition metal-free carbon-carbon coupling reactions provided limited information on the possible underlying mechanism at work in these reactions, with the likely involvement of radical intermediates being the main piece of mechanistic information gleaned from these publications. Despite this, in 2011 Studer and Curran[11] published what has now become the widely accepted mechanism of these reactions – the base-promoted homolytic aromatic substitution reaction.

2.1 Base-Promoted Homolytic Aromatic Substitution

Studer and Curran proposed the BHAS mechanism after noticing similarities between the reactivity reported by those conducting transition metal-free coupling reactions and the already formalised mechanism of homolytic aromatic substitution (HAS). HAS reactions involving the arylation of haloarenes in the presence of stoichiometric amounts of a radical initiator (Scheme 2.3), take place by addition of aryl radicals to arenes with high selectivity for *ortho* addition – a feature also noted in transition metal-free coupling reactions.
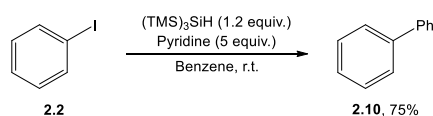
Scheme 2.3: Example of a HAS reaction initiated by a stoichiometric amount of (TMS)$_3$SiH.[12]

Addition of an aryl radical to an arene affords a cyclohexadienyl radical (**2.11**), which can be rearomatised in one of two ways: (i) electron transfer followed by proton transfer; or (ii) proton transfer followed by electron transfer (Scheme 2.4).
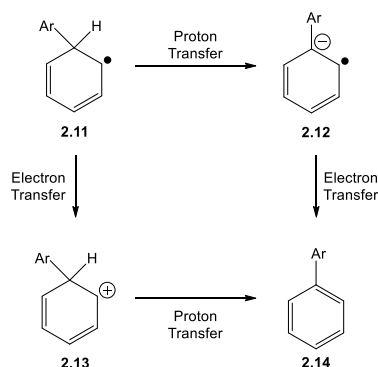
Scheme 2.4: Two possible routes to rearomatise a cyclohexadienyl radical.[13]

Given the presence of strong bases like NaO^{t}Bu or KO^{t}Bu in the transition metal-free coupling reactions, Studer and Curran concluded that proton transfer to afford a biaryl

radical anion (**2.12**, a strong reducing agent) would occur first. This would then be followed by electron transfer to another molecule of starting haloarene to propagate the radical chain (Scheme 2.5).
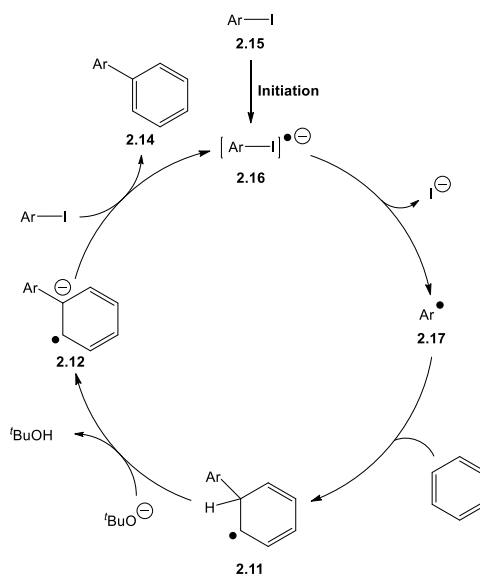
Scheme 2.5: The, now widely accepted, BHAS mechanism proposed by Studer and Curran[11] in 2011 for transition metal-free cross coupling reactions of haloarenes with arenes in the presence of a strong base and an organic additive.

At this early stage of research into BHAS reactions, little was understood about the initiation step to form the haloarene radical anion **2.16**. Indeed, it was known that electron transfer must be occurring to furnish this intermediate which then undergoes dissociation to afford an aryl radical, **2.17**. The early proposal for initiation focused on electron transfer occurring from a complex between *tert*-butoxide and the organic additive (*i.e.*, phenanthroline, Figure 2.1).[9-10]
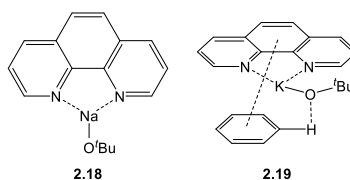
Figure 2.1: Phenanthroline – *tert*-butoxide complexes proposed to act as electron donors by Hayashi *et al.*[9] and Shi *et al.*[10]

A range of publications have since demonstrated other organic additives to be effective at initiating BHAS reactions in the presence *tert*-butoxide, whilst invoking the idea of a complex between the additive and *tert*-butoxide as the electron donating species

responsible for initiation. These additives have included amino acids,[7, 14] alcohols,[15] diols,[7, 16] and diamines.[7, 16-18] However, further mechanistic detail about the mode of BHAS initiation in the presence of these organic additives were not reported until the seminal work of Murphy, Tuttle and co-workers in 2014.[19-20] The following sections will discuss what is now understood about the modes of initiation for BHAS reactions under transition metal-free conditions, and how this differs from the early idea of a *tert*-butoxide – organic additive complex being responsible for initiation.

2.2 Initiation of BHAS Reactions

2.2.1 Organic Additives as Electron Donor Precursors

As previously mentioned, in 2014 Murphy, Tuttle and co-workers published two important papers on the topic of BHAS initiation where organic additives were used in the presence of *tert*-butoxide.[19-20] Since 2014 a number of other publications have contributed to the understanding of how organic additives react with *tert*-butoxide to form organic electron donors *in situ*. This section will discuss a range of organic additives and their reactions with *tert*-butoxide resulting in formation of such organic electron donor species.

The contribution of Murphy, Tuttle and co-workers[19-20] extended their previous interest in the field of organic electron donor molecules, in which they have developed powerful organic reducing agents (super electron donors) to effect a range of difficult transformations. (These previous works are well reviewed[21-22] and will not be discussed further in this chapter.) Drawing on this previous knowledge in organic super electron donor reactivity, they were able to apply a previously studied super electron donor as the initiator in the coupling of iodobenzene or 4-iodoanisole with benzene, Scheme 2.6.
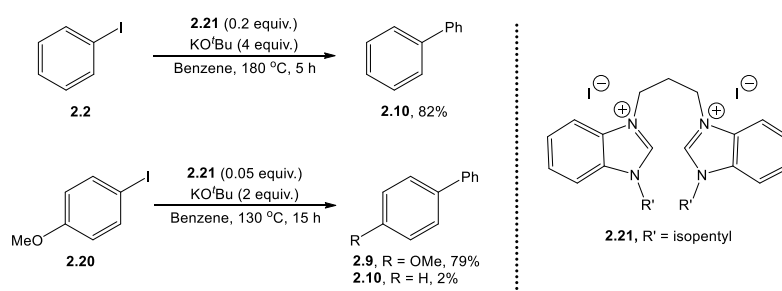
Scheme 2.6: Coupling of iodobenzene or 4-iodoanisole with benzene in the presence of super electron donor precursor salt (**2.21**) and KO*t*Bu.

Detailed experimental and computational investigations were also carried out by Murphy, Tuttle and co-workers to understand how organic additives and *tert*-butoxide initiated

BHAS reactions of haloarenes with arenes. The results of these studies and the most up to date mechanistic information will be discussed below for each of the most common organic additive types – alcohols/diols, diamines, nitrogen heterocycles and amino acids and diketopiperazines.

2.2.1.1 Alcohols and Diols

Alcohols were first reported to initiate BHAS reactions of haloarenes with arenes, alongside KO^{t}Bu by Liu *et al.*[15] in 2013 when they were able to utilise a large number of alcohols ranging from methanol to benzyl alcohol. Using *n*-butanol (40 mol%) and KO^{t}Bu (3 equiv.) Liu *et al.*[15] were able to couple iodo- or bromobenzene with benzene at 80 °C in an 82% or 30% yield, respectively.

^{n}BuOH (0.4 equiv.)
KO^{t}Bu (3 equiv.)
Benzene, 80 °C, 24 h

2.2, X = I
2.8, X = Br

2.10
X = I, 82%
X = Br, 30%
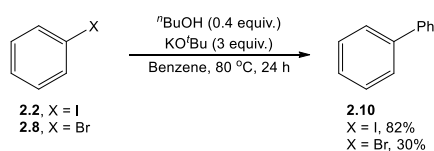
Scheme 2.7: Coupling of iodo- or bromobenzene with benzene in the presence of *n*-butanol and KO^{t}Bu.[15]

Lei *et al.*[7] became the first to report diols as initiators of BHAS reactions with their application of *cis-* and *trans*-cyclohexane-1,2-diol as additives in the coupling of 4-iodotoluene with benzene, Scheme 2.8a. The acyclic diols ethane-1,2-diol, propane-1,3-diol and butane-1,4-diol were utilised as initiators by Kwong *et al.*[16] for intramolecular haloarene coupling to afford phenanthridines, Scheme 2.8b.
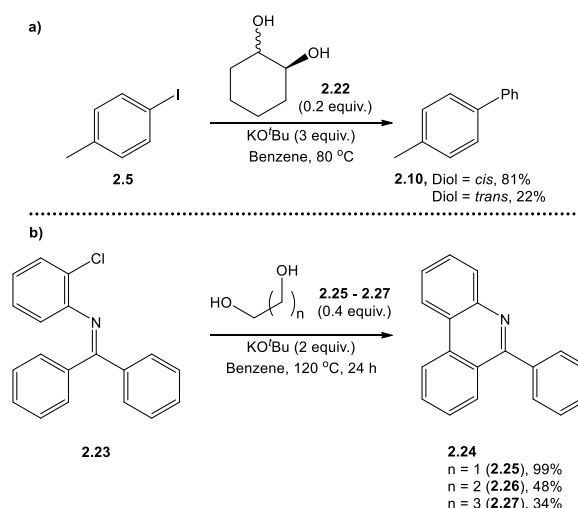
Scheme 2.8: a) Coupling of 4-iodotoluene and benzene initiated by cyclohexane-1,2-diol and KO*t*Bu.[7] **b)** Synthesis of phenanthridines (**2.24**) by intramolecular transition metal-free coupling initiated by acyclic diols and KO*t*Bu.[16]

Murphy, Tuttle and co-workers[19] proposed that under the transition metal-free coupling reaction conditions, alcohols and diols could be converted, *in situ*, to organic electron donors. This could occur by oxidation of an alcohol moiety to its corresponding ketone; oxidation of an alcohol to its corresponding ketone in the presence of KO*t*Bu and an electrophile (another ketone) was previously demonstrated by Woodward *et al.*[23] in 1945. Subsequent deprotonation of the α-carbon would afford an enolate, a potential electron donor species. This proposal is supported in part by the very low yields observed by Liu *et al.*[15] when utilising the alcohol *tert*-butanol, which is unable to undergo oxidation to a ketone, and also 2,2,2-trifluoroethanol which bears no α-hydrogens.

In order to test their proposed mechanism, Murphy, Tuttle and co-workers[19] heated *cis-4-tert*-butylcyclohexan-1-ol (**2.28**) in benzene to 170 °C with 10 equiv. of KO*t*Bu for 16 h and observed a mixture of *cis-* and *trans-4-tert*-butylcyclohexan-1-ol with small amounts of 4-*tert*-butylcyclohexan-1-one (**2.30**). Similar results were obtained upon starting from *trans-4-tert*-butylcyclohexan-1-ol (**2.33**). To verify if enolate **2.31** could indeed act as an initiator, Murphy, Tuttle and co-workers prepared it by reacting 4-*tert*-butylcyclohexan-1-one (**2.30**) with potassium hydride, and following isolation used the enolate to successfully initiate a coupling reaction between iodo-*meta*-xylene and benzene.
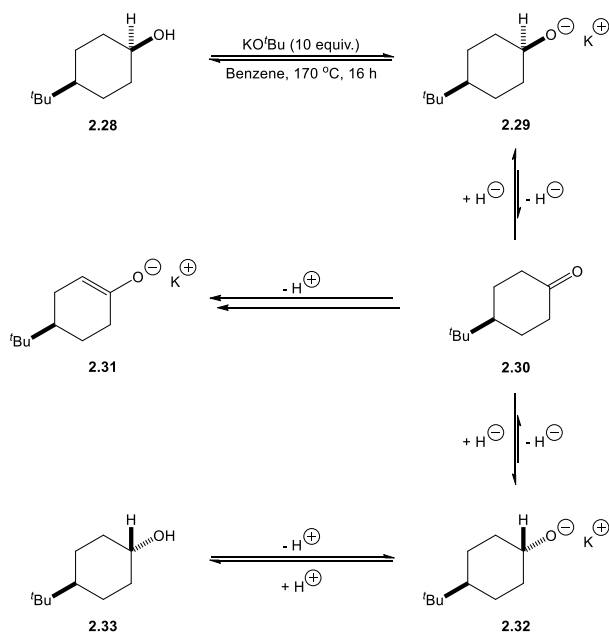
Scheme 2.9: Reaction of *cis-tert*-butylcyclohexanol (**2.28**) with KO*t*Bu carried out by Murphy *et al.*[19] which formed small amounts of ketone **2.30** and a mixture of **2.28** and **2.33**.

Diols have also been shown to react in a similar manner, for example, treating *cis*-cyclohexan-1,2-diol (**2.34**) with 3.5 equiv. of KO*t*Bu formed 2-hydroxycyclohexan-1-one (**2.36**) and *trans*-cyclohexan-1,2-diol (**2.40**, Scheme 2.10). It was therefore proposed by Murphy, Tuttle and co-workers[19] that diols could ultimately form enolates (**2.37** or **2.38**) or enediolates which could both act as organic electron donors.
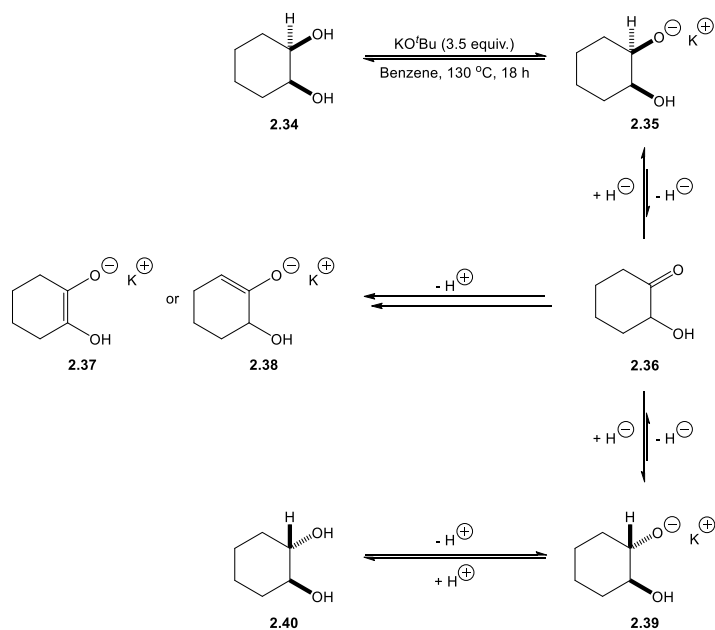
Scheme 2.10: Conversion of diol **2.34** to a mixture of **2.34**, **2.36** and **2.40**. Upon deprotonation **2.36** could form potential electron donors **2.37** and **2.38**.

2016 saw Murphy *et al*. investigate 2-pyridinecarbinol (**2.44**) as an initiator for transition metal-free coupling reactions.[24] By utilising 2-pyridinecarbinol and several other molecules as initiators, in the presence of KO*t*Bu, they were able to show that 2-pyridinecarbinol was the most effective initiator tested, Scheme 2.11. Testing additional initiator molecules was however to provide mechanistic information. For example, protecting the hydroxy group as its methyl ester (**2.45**, Scheme 2.11, entry 3) or replacing the methylene hydrogens by methyl groups (**2.46**, Scheme 2.11, entry 4) reduced the initiation activity in the test BHAS reaction by an order of magnitude.

Additive	Blank	OH 2.44	OMe 2.45	OH 2.46
Combined Yield 2.42 & 2.10	1.5 mg	34 mg	3.1 mg	4 mg
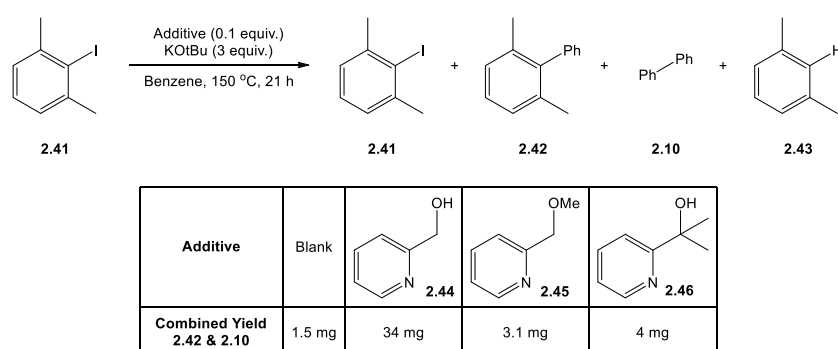
Scheme 2.11: 2-pyridinecarbinol and derivates tested as initiators for the coupling between iodo-*meta*-xylene and benzene by Murphy *et al*.[24]

These reactions, along with deuterium incorporation studies allowed Murphy *et al*.[24] to propose that the main source of electron donor was *via* double deprotonation of 2-pyridinecarbinol – first at the hydroxyl group then at the adjacent methylene, Scheme 2.12a. They further proposed that another electron donor may be formed as part of a minor pathway; through deprotonation then hydride loss to yield aldehyde **2.49**. Addition of KO*t*Bu to the aldehyde would follow, then electron donor species **2.51** could be formed by deprotonation of **2.50**, Scheme 2.12b.
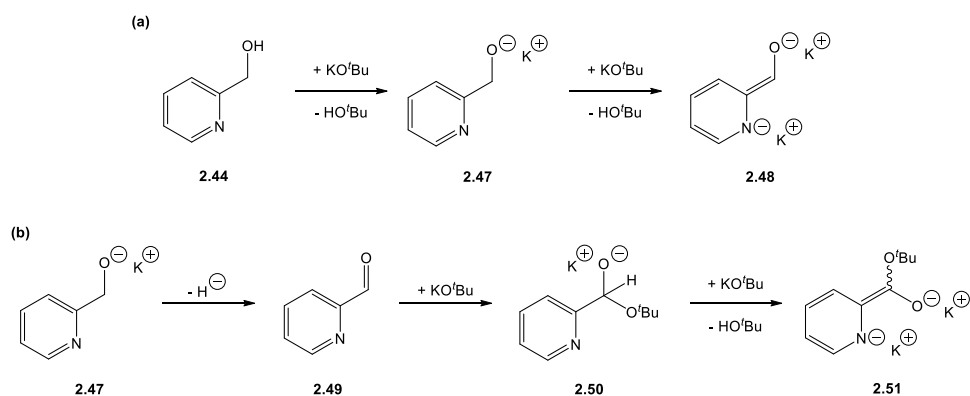
Scheme 2.12: Two proposed routes to electron donor species from 2-pyridinecarbinol proposed by Murphy *et al*.[24]

2.2.1.2 Diamines

One of the most widely utilised classes of additives in transition metal-free BHAS coupling reactions are the diamines. To date, several diamines have been studied and these include: ethylenediamine (**2.52**),[7] N,N'-disubstituted ethylenediamines (**2.53** - **2.54**),[7, 16, 18-19, 25-27] cyclohexane-1,2-diamine (**2.55**)[16, 18-19, 27] and N-substituted cyclohexane-1,2-diamines (**2.56** - **2.57**).[18, 27]

2.52, R = H
2.53, R = Me
2.54, R = -(CH₂)₃(CF₂)₅CF₃

2.55, R = H
2.56, R = Bz
2.57, R = Ts
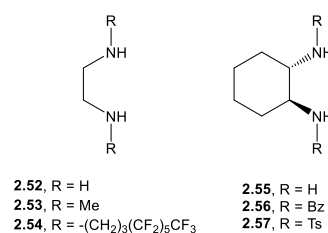
Figure 2.2: Diamines used as additives in transition metal-free BHAS coupling reactions.

The early mechanistic proposal[18] for reactions initiated by a diamine and KO*t*Bu followed from the mechanism proposed by Hayashi *et al*.[9] for initiations by phenanthroline and bipyridine type additives in combination with KO*t*Bu. It suggested that a complex between KO*t*Bu and diamine (**2.60**) was able to transfer an electron to an aryl halide substrate (**2.58**) thus initiating the BHAS mechanism.
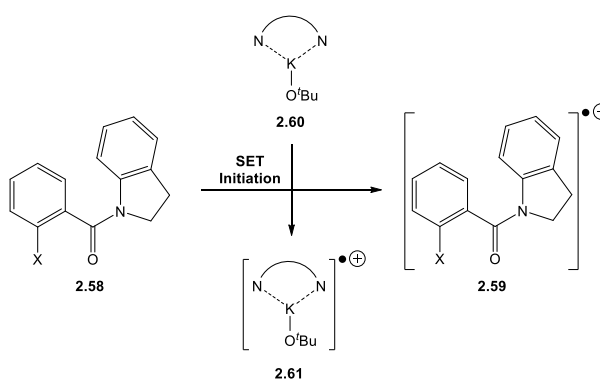
Scheme 2.13: Diamine - KO*t*Bu complex (**2.60**) proposed by Bisai *et al*.[18] to act as a single electron donor towards substrate **2.58**.

Since this initial mechanistic proposal, the mechanism of initiation using the combination of diamine and KO*t*Bu has been well studied by experimental and computational techniques. The first published mechanistic study saw Murphy, Tuttle and co-workers[19] experimentally investigate how DMEDA and KO*t*Bu could initiate transition metal-free BHAS coupling reactions between haloarenes and arenes. After conducting coupling

reactions with DMEDA or cyclohexane-1,2-diamines as additives, coloured reaction mixtures were observed (Scheme 2.14).
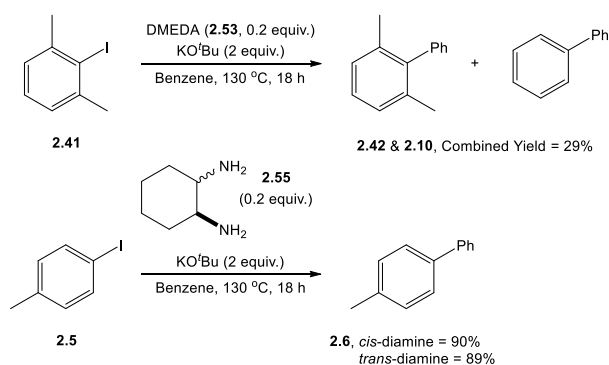
Scheme 2.14: Transition metal-free coupling reactions initiated by diamine additives and KO^{t}Bu conducted by Murphy, Tuttle and co-workers.[19]

The appearance of colour in the reaction mixture is indicative of the formation of a conjugated species, and thus prompted Murphy, Tuttle and co-workers[19] to consider whether, like alcohols and diols electron donor species could be formed *in situ* by reaction of the diamine with KO^{t}Bu. Attempts were therefore made to isolate products from reactions of DMEDA or cyclohexan-1,2-diamine with KO^{t}Bu in benzene, however these proved unsuccessful. As mentioned earlier, it is known in the literature that treating ethylenediamine with base (^{n}BuLi) forms a pyrazine radical anion;[8] this is likely to occur via deprotonation, loss of hydride[28] and subsequent condensation of the imine. To probe if similar reactions were occurring between DMEDA and KO^{t}Bu, Murphy, Tuttle and co-workers synthesised three deuterated analogues of DMEDA. These were then utilised as additives in coupling reactions between iodo-*meta*-xylene and benzene. The coupling reaction yields displayed a primary kinetic isotope effect for cleavage of a methylene C-H/D bond, which indicated that this was the rate-limiting step in the formation of an initiator species.
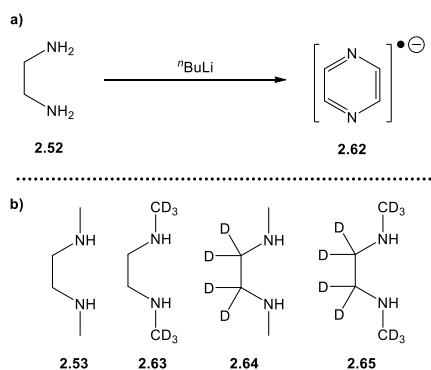
Scheme 2.15: a) Formation of pyrazine radical anion (**2.62**) from reaction of ethylenediamine (**2.52**) with ^{n}BuLi observed by Koster *et al.*[8] **b)** DMEDA analogues (**2.53**, **2.63 - 2.65**) studied by Murphy, Tuttle and co-workers.[19]

More recently, Jiao *et al.*[25] published a detailed kinetic and computational study of transition metal-free cross coupling reactions in the presence of DMEDA and KO^{t}Bu, proposing a novel initiation scheme. They proposed that a small amount of aryl radical could be produced initially by a background reaction such as the benzyne initiation published by Murphy, Tuttle and co-workers (see Section 2.2.3).[20] The aryl radical could then abstract a hydrogen atom from the ethylene backbone or an amine of DMEDA, producing radical **2.66** or **2.67**, respectively. Radical **2.66** or **2.67** could then be deprotonated by KO^{t}Bu to form radical anion **2.68**, which would act as a strong electron donor; this is paralleled by the work of Studer *et al.*[29] who have proposed radical anions of alcohols to be initiators in hydrodeiodination of aryl, alkynyl, alkenyl and alkyl iodides. The neutral imine, **2.69**, formed after single electron transfer (SET) could then undergo hydrogen atom abstraction by an aryl radical forming **2.71** or be deprotonated to form a different electron donor **2.70**. This electron donor could then initiate another BHAS radical chain. Radical **2.71** could then be further deprotonated to generate another electron donor species, **2.72**, which upon initiating another BHAS radical chain would form diimine **2.73**. This mechanistic proposal is supported by the observed kinetic profile for the coupling reaction of 4-iodoanisole with benzene in the presence of KO^{t}Bu and either DMEDA or **2.69** as additive. DMEDA exhibits an induction period whereas imine **2.69** does not, supporting the view that imine **2.69** alone promotes the 'proliferation' pathway.
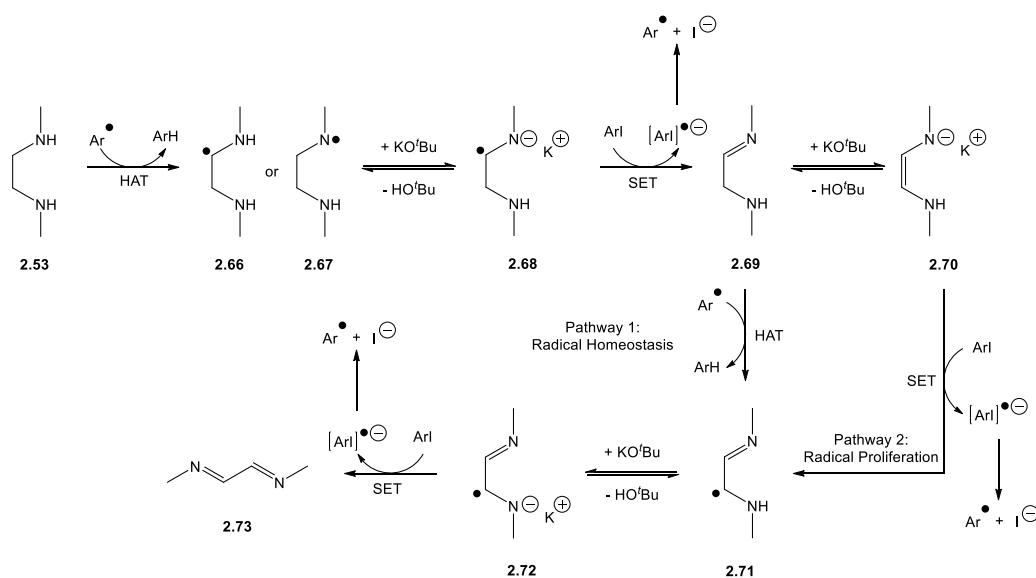
Scheme 2.16: Proposed mechanism of initiation by DMEDA additive plus KO^{t}Bu by Jiao *et al.*[25] utilising aryl radicals generated by background benzyne initiation.[20]

2.2.1.3 Nitrogen Heterocycles

Amongst the early reports of transition metal-free cross coupling of haloarenes with arenes, nitrogen heterocycles were commonly the additives used in conjunction with KO^{t}Bu to initiate the reaction, Figure 2.3.[6, 9-10] Despite this, few mechanistic details were known about how these nitrogen heterocycles in conjunction with KO^{t}Bu were able to initiate BHAS reactions.
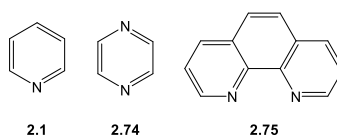
Figure 2.3: Nitrogen-containing heterocycles used in the early reports of transition metal-free haloarene – arene cross coupling.

What had been proposed in the original publications utilising phenanthrolines by Hayashi *et al.*[9] and Shi *et al.*[10, 17] was that a complex formed between *tert*-butoxide (NaO^{t}Bu or KO^{t}Bu) and phenanthroline (**2.75**) would be able to act as an electron donor towards haloarene substrates. However, no evidence to support this hypothesis was presented.

In 2014, Murphy, Tuttle and co-workers published the results of their investigations into pyridine and phenanthrolines as additives in transition metal-free cross coupling in the presence of KO^{t}Bu.[20] Initially they tested the hypothesis of Hayashi *et al.*[9] and Shi *et al.*[10, 17] by calculating the thermodynamics of the single electron transfer from **2.76/2.77**

(M = Na or K) to iodobenzene (**2.2**), Scheme 2.17. In the case of NaO^{t}Bu single electron transfer was endergonic by 63.9 kcal/mol, whilst KO^{t}Bu was similarly endergonic (59.5 kcal/mol).
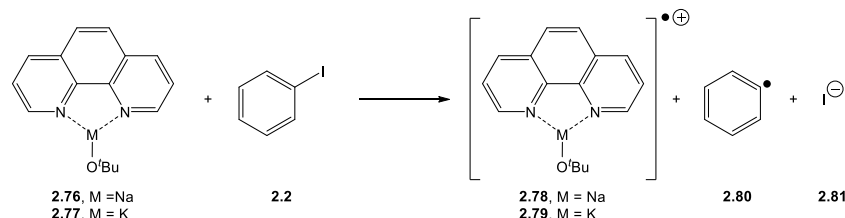
Scheme 2.17: Single electron transfer reaction between *tert*-butoxide - phenanthroline complex and iodobenzene studied by Murphy, Tuttle and co-workers using DFT calculations (M06L/6-311G(d,p), benzene modelled using CPCM solvation).

They therefore returned to experiment in order to investigate the roles of KO^{t}Bu and phenanthroline, by first performing a blank reaction of 1,10-phenanthroline and KO^{t}Bu in benzene with heating, to test for formation of potential electron donor species. Indeed, they were able to isolate **2.85** following quenching of the pyrophoric reaction product with iodine, indicating that **2.84'** was the product of the reaction between KO^{t}Bu and phenanthroline. Candidate electron donor **2.84'** is proposed to form by deprotonation of 1,10-phenanthroline – KO^{t}Bu complex **2.77** by another KO^{t}Bu molecule, **2.82** could then act as a nucleophile towards another molecule of phenanthroline affording **2.83**. Deprotonation of this anion would lead to **2.84** which has a resonance form **2.84'**, which possesses an electron rich alkene moiety – a known characteristic of organic electron donors.[22, 30-32]

In addition to this experimental evidence, Murphy, Tuttle and co-workers conducted DFT calculations to understand the energetic profile for formation of dianion **2.84'**, finding that the initial *ortho* deprotonation of phenanthroline was endergonic by 15.8 kcal/mol. Subsequent addition to neutral phenanthroline and deprotonation to afford **2.84'** would occur readily (small free energy of activation) and favourably (exergonic). These findings show that phenanthroline would indeed be able to form an electron donor *in situ* which could subsequently act as a BHAS initiator. The largest energy span found for formation of **2.84'** was 26.3 kcal/mol which was made up of the endergonic deprotonation of phenanthroline and the free energy of activation for addition to a subsequent phenanthroline molecule ($\Delta G^{\ddagger}$ = 10.5 kcal/mol).
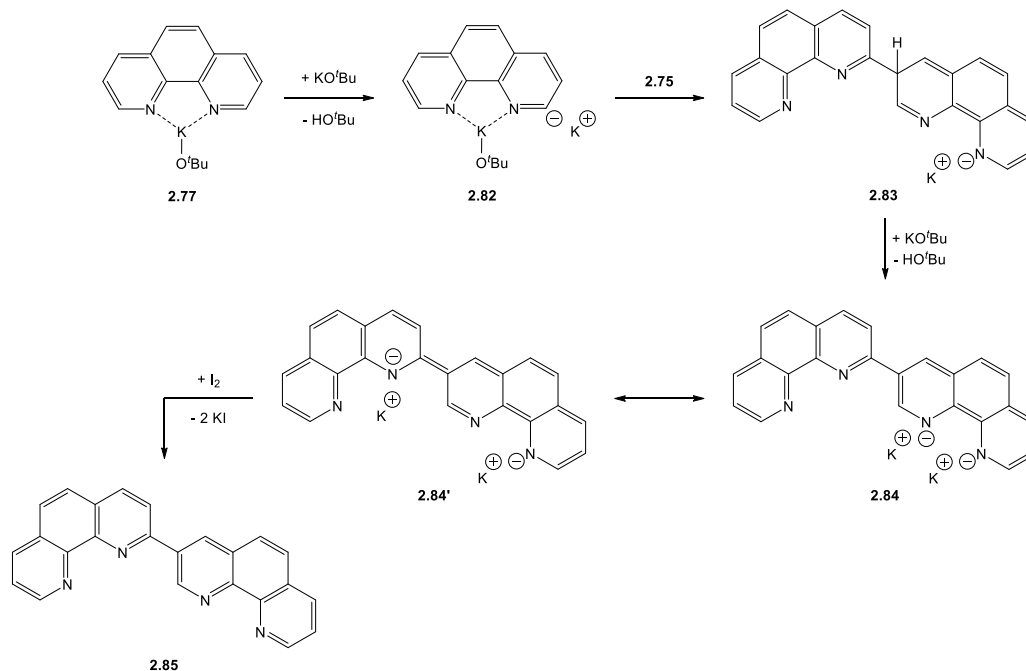
Scheme 2.18: Formation of dianionic phenanthroline dimer **2.84'**, a candidate electron donor.

Murphy, Tuttle and co-workers then turned their attentions to the use of pyridine in transition metal-free coupling reactions, and whether it could be forming an electron donor species *in situ*. In analogy to the 1,10-phenanthroline investigations they reacted pyridine with KO^{t}Bu under heating followed by quenching with iodine. This yielded both 2,2'- and 4,4'-bipyridine, but no 2,4'-bipyridine, indicating that pyridine was reacting in a similar manner to phenanthroline. Deprotonation of pyridine at the 2- or 4- position, followed by addition of the anion to the same position on another pyridine molecule would lead to **2.91** or **2.87** respectively. Subsequent deprotonation of **2.91** or **2.87** would lead to dianions **2.92** or **2.88**, both of which possess the characteristics of a good organic electron donor – namely, an electron rich double bond and the potential to gain aromaticity upon loss of electrons.
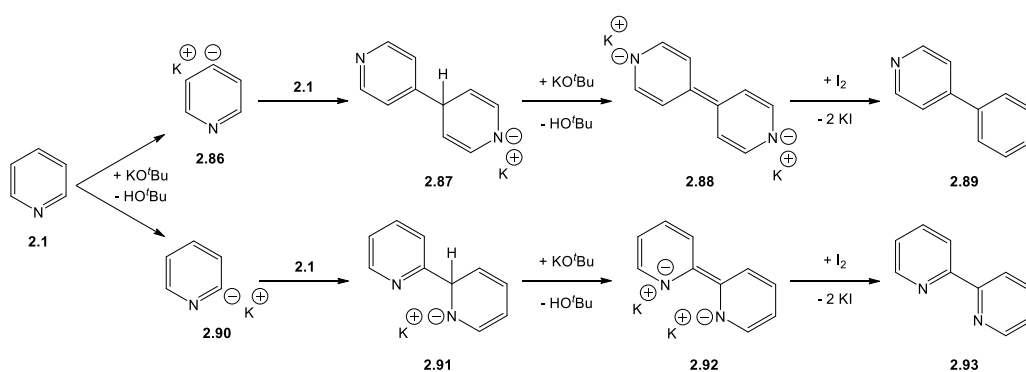
Scheme 2.19: Proposed formation of bipyridine electron donors **2.88** and **2.92** by reaction of pyridine and KO^{t}Bu.[20]

2.2.2 Additive-Free Reactions

Whilst the combination of *tert*-butoxide (typically KO*t*Bu) and an organic additive have proven very successful for the initiation of transition metal-free coupling between a haloarene and another arene substrate, there is also evidence that this reactivity is indeed possible without the organic additive, Scheme 2.20.[20, 33] This invited the question: how are these BHAS reactions being initiated in the absence of organic additives, such as those mentioned previously, which can form organic electron donors *in situ*?

a)

Temperature (°C)	Time (h)	Yield
85	3	0%
110	3	3%
160	3	38%
160	6	66%

b)

Temperature (°C)	Time (h)	KO*t*Bu Equivalents	Yield
110	3.5	2	27%
130	3.5	2	30%
185	14	4	48%
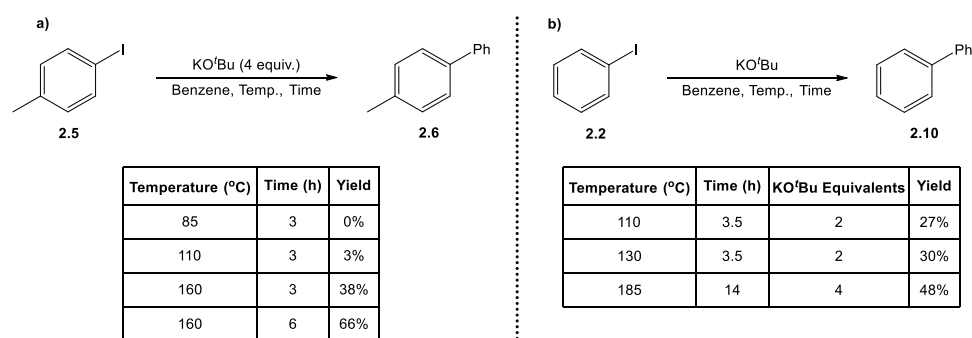
Scheme 2.20: a) Additive-free coupling of iodotoluene and benzene reported by Wilden *et al*.[33] **b)** Additive-free coupling of iodobenzene and benzene reported by Murphy *et al*.[20]

Upon surveying the literature, two possible modes of initiation with only KO*t*Bu can be found: (i) KO*t*Bu itself acting as an electron donor; or (ii) the formation of benzyne intermediates, which can then act as radical initiators.

2.2.3 Benzyne Initiation

Murphy, Tuttle and co-workers were the first to discuss the involvement of benzyne intermediates as initiators of BHAS reactions between iodobenzene and benzene in the presence of only KO*t*Bu.[20] The ability of KO*t*Bu to form benzyne upon reaction with an iodoarene had already been demonstrated by Bajracharya and Daugulis, in their report of intramolecular arylation of phenols.[34] It was shown using DFT calculations that formation of benzyne (**2.94**) from iodobenzene (**2.2**), by first deprotonation (using KO*t*Bu) then expulsion of iodide (as potassium iodide), is an endergonic process (ΔG = 18.6 kcal/mol). The subsequent step of benzyne addition to benzene has an associated free energy of activation of 5.7 kcal/mol making the energy span 24.3 kcal/mol to access the transition state for formation of **2.95**. Intermediate **2.95** was found to be 7.9 kcal/mol lower in energy than **2.94** plus **2.4**. With the subsequent steps exhibiting accessible barriers and favourable relative energies, the results would suggest that benzyne could be readily formed under the high temperature reaction conditions.
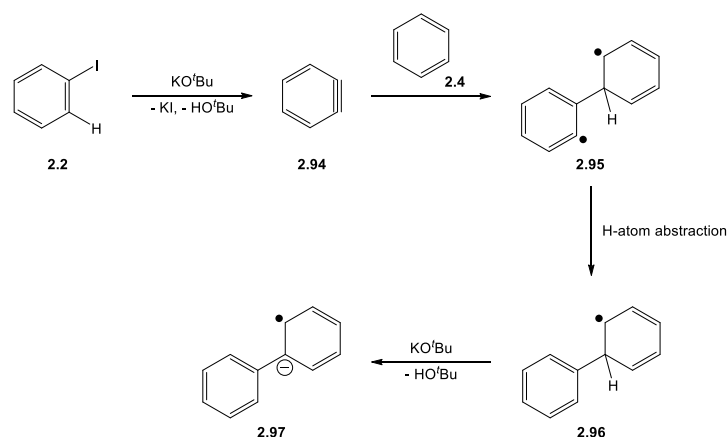
Scheme 2.21: Formation of an electron donor from iodobenzene through a benzyne intermediate.[20]

2.3 KO*t*Bu as an Electron Donor

Potassium *tert*-butoxide has long been discussed as an electron donor, with Ashby *et al*.[35] first reporting the single electron reduction of benzophenone by KO*t*Bu in 1982. Whilst studying the reduction of benzophenone to benzhydrol with a selection of lithium alkoxides bearing an α-hydrogen, it was noted that the distinctive blue colouration of benzophenone ketyl radical anion was formed. This same blue colouration was also observed in the case of KO*t*Bu. In addition, the formation of radical intermediates in these reactions was confirmed by electron paramagnetic resonance (EPR) spectroscopy.[2, 35-36] The mechanism of reduction was proposed to be an initial single electron transfer from alkoxide to benzophenone (**2.98**), followed by abstraction of the α-hydrogen from the alkoxyl radical by the benzophenone ketyl radical anion (**2.100**). For those alkoxides bearing no α-hydrogen (i.e. *tert*-butoxides) no benzhydrol (**2.103**) is observed, only the benzophenone ketyl radical anion.
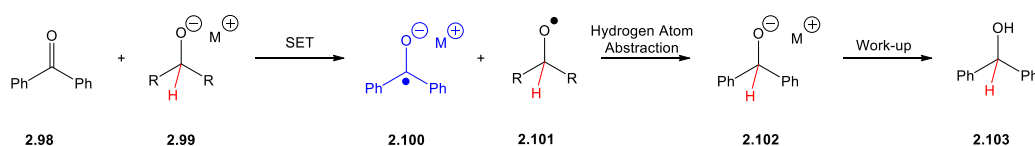
Scheme 2.22: Proposed reaction mechanism of Ashby *et al*.[2, 35-36] for reduction of benzophenone by alkali metal alkoxides bearing an α-hydrogen.

The work of Ashby *et al*.[2, 35-36] later prompted Wilden *et al*.[33] to propose that KO*t*Bu could donate an electron to haloarenes in order to initiate coupling with benzene. Wilden *et al*. described how alkali metal alkoxides could be thought to exist in an equilibrium between a covalent and a charge-separated form, the latter charge-separated form also existing

in an equilibrium with the corresponding alkoxyl radical and a loosely bound electron. On this basis, Wilden *et al*. rationalised their observed higher yields when using different alkali metal *tert*-butoxides by stating that the equilibrium for KO*t*Bu lies towards the charge-separated form more so than NaO*t*Bu, whereas the equilibrium for LiO*t*Bu lies more towards the covalent form. For all three *tert*-butoxides they state that the equilibrium between the charge-separated form and the alkoxyl radical-loosely bound electron heavily favours the charge-separated form. As such it is proposed that high temperatures would be required for the loosely bound electron to be transferred to a haloarene in all of these cases.
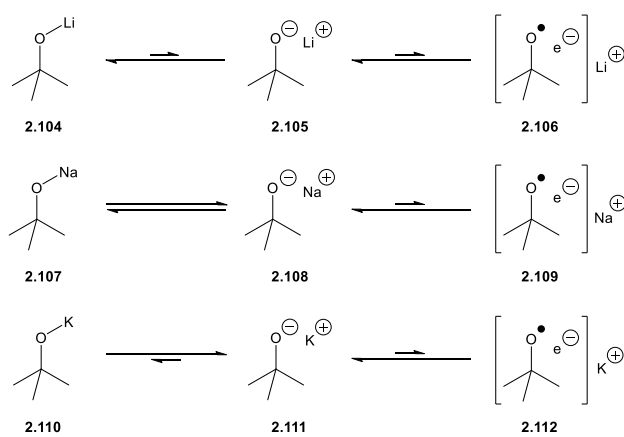
Scheme 2.23: Equilibria between covalent, charge-separated and loosely bound electron for alkali metal *tert*-butoxides, proposed by Wilden *et al*.[33]

The proposal that KO*t*Bu acts as an electron donor was further extended by Wilden *et al*. to reactions where 1,10-phenanthroline was present as an additive. It was suggested that 1,10-phenanthroline would act as an electron acceptor, removing the loosely bound electron and thus shifting both equilibria to the right, Scheme 2.23. To obtain evidence for this process, Wilden *et al*. reacted potassium *tert*-pentoxide and 1,10-phenanthroline, observing butanone (formed by fragmentation of the *tert*-pentoxyl radical into methyl radical and butanone) by mass spectrometry. However, since these reactions were run with THF as solvent which has the same molecular weight as butanone, the results cannot be taken as conclusive evidence for formation of *tert*-pentoxyl radicals. Further evidence for butanone formation was provided by means of a Janovsky test, where *meta*-dinitrobenzene was added to the reaction of potassium *tert*-pentoxide and 1,10-phenanthroline. This provided a positive purple colour, indicating that the enolate of a ketone had reacted with the *meta*-dinitrobenzene.[37-39]

Lei *et al.*[40] also studied the reaction between KO*t*Bu and 1,10-phenanthroline performing a range of EPR and cyclic voltammetry (CV) experiments. They concluded that an interaction between the two reactants led to an inner-sphere electron transfer (ISET) from KO*t*Bu to 1,10-phenanthroline. This was due to fast outer-sphere electron transfer (OSET) being ruled out by the large measured difference in the oxidation peak potential of KO*t*Bu (0.1 V in DMF, *vs* SCE) and the first reduction potential of 1,10-phenanthroline (-2.06 V in DMF, *vs* SCE). The 1,10-phenanthroline radical anion generated by ISET was then said to donate an electron to haloarenes *via* OSET to generate aryl radicals, thus initiating the BHAS mechanism.
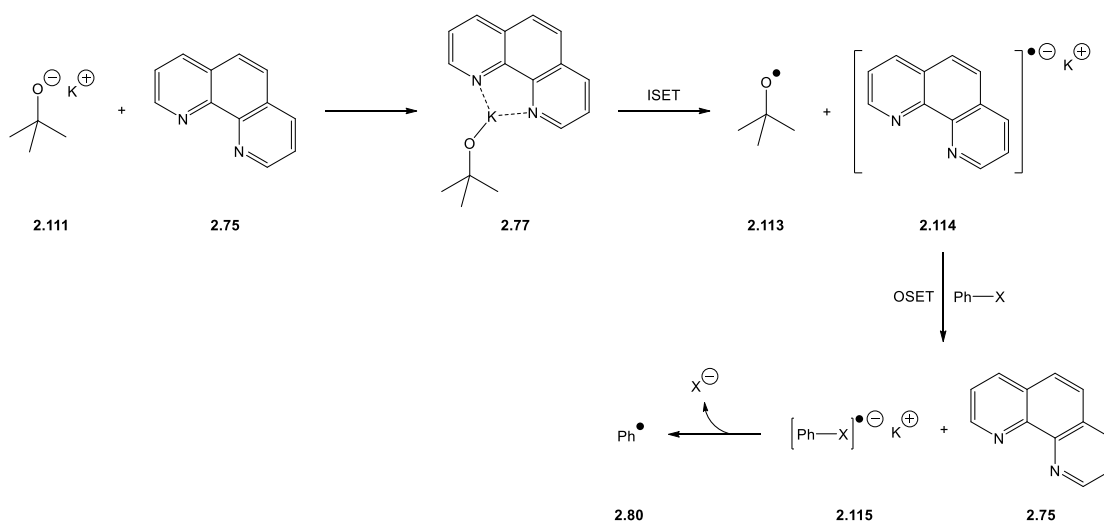
Scheme 2.24: Mechanism of initiation proposed by Lei *et al.*[40] involving initial inner-sphere electron transfer from KO*t*Bu to 1,10-phenanthroline, followed by outer-sphere electron transfer from phenanthroline radical anion to haloarene substrate.

In 2016, Murphy *et al.*[41] published a wide ranging study on the ability of KO*t*Bu to act as an electron donor; significantly, they further studied whether KO*t*Bu could act as an electron donor towards 1,10-phenanthroline. As previously mentioned in Section 2.2.1.3, Murphy *et al.*[20] have isolated a phenanthroline dimer upon reacting 1,10-phenanthroline with KO*t*Bu. They and others[42-43] have also demonstrated, through DFT calculations, that SET from a KO*t*Bu-phenanthroline complex to a haloarene is a highly endergonic reaction (>50 kcal/mol). Despite this they undertook further investigations into the reactivity of KO*t*Bu with 1,10-phenanthroline.

First they studied both 1,10-phenanthroline (**2.75**) and its dianionic dimer (**2.84'**) by CV, with the voltammogram for 1,10-phenanthroline matching that of Lei *et al.*,[40] whilst observing three peaks for the dimer at -1.70, -1.94 and -2.19 V (in DMF *vs* SCE). Upon

calibrating the dimer voltammogram with Fc/Fc$^+$, Murphy *et al*. were able to show that these peaks corresponded to 1e$^-$, 1e$^-$ and 2e$^-$, respectively. Since the first potential of the dimer matches more closely with the first reduction potential of 1,10-phenanthroline, Murphy *et al.* suggest that in the experiment of Lei *et al*. the dimer could be responsible for reducing 1,10-phenanthroline. This could explain the existence of the non-symmetrical EPR spectrum measured by Lei *et al*. in which two phenanthroline related radical anions may be present.

With both experimental and computational observations indicating direct electron transfer from KO^{t}Bu to haloarenes (or organic additives) as highly unlikely, Murphy and co-workers set out an alternative initiation mechanism for the BHAS reaction in the presence of only KO^{t}Bu and a haloarene substrate; namely, that the initiation mechanism involves a benzyne intermediate.[20, 41]

2.4 Solvents as Electron Donor Precursors

The previous sections have focussed on reactions where additives have been added to systems in addition to substrates, solvents and base. However, there exist reports in the literature where the solvent used in BHAS reactions has been implicated as the 'additive,' in the sense which we have been describing the organic molecules previously.

The group of Yan have proposed that in reactions where KO^{t}Bu and DMF (**2.116**) are present, a complex between these two can transfer an electron to another molecule of DMF yielding a DMF radical anion (**2.118**) and a carbamoyl radical (**2.119**). In this case, the carbamoyl radical has been postulated to initiate the intramolecular coupling of tertiary amines with ketones to yield indoles,[44] as well as the intramolecular cyclisation of 1,1'-biphenyl aldehydes and ketones to form phenanthrenes (Scheme 2.25).[45]
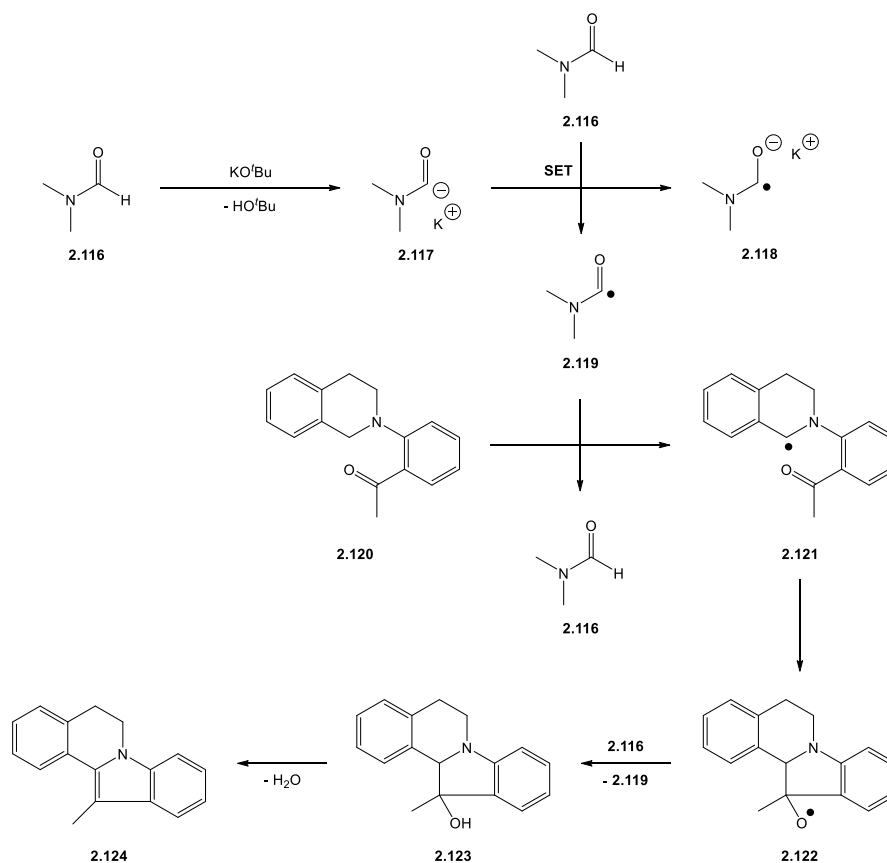
Scheme 2.25: Proposal of Yan *et al.* that sees a carbamoyl anion act as an electron donor towards DMF yielding a carbamoyl radical, which can then initiate radical cyclisation reactions.

In the work of Taillifer *et al.*[43] DMF, which was being used as the solvent for the α-arylation of enolisable aryl ketones, was found to be a vital reactant, as when the solvent was switched to toluene, acetonitrile (MeCN) or dimethylsulfoxide (DMSO) no reaction was observed. The deprotonation of DMF by KO*t*Bu was said to be affording the carbamoyl anion which could then act as a single electron reductant towards the haloarene substrate, the resultant radical anion fragments to afford halide anion and aryl radical. An $S_{RN}1$ reaction then occurs between the aryl enolate (**2.127**) and the aryl radical (**2.80**) to afford ketyl radical anion, which can propagate the radical chain by acting as a single electron reductant.
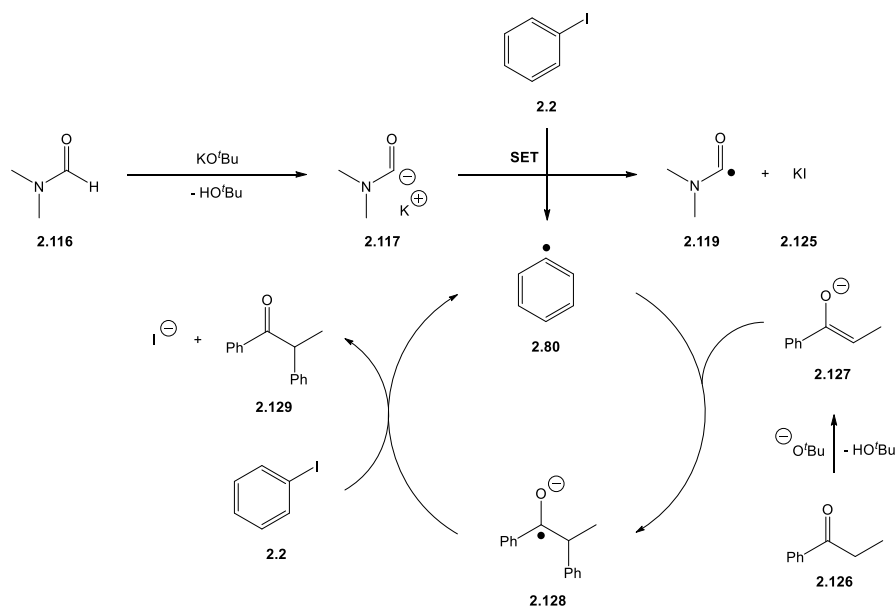
Scheme 2.26: Proposal by Taillifer *et al*. that carbamoyl anion acts as a single electron reductant towards haloarenes.

More recently, Murphy, Tuttle and co-workers[41] investigated the reaction between KO*t*Bu, DMF (**2.116**) and diformamides **2.133** and **2.136**. They were able to test their theory that upon deprotonation of a formamide to afford a carbamoyl anion, this would attack another formamide to afford a dimer. Using the three formamides as additives for the BHAS reaction depicted in Scheme 2.27, showed that 0.2 equiv. of DMF afforded 0.6% yield of coupled products, whereas using 0.1 equiv. of diformamides **2.133** & **2.136** afforded increased yields of 8.0% and 16.1%, respectively. These results suggest that intermolecular dimerization would occur less readily than intramolecular dimerisation of the linear diformamide, whilst conformationally restricted cyclic diformamide **2.136** should cyclise more readily than **2.133**. This work serves to offer an alternative mechanistic explanation for electron transfer occurring from a DMF derived electron donor, to that of Yan or Taillefer. The example of DMF should act as another reminder that the seemingly simple reactions can have widely different mechanistic possibilities, and that the operative reaction mechanism can be very elusive.
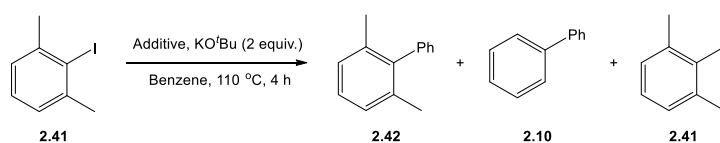
Scheme 2.27: BHAS reaction used by Murphy, Tuttle and co-workers to assess the initiation ability of **2.116**, **2.133** and **2.136**.
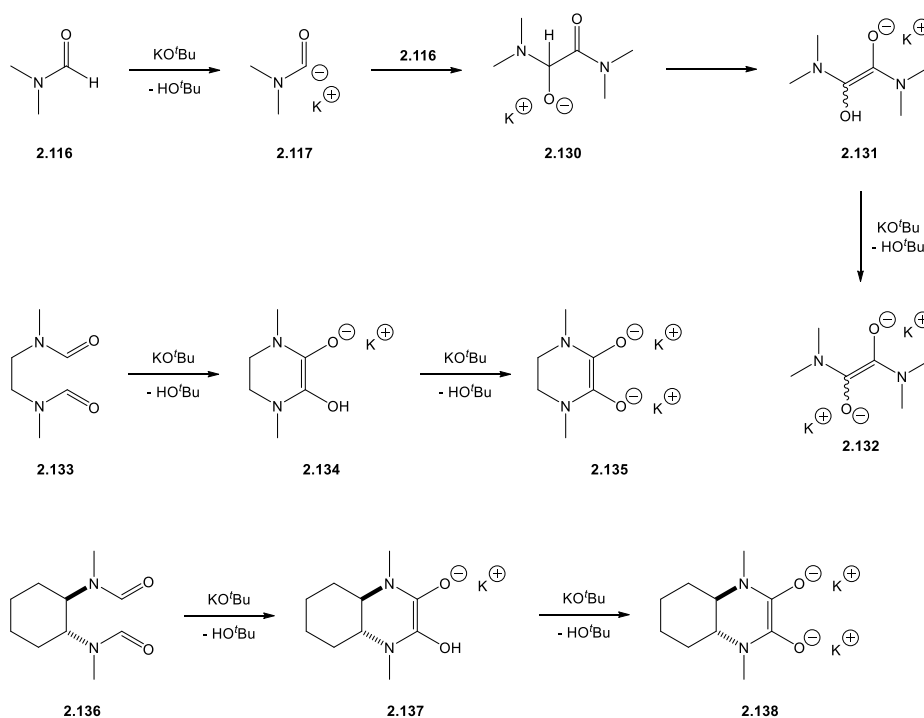
Scheme 2.28: Formamides studied by Murphy, Tuttle and co-workers as additives for BHAS initiation.[41]

In analogy to DMF, the solvent DMSO has recently been linked to electron transfer reactions whilst in the presence of KO^{t}Bu (or other strong bases). Murphy, Tuttle and co-workers studied the reduction of 1,3-dithianes in the presence of KO^{t}Bu with DMSO as solvent, which had previously been reported by Peñéñory *et al.*[46] In the original publication, the authors concluded that a charge transfer complex between KO^{t}Bu and the dithiane (**2.139**) was the species being photoexcited, obtaining the dithiane radical anion as product. Upon C–S bond cleavage this could abstract a hydrogen from the 1,4-cyclohexadiene present and then receive another electron and undergo the second C–S cleavage to afford the product. Upon revisiting this reaction, Murphy, Tuttle and co-workers used UV-vis spectroscopy to study mixtures of DMSO or DMF, dithiane and KO^{t}Bu or KH. They observed a peak at 466 nm for the mixture of DMSO, dithiane and KO^{t}Bu, upon changing the base to KH a similar peak at 466 nm was still observed. When swapping out the DMSO for DMF, no new peak at 466 nm was observed therefore the conclusion was made that the charge transfer complex was likely between dimsyl anion and dithiane.
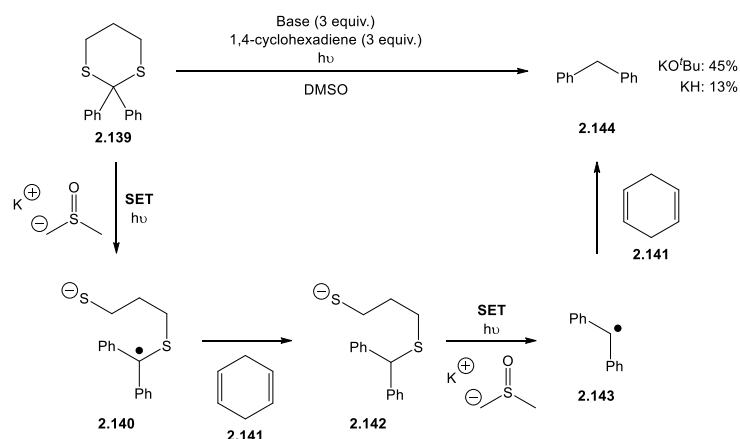
Scheme 2.29: Reduction of the 1,3-dithiane **2.139** reported by Peñéñory *et al.*[46] and further studied by Murphy, Tuttle and co-workers.[41]

Another case of the dimsyl anion acting as an electron donor under irradiation was demonstrated by Rossi *et al.*[47] for the photoinitiation of BHAS and other reduction reactions. Using a blue LED (3 W) to irradiate reactions of KO^{t}Bu, adamantyl iodide (**2.145**) and benzene (**2.4**) in DMSO they were able to form coupled product **2.146** with an excellent yield.
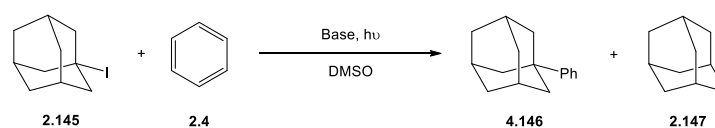
Entry	Benzene (equiv.)	Base (equiv.)	Time (h)	Conversion	Product Yields (%)
1	20	KO^{t}Bu	3	100	**2.146** (95)
2	10	KO^{t}Bu	3	100	**2.146** (91) **2.147** (6)
3	50	KO^{t}Bu	3 (dark)	4	(-)
4	10	NaH	3	100	**2.146** (76) **2.147** (5)

Scheme 2.30: BHAS initiation carried out by Rossi *et al.* utilising light, DMSO and a strong base.

2.5 KO^{t}Bu – Triethylsilane Reducing System

Organosilanes have long been utilised as reducing agents in organic chemistry, in radical based reductions[48] or in combination with an acid (typically trifluoroacetic acid) to afford 'ionic hydrogenations'.[49] A novel application of organosilanes as reducing agents appeared in the 1980s when activation of organosilanes by a nucleophile (typically fluoride or alkoxides) enhanced their reducing ability.

Activation of alkylsilanes by fluoride, to form pentavalent silicates was reported in 1986 by Yang and Tanner,[50] who were studying the mechanism of reduction of ketones, a reaction which had been proposed to occur by hydride transfer or SET, Scheme 2.31. They proposed that fluoride anion adds to trialkylsilane forming a pentavalent silicate, which can then deliver a hydride to ketones (Scheme 2.31a) or alternatively transfer an electron to generate the ketyl radical anion (Scheme 2.31b). Reduction by SET would lead to opening of the cyclopropyl substituent, and following hydrogen atom abstraction and subsequent protonation would yield **2.159**. On the other hand, hydride transfer followed by protonation would afford alcohol **2.154**. The major product of the reaction was **2.154**, indicating that hydride transfer is the predominant mode of reactivity of **2.150** with ketones. However, small amounts of **2.159** were detected at the end of the reaction indicating that pentavalent silicate **2.150** was indeed capable of donating an electron to ketone **2.151**.
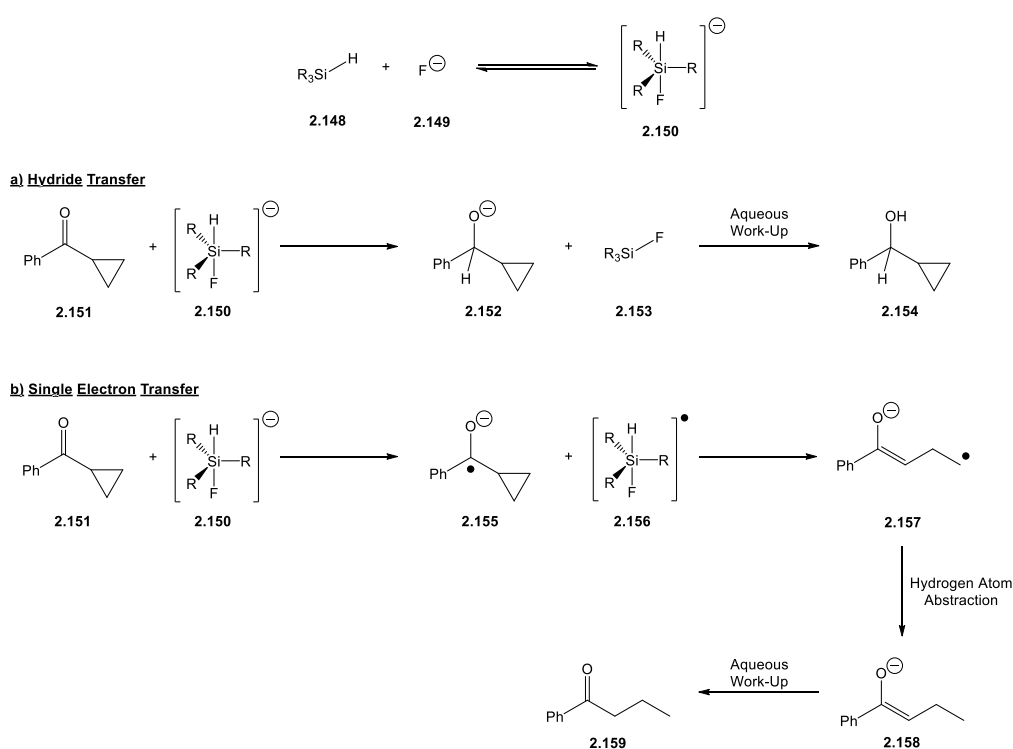
Scheme 2.31: Formation of pentavalent silicate (**2.150**) by nucleophilic addition of fluoride anion to trialkylsilane. Reduction of ketone **2.151**, by **a)** hydride transfer pathway or **b)** single electron transfer pathway as proposed by Yang and Tanner.[50]

Similarly, activation of trialkoxysilanes by alkali metal alkoxides has been previously demonstrated by Corriu *et al.*[51-55] For example, they were able to react triethoxy-, tri*iso*-propoxy- or triphenoxysilane with the corresponding alkali metal alkoxide to yield pentavalent hydridosilicates (Scheme 2.32).[54]
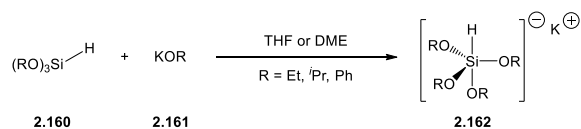
Scheme 2.32: Formation of hydridosilicates reported by Corriu *et al.*[54]

These pentavalent hydridosilicates were then utilised to reduce aldehydes and ketones, as well as alkyl or benzyl halides (Scheme 2.33).

R^1	R^2	OH $R^1\!-\!R^2$ H
Ph	H	90 %
$CH_3(CH_2)_3$	H	80 %
Ph	Ph	73 %
Ph	CH_3	44 %

R	X	$R\!-\!H$	$R\!-\!R$
$C_{12}H_{25}$	Cl	33 %	-
$C_{12}H_{25}$	Br	47 %	-
$PhCH_2$	Br	20 %	30 %
Ph_2CH	Cl	12 %	40 %
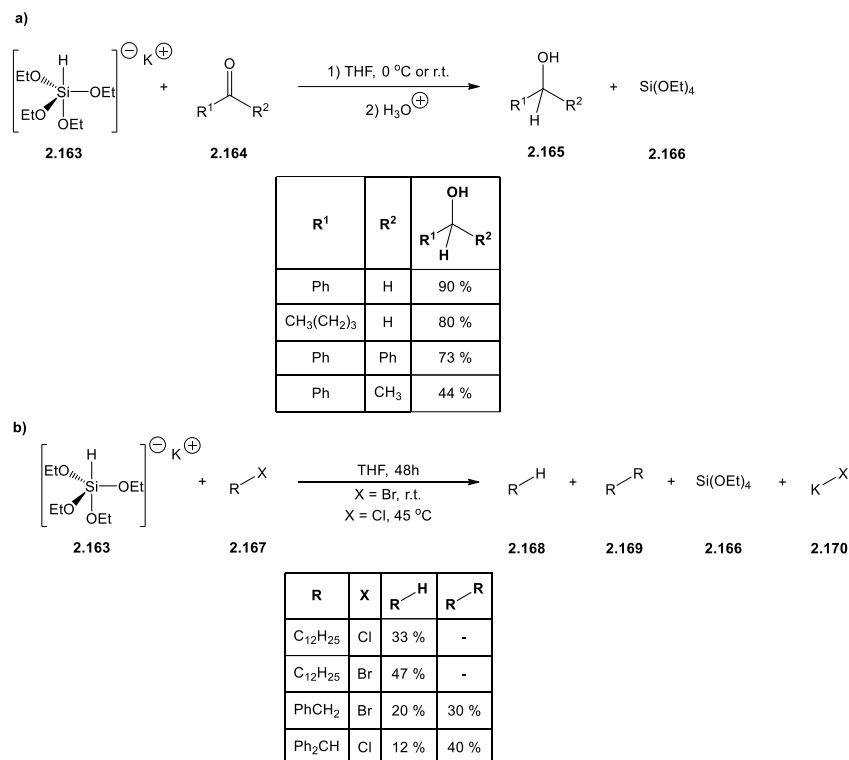
Scheme 2.33: a) Reduction of aldehydes and ketones by **2.163**, **b)** Reduction of organic halides by **2.163**.[51]

Reduction of carbonyl substrates was reported to occur *via* a hydride transfer mechanism (Scheme 2.34), with the reduction of benzophenone yielding only benzhydrol; no blue coloured benzophenone ketyl radical anion was observed during the reaction and no benzopinacol was isolated at the end of the reaction.
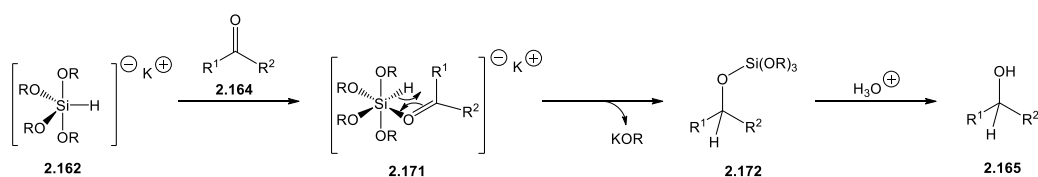
Scheme 2.34: Proposed hydride transfer mechanism for reduction of aldehydes and ketones by Corriu *et al.*[51]

Reduction of alkyl halides led to the formation of the corresponding alkanes as expected, however, reduction of benzyl bromide or chlorodiphenylmethane yielded the reduced dimers as the major products (Scheme 2.33b). The formation of the reduced dimer hints at the reaction for these halides proceeding *via* a SET mechanism to form benzyl or diphenylmethyl radicals which then dimerise.

More recently, in 2013, Grubbs *et al*. published a reductive system comprised of the reagents KO^{t}Bu and Et$_3$SiH, capable of reducing dibenzofuran.[56] In their initial screening reactions, Grubbs *et al.* found that 3 equivalents of both KO^{t}Bu and Et$_3$SiH in mesitylene at 165 °C afforded the highest yield of the desired cleavage product **2.174**. Meanwhile, a range of other cleavage and/or silylation products were found in small amounts or were not detected. (Varying amounts of the below products were formed under differing reaction conditions, see the original publication[56] for details).
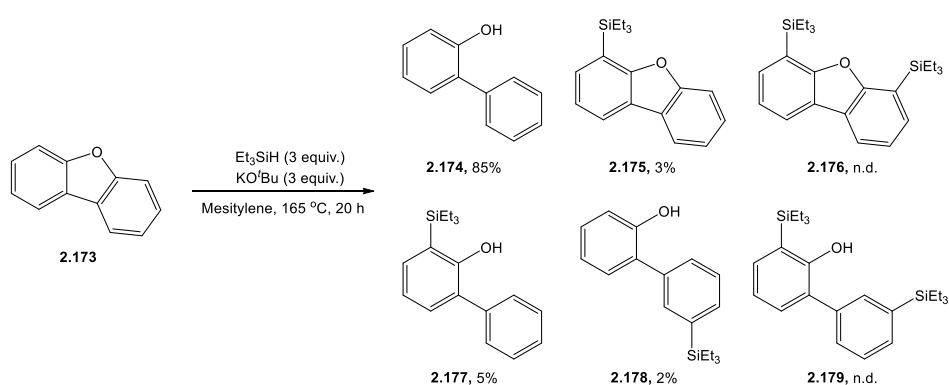
Scheme 2.35: Optimised conditions for reductive cleavage and/or silylation of dibenzofuran observed by Grubbs *et al.* upon reaction with KO^{t}Bu and Et$_3$SiH.

These conditions were then further extended to the reductive cleavage of a range of other diaryl ethers and alkyl aryl ethers, such as those shown in Scheme 2.36. In this initial publication, only some formative mechanistic information was reported, and this ruled out the reaction occurring *via* a benzyne intermediate. At this stage Grubbs *et al.* suggested that the key reactive intermediate was likely to be a hydridosilicate such as those formed by Corriu *et al*.[51]
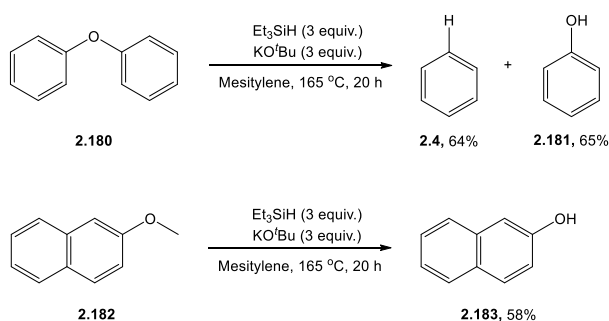
Scheme 2.36: Reductive cleavage of diphenyl ether **2.180** and methyl 2-naphthyl ether **2.182** by the KO*t*Bu/Et$_3$SiH system.

Following their initial report on dibenzofuran reduction and silylation, Grubbs, Stoltz and co-workers[57] found that catalytic amounts of KO*t*Bu plus a silane (3 equiv.) was also capable of C2-silylation of N-substituted indoles, with greater than 20:1 regioselectivity over C3-silylation. Indoles bearing electron withdrawing substituents were found to be unreactive, while electron rich substituents provided good to excellent yields. These conditions were also applicable to the *ortho*-silylation of N-, S- and O-containing heteroarenes. As well as triethylsilane, several other silanes including phenyldimethylsilane were also effective for the silylation of indoles. Notably, the conditions for these silylation reactions were somewhat less harsh than those employed for the reductive cleavage of dibenzofuran mentioned earlier: 25 – 65 °C *vs.* 165 °C.

R^1 = Me, Et, Ph, Bn, Methoxylmethyl, 2-[(trimethylsilyl)ethoxy]methyl
R^2 = Me, OMe, OBn, CH$_2$OMe, Ph
|Si| = SiEt$_3$, SiHEt$_2$, SiPhMe$_2$, Si^{n}Bu$_3$

Yield: 45 - 83 %
With C2:C3, >20:1
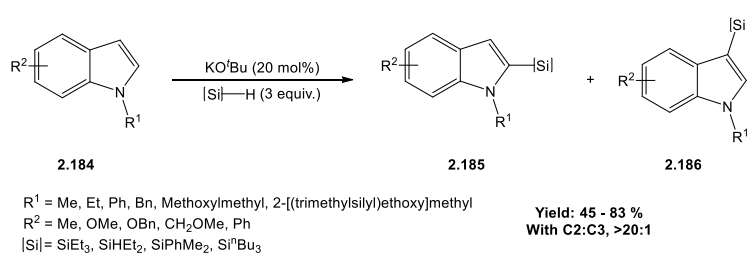
Scheme 2.37: Silylation of indoles bearing various N-substituents and ring substituents.[57]

The combination of KO*t*Bu and Et$_3$SiH was also found to be able to silylate the sp^3 carbons of toluene (**2.187**, 24%), 2,6-lutidine (**2.188**, mono-silylation: 53%) and benzyl ether **2.189** (46%).

2.187, 24%   **2.188**, 53%   **2.189**, 46%
sp^3:sp^2 = 18:1   mono:bis = >20:1
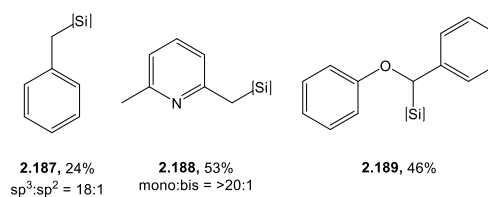
Scheme 2.38: Examples of C-sp^3 silylation carried out by Grubbs, Stoltz and co-workers.[57]

In 2017, Grubbs, Stoltz and co-workers published two papers dedicated to investigating the mechanism of indole silylation by the KO^{t}Bu plus Et$_3$SiH system.[58-59] Both papers presented extensive experimental and computational studies investigating whether the reaction could occur *via* an ionic, neutral or radical mechanism.

In the first of their papers, Grubbs, Stoltz and co-workers investigated the involvement of radical intermediates in the C2-silylation of N-methylindole by KO^{t}Bu plus Et$_3$SiH. It was proposed that formation of a pentavalent silicate species (**2.190**) by addition of KO^{t}Bu to Et$_3$SiH would ultimately furnish triethylsilyl radicals by homolysis of the Si–H bond. The DFT calculated Gibbs free energy (ΔG) for this reaction however was high, 70.2 kcal/mol for homolysis, suggesting that homolysis under thermal conditions would not be possible.[59] Nevertheless, Grubbs, Stoltz and co-workers observed experimental evidence for the formation of radical intermediates through radical clock experiments and trapping experiments with TEMPO.

An alternative formation of triethysilyl radicals due to the presence of trace quantities of oxygen in the reaction vessel was then investigated using DFT methods by Grubbs *et al*. Upon reaction of molecular oxygen with KO^{t}Bu tetramer, *tert*-butoxyl radical and potassium peroxide radical **2.191** would be formed, this reaction was found to be endergonic by 23.4 kcal/mol, while the same reaction with NaO^{t}Bu requires 30.7 kcal/mol (**2.195**). Grubbs *et al*. rationalised the lack of reactivity for NaO^{t}Bu to this highly endergonic reaction and were also able to show that the smaller size of the sodium cation would lead to a larger distortion from the tetramer to **2.195**, in comparison to KO^{t}Bu. The *tert*-butoxyl radical could then react with trimethylsilane to generate the silyl radical via transition state **TS 2.192**, which was found to be 36.0 kcal/mol higher in energy than the reactants. The total process of silyl radical generation was found to be endergonic by 8.6 kcal/mol, consistent with formation of trace amounts of silyl radicals required to initiate the subsequently proposed radical chain mechanism.
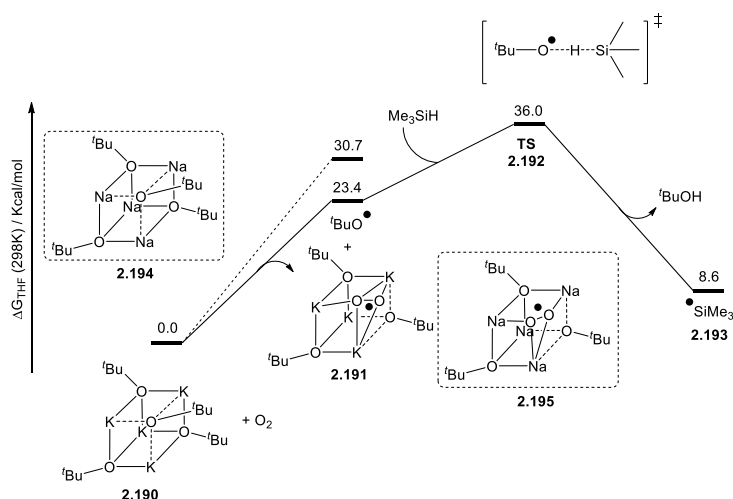
Scheme 2.39: Free energy profile calculated by Grubbs *et al*. for the generation of silyl radical involving traces of oxygen. (Trimethylsilane was utilised in place of triethylsilane for calculations).

Silyl radicals could silylate the C2 position of N-methylindole in conjunction with either pentavalent silicate **2.196** (Scheme 2.40a) or a tetramer of KO*t*Bu (Scheme 2.40b). Using DFT calculations (trimethylsilyl radical in place of triethylsilyl radicals) Grubbs, Stoltz and co-workers determined that addition to the C2 position occurred with a free energy barrier of 13.4 kcal/mol and was exergonic by 4.1 kcal/mol. Similarly, addition at C3 exhibited a barrier of 15.6 kcal/mol whilst being exergonic by 0.8 kcal/mol. This demonstrated that addition at both C2 and C3 is facile and reversible.
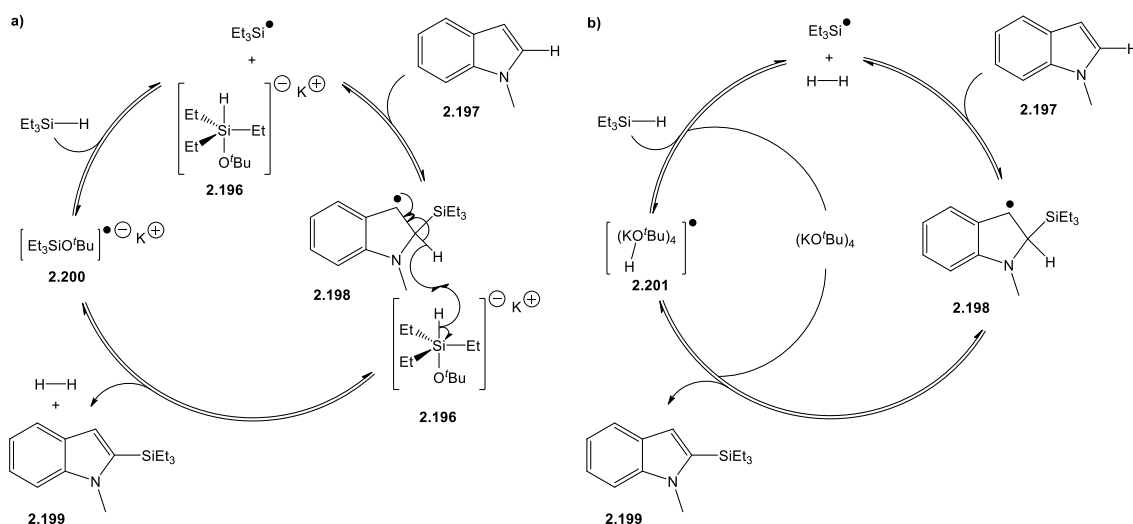
Scheme 2.40: Radical mechanisms for the C2-silylation of N-methylindole proposed by Grubbs, Stoltz and co-workers,[59] **a)** mediated by pentacoordinate silicate anion **2.190**, **b)** mediated by KO*t*Bu tetramer.

Loss of the *ipso* hydrogen atom was postulated to occur by abstraction with **2.196** or by a KO*t*Bu tetramer. Abstraction by **2.196** and loss of hydrogen gas was found to be possible at the C2 position with a barrier of 21.0 kcal/mol while at C3 the barrier was higher at 24.4 kcal/mol, both reactions were endergonic (C2 = 7.1 kcal/mol, C3 = 1.5 kcal/mol). It can therefore be seen that C2 silylation is favoured over C3 since the abstraction at C2 occurs *via* the lower energy transition state in an irreversible reaction (elimination of hydrogen gas). In the alternative mechanism, where the KO*t*Bu tetramer acts to abstract the hydrogen atom, C2 abstraction occurs with a barrier of 19.1 kcal/mol whilst C3 abstraction occurs with a barrier of 20.8 kcal/mol. Both steps were again found to be endergonic (C2 = 11.6 kcal/mol, C3 = 6.0 kcal/mol), and the subsequent step to form H_2 by reaction of **2.201** with trimethylsilane was exergonic by 4.5 kcal/mol. These computational results suggest that hydrogen atom abstraction by the KO*t*Bu tetramer was the likely mechanism for this reaction owing to the lower barrier for the rate determining hydrogen abstraction. The DFT data indicated that the C3 product would be the thermodynamic product and this was indeed observed when the reaction was heated to higher temperatures or for longer reaction times. The formation of the thermodynamic (C3) product would be possible as the reaction overall would be reversible due to the generated H_2 still being present within the reaction vessel.

The subsequent publication by Grubbs, Stoltz and co-workers[58] focused on whether the reaction could be proceeding *via* an ionic or neutral mechanism, involving either **2.196** or KO*t*Bu tetramer, respectively. Again, DFT calculations were employed to probe both mechanistic possibilities, with the results for the ionic mechanism displayed in Scheme 2.41 and for the neutral mechanism in Scheme 2.42.
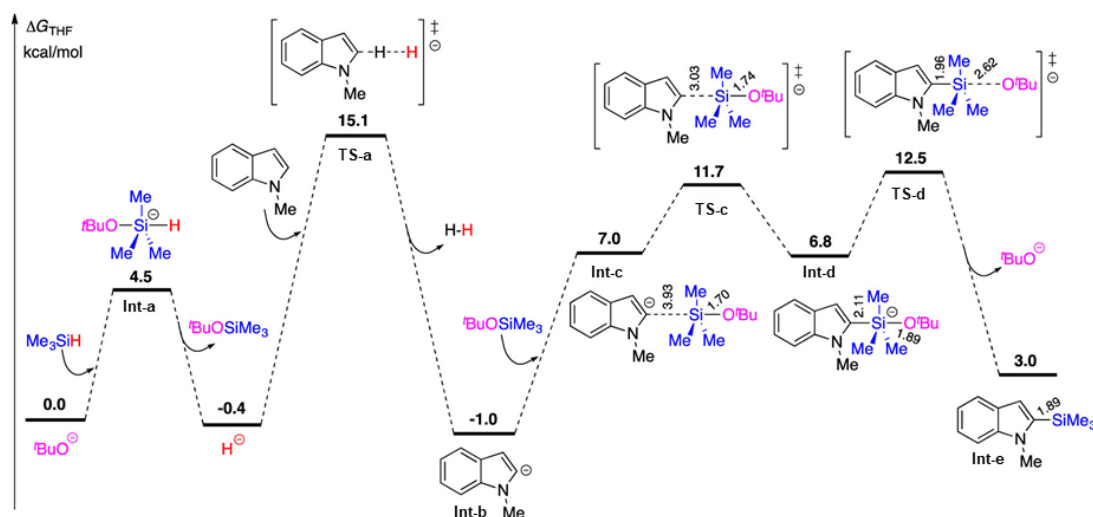
Scheme 2.41: Gibbs Free Energy plot for the KO*t*Bu catalysed silylation of 1-methylindole *via* an ionic mechanism. Reprinted (adapted) with permission from (Shibdas Banerjee; Yun-Fang Yang; Ian D. Jenkins; Yong Liang; Anton A. Toutov; Wen-Bo Liu; David P. Schuman; Robert H. Grubbs; Brian M. Stoltz; Elizabeth H. Krenske; Kendall N. Houk; Richard N. Zare; *J. Am. Chem. Soc.* **2017**, 139, 6880-6887). Copyright (2018) American Chemical Society.

Whilst the rate-determining deprotonation of N-methylindole at the C2 position has a lower barrier for the ionic mechanism, this mechanism does not take into account the unfavourable dissociation of KO*t*Bu tetramer into monomer components. Perhaps more importantly, Grubbs, Stoltz and co-workers found that for the neutral mechanism, when substituting KO*t*Bu tetramer for NaO*t*Bu tetramer the barrier to C2 deprotonation was around 10 kcal/mol higher.[58] When extending their DFT studies to other heteroarene substrates, Grubbs, Stoltz and co-workers also found that the barrier for the deprotonation step of the neutral mechanism was able to account for the observed experimental trends. Across both studies, Grubbs, Stoltz and co-workers concluded that the radical, neutral or ionic mechanisms could be operative and were able to provide both experimental and computational evidence to this end.
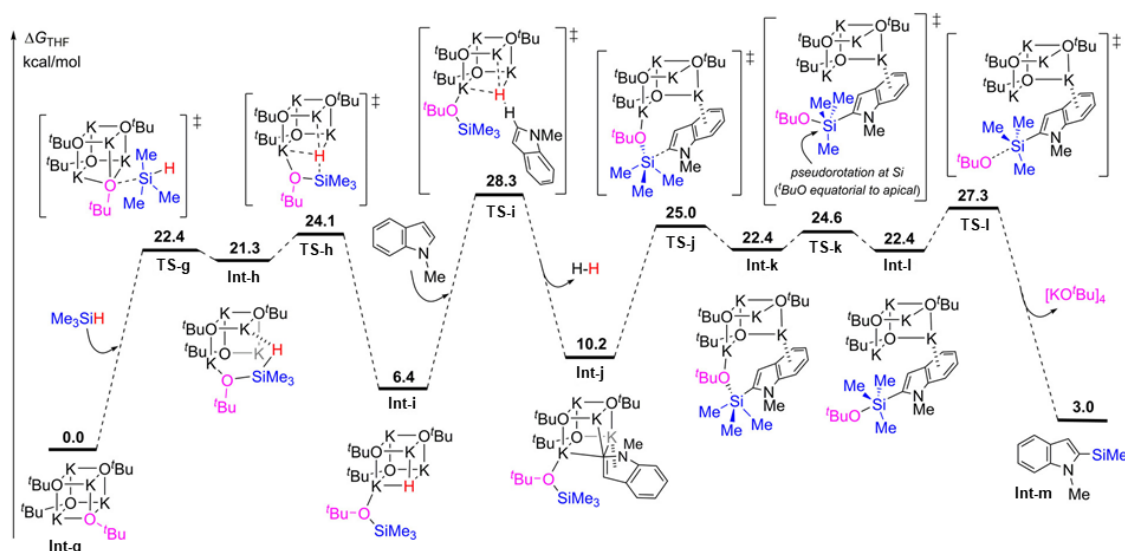
Scheme 2.42: Gibbs Free Energy plot for the KO*t*Bu catalysed silylation of 1-methylindole *via* a neutral mechanism. Reprinted (adapted) with permission from (Shibdas Banerjee; Yun-Fang Yang; Ian D. Jenkins; Yong Liang; Anton A. Toutov; Wen-Bo Liu; David P. Schuman; Robert H. Grubbs; Brian M. Stoltz; Elizabeth H. Krenske; Kendall N. Houk; Richard N. Zare; *J. Am. Chem. Soc.* **2017**, 139, 6880-6887). Copyright (2018) American Chemical Society.

A further practical application of the KO*t*Bu plus Et$_3$SiH reducing system was published in 2017 by Grubbs *et al.*[60] for the hydrodesulfurisation of fuels. They were able to demonstrate on a model substrate, dibenzothiophene, that KO*t*Bu plus Et$_3$SiH at high temperature (165 °C) could yield 82% of the desulfurised product, biphenyl. They also extended this to non-heterocyclic, sulfur containing substrates such as naphthalene thiol and 4,4'-thiodibenzenethiol affording desulfurized products in excellent yields. Notably, in the desulfurisation of naphthalene thiol a small quantity (<5%) of the reduction product 1,2,3,4-tetrahydronaphthalene (**2.205**) was also formed. In the desulfurisation reaction of 4,4'-thiodibenzenethiol, the major product was biphenyl which similarly indicated a reductive process was at work.
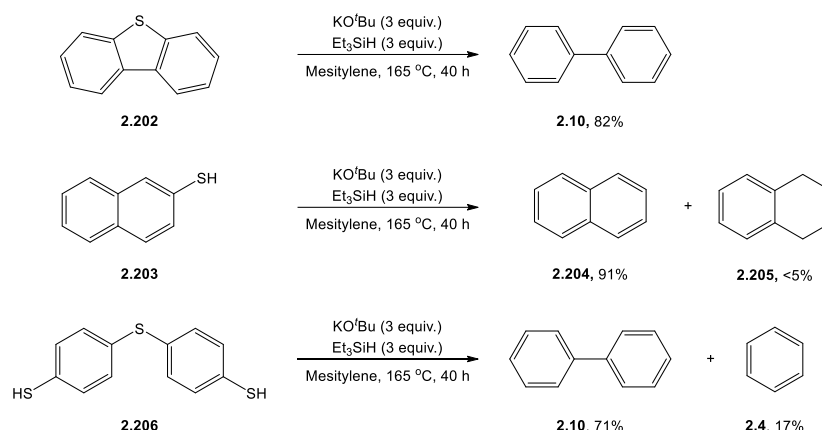
Scheme 2.43: Desulfurisation of heterocyclic and non-heterocyclic substrates by Grubbs *et al.*[60] using KO*t*Bu plus Et₃SiH.

The mechanism of desulfurisation of 4,6-dimethyldibenzothiophene was studied using DFT calculations alongside 4,6-dimethyldibenzofuran, with dibenzofuran having been previously studied experimentally by Grubbs *et al.*[56] and failed to undergo deoxygenation. Direct addition of trimethylsilyl radical to sulfur causing C–S cleavage was shown to be accessible, Scheme 2.44. In order to afford the second C–S cleavage, a similar mechanism is followed – trimethylsilyl radical addition and accompanying C–S bond cleavage exhibits a barrier of 15.4 kcal/mol and is exergonic by 8.7 kcal/mol.[60]
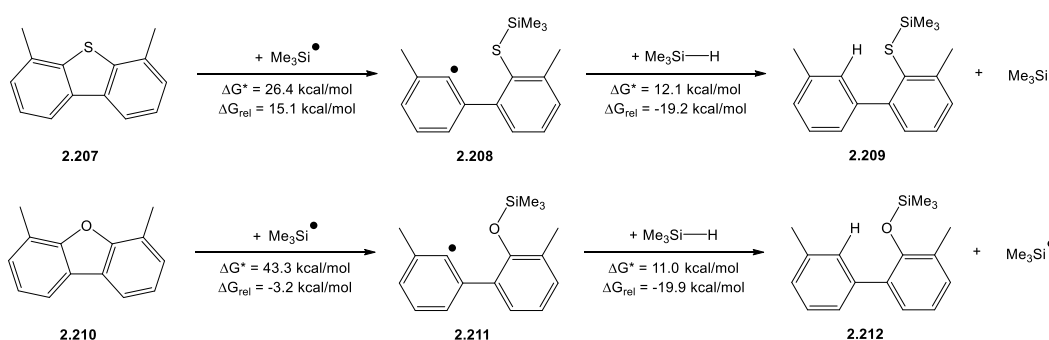
Scheme 2.44: DFT results of Grubbs *et al.*[60] for the first C-S/O cleavage by direct silyl radical addition to the heteroatom.

For 4,6-dimethyldibenzofuran however, the direct addition of trimethylsilyl radical to oxygen causing C-O bond cleavage has a larger free energy barrier and was therefore determined to occur *via* a lower energy pathway, Scheme 2.45. The key distinction between the reactivities 4,6-dimethyldibenzothiophene and 4,6-dimethyldibenzofuran was manifested in the second trimethylsilyl radical addition C–O cleavage step, with the barrier for addition/cleavage in **2.212** being 37.5 kcal/mol, in comparison to 15.4 kcal/mol for **2.209**. This was further backed up by the experimental observation that

deoxygenation of dibenzofuran could indeed be observed in small quantities at a higher temperature of 200 °C.

The work of Grubbs *et al*. further demonstrates the versatility of KO^{t}Bu to react with small molecules to form reactive intermediates which can afford remarkable transformations.
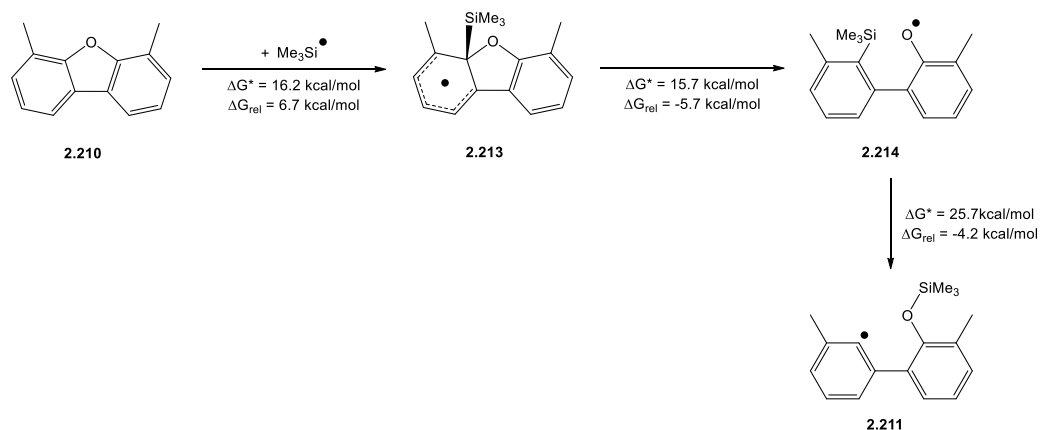
Scheme 2.45: DFT results of Grubbs *et al.*[60] for an alternative C-O cleavage by initial *ipso* trimethylsilyl addition.

Throughout the literature review, examples of numerous types of reactivity have been presented, including single electron transfer, reductive bond cleavage and aromatic silylation. Common to all of the literature discussed has been that aspects of mechanism have been up for debate between different research groups and often also by the proposers themselves. In most cases, a consensus view or well-evidenced proposal has been reached in terms of mechanism (i.e. the BHAS mechanism and the mechanisms of initiation for BHAS reactions). In order to achieve these well evidenced mechanistic proposals, research groups have had to utilise not only experimental techniques but also computational methods, with the latter providing invaluable insights into mechanistic details which would simply be unrealistic to obtain by experimental means. A case in point would be the work of Murphy, Tuttle and co-workers in understanding the reactions which take place between KO^{t}Bu and small organic molecules such as alcohols (Section 2.2.1.1), diamines (Section 2.2.1.2) and nitrogen heterocycles (Section 2.2.1.3). DFT calculations proved invaluable in this work by providing a means to corroborate experimental observations, for example, where phenanthroline dimers were isolated following reaction of KO^{t}Bu with 1,10-phenanthroline. This alone does not provide enough support for phenanthroline dimers being involved as electron donors. However, using DFT calculations to calculate the free energy profile for forming the dimers and for electron transfer to the haloarene substrate Murphy, Tuttle and co-workers were able to

more convincingly conclude that the dimers were indeed responsible for initiation. DFT calculations were also utilised to rule out alternatives to the mechanism settled on by Murphy, Tuttle and co-workers, namely that a complex between KO^tBu and phenanthroline was not able to act as a single electron reductant towards haloarenes.

In a similar manner Grubbs, Stoltz and co-workers utilised DFT calculations to complement their wide-ranging experimental studies, when investigating reactions of the KO^tBu/Et_3SiH reducing system. They were able to rationalise the observed difference in reactivity of dibenzothiophene (desulfurisation) and dibenzofuran (single C-O bond cleavage) when treated with KO^tBu and Et_3SiH, through calculation of the free energy profile of the reaction. This allowed them to determine that an alternative lower energy pathway was accessible for dibenzofuran by first addition of the silyl radical to the *ipso* position rather than direct addition to the heteroatom.

Computational methods have been used throughout the research presented herein to do exactly this: provide insights not readily accessible by experimental means and to complement and further inform experimental studies. The method of choice throughout has been density functional theory (or a variant of) and the next section provides a theoretical background for the methods applied.

3. Quantum Chemistry

Quantum chemistry has been defined as "the study of chemistry through the use of approximate solutions to the electronic Schrödinger equation."[61] The choice of quantum chemistry technique utilised throughout this work is Density Functional Theory (DFT), and the theoretical underpinnings of this technique will be discussed in this chapter. First, the wavefunction, Hamiltonian Operator and the Schrödinger Equation are introduced, followed by representation of the wavefunction within Hartree-Fock (H-F) theory. From here utilising the electron density to retrieve the physical properties of a system is discussed in terms of the ground-breaking work of Hohenberg and Kohn, as well as that of Kohn and Sham. Use of time-dependent (TD) DFT to find an approximate solution to the time-dependent Schrödinger equation will also be discussed. Finally, a discussion of DFT methods (functionals), basis sets, solvation and methodologies for studying electron transfer will close the chapter.

This chapter is not intended to serve as a full description of quantum chemistry, merely an introduction to the techniques utilised within this work. For more detailed explanations of quantum chemistry and DFT see works by Harvey,[61] Cramer[62] or Koch and Holthausen.[63]

3.1 Quantum Mechanics

3.1.1 The Wavefunction

When studying a system in quantum theory, the positions of the n particles in the system can be represented by $3n$ coordinates (q_1, q_2, ..., q_{3n}). This allows the system to be described by a wavefunction which is related to the coordinates and time (t): $\Psi(q_1, q_2, ..., q_{3n}, t)$. The square of the wavefunction is a measure of the probability of finding the n particles of the system in a given volume of space, V.

$$\int \Psi^2 \, dV$$

<div align="right">**Equation 3.1**</div>

Since the particle must exist somewhere in the region of space, the normalisation condition is introduced whereby the total probability is 1:

$$\int_0^\infty \Psi^2 \, dV = 1$$

<div align="right">**Equation 3.2**</div>

This is the first of five conditions placed upon the wavefunction for it to be physically acceptable, the remaining four state that it should be: single-valued, finite over an infinite range, continuous everywhere and have a continuous first derivative. As a result, only certain wavefunctions are allowed.

To extract information from a wavefunction it must be operated on, that is, to obtain an observable (o), a measurable physical property, an operator ($\hat{O}$) is required. To find the exact value of an observable, an eigenvalue equation is formed. Therefore, if we wish to extract the energy E, the Hamiltonian operator $\hat{H}$ is applied, producing the famous Schrödinger equation:

$$\hat{H}\Psi = E\Psi$$

<div align="right">**Equation 3.3**</div>

The Hamiltonian operator contains terms relating to the kinetic and potential energy of all the particles in a given system, that is all electrons and nuclei in the absence of an external field. The Hamiltonian operator has the following form:

$$\hat{H} = -\frac{1}{2}\sum_{i=1}^{N}\nabla_i^2 - \frac{1}{2}\sum_{A=1}^{M}\frac{1}{m_A}\nabla_A^2 - \sum_{i=1}^{N}\sum_{A=1}^{M}\frac{Z_A}{r_{iA}} + \sum_{i=1}^{N}\sum_{j>i}^{N}\frac{1}{r_{ij}} + \sum_{A=1}^{M}\sum_{B>A}^{M}\frac{Z_A Z_B}{R_{AB}}$$
Equation 3.4

Where i and j represent the N electrons and A and B refer to the M nuclei in the system, m_A is the mass of nucleus A in multiples of the mass of an electron, Z_A is the charge on nucleus A, r_{iA} is the distance between electron i and nucleus A and R_{AB} is the distance between nuclei A and B. The first two terms determine the kinetic energy of the electrons and nuclei respectively, where ∇^2 is the Laplacian operator (sum of the differential operators in Cartesian coordinates):

$$\nabla^2 = \frac{\delta^2}{\delta x^2} + \frac{\delta^2}{\delta y^2} + \frac{\delta^2}{\delta z^2}$$
Equation 3.5

The remaining three terms represent the potential energy of the system arising from: electron - nucleus attraction, electron - electron repulsion and nucleus - nucleus repulsion, respectively.

The Hamiltonian operator can be simplified to the electronic Hamiltonian ($\hat{H}_{elec}$) by applying the Born-Oppenheimer Approximation, which states that the nuclei are fixed relative to the electrons. This is a result of the masses of nuclei being much larger than that of an electron, for example, a ^{1}H nucleus is 1800 times heavier than the mass of an electron, therefore nuclei will move much slower than electrons. No kinetic energy terms for nuclei are therefore required and the nucleus - nucleus repulsion term becomes constant. The electronic Hamiltonian thus has the following form:

$$\hat{H}_{elec} = -\frac{1}{2}\sum_{i=1}^{N}\nabla_i^2 - \sum_{i=1}^{N}\sum_{A=1}^{M}\frac{Z_A}{r_{iA}} + \sum_{i=1}^{N}\sum_{j>i}^{N}\frac{1}{r_{ij}}$$
Equation 3.6

Which is often written as:

$$\hat{H}_{elec} = \hat{T} + \hat{V}_{Ne} + \hat{V}_{ee}$$
Equation 3.7

Applying the electronic Hamiltonian to the Schrödinger equation leads to the solution containing the electronic wavefunction (Ψ_{elec}) and electronic energy (E_{elec}).

$$\widehat{H}_{elec}\Psi_{elec} = E_{elec}\Psi_{elec}$$

Equation 3.8

By solving the electronic Schrödinger equation (Equation 3.8) for a given set of nuclear coordinates, R_M, a wavefunction $\Psi(r)$ describing the different electron arrangements, and the associated energy (E) are obtained. Even for simple systems this becomes complex, since after assuming the positions of the nuclei we must find the function $\Psi(r)$ that depends on the coordinates of all the electrons, such that when operated on by the electronic Hamiltonian, the function multiplied by a constant is obtained. This constant is the energy of the system. Multiple solutions to Equation 3.8 are produced, each with a different wavefunction and energy, however the wavefunction we desire has the lowest associated energy and is therefore termed the ground state.

The following section will discuss one method to approximate the ground state wavefunction and energy, the Hartree-Fock theory.

3.1.2 Hartree-Fock Theory

Fundamental to Hartree-Fock (H-F) Theory is the assumption that electrons move independently of each other within a molecular system. This is a good approximation even though it discounts the strong repulsive Coulombic interactions that electrons experience, this is due in part to the very fast motion of electrons in molecular systems. This approximation allows the overall *N* electron wavefunction to be written as a product of *N*-one electron wavefunctions, ψ, termed molecular orbitals.

$$\Psi(r_1, r_2, r_3, \dots, r_n) \cong \psi_1(r_1) \times \psi_2(r_2) \times \psi_3(r_3) \times \dots \times \psi_n(r_n)$$

Equation 3.9

At first this may seem to increase the number of wavefunctions to be determined, however, determining the shape of many individual molecular orbitals is far easier than determining the shape of the overall wavefunction. These individual molecular orbitals are chosen to be orthogonal such that the integral over all space, of the product of two different molecular orbitals is zero.

To correctly utilise this approximation, the fact that electrons have quantised spin must also be considered. This is applied by replacing the molecular orbitals *ψ(r)* by spin orbitals *χ(r;ω)*, which can be written as the product of a spatial (*ψ(r)*) and spin component (*α(ω)* or *β(ω)*). The spatial and spin functions of an electron (r_i, ω_i) are often represented by x_i.

Since electrons are indistinguishable, it is not possible to assign individual electrons specific one electron wavefunctions, which rules out the use of the previously mentioned, simple product of *N*-one electron wavefunctions to approximate the overall wavefunction. However, by taking the antisymmetric product of *N*-one electron wavefunctions, it is possible to approximate the *N*-electron wavefunction. This antisymmetric combination of products can be written as the determinant of a matrix, with *N* columns and rows. In Hartree-Fock theory these determinants are known as Slater Determinants:

$$\Psi(x_1, x_2, \dots, x_N) = \Phi_{SD} = \frac{1}{\sqrt{N!}} \begin{vmatrix} \chi_1(x_1) & \chi_2(x_1) & \cdots & \chi_N(x_1) \\ \chi_1(x_2) & \chi_2(x_2) & & \chi_N(x_2) \\ \vdots & \vdots & & \vdots \\ \chi_1(x_N) & \chi_2(x_N) & \cdots & \chi_N(x_N) \end{vmatrix}$$

Equation 3.10

Applying the Hartree-Fock approximation allows the electronic Schrödinger equation to be 'solved,' yielding an approximate energy (the Hartree-Fock wavefunction does not equal the true *N*-electron wavefunction therefore it cannot yield the exact energy).

The approximate energy must be greater than or equal to the true ground state energy – this is known as the Variational Principle (this does not apply to all methods i.e. Møller-Plesset, MPn, methods). By applying the Variational Principle to the Slater Determinant, it is possible to access the Hartree-Fock wavefunction with a set of orthogonal orbitals which produces the lowest possible energy. The Hartree-Fock energy is obtained by inserting the Slater Determinant into the electronic Schrödinger equation (re-written to equal the energy), which yields:

$$E_{HF} = \sum_{i=1}^{N} h_{ii} + \sum_{i=1}^{N} \sum_{j=i+1}^{N} (J_{ij} - K_{ij})$$

Equation 3.11

Where the h_{ii} integrals are one electron terms, containing kinetic energy and potential energy from electron-nucleus attraction. The J_{ii} integrals contain the potential energy as a result of Coulombic repulsion between two electrons, and the K_{ij} integrals are two electron terms which correct the Coulombic repulsion required due to exchange of electrons.

To solve for the lowest Hartree-Fock energy, the spin orbitals must be varied whilst remaining orthonormal. This is achieved by utilising Fock equations:

$$\hat{f}_i \chi_i = \varepsilon_i \chi_i$$

Equation 3.12

Where $\hat{f}_i$ is the one electron Fock operator (a modified Hamiltonian operator), ε_i is an energy and χ_i is a molecular orbital. The orbitals obtained by solving the Fock equations yield the Hartree-Fock many electron wavefunction, since the Fock operator contains a term accounting for electron-electron repulsion, V_{HF}:

$$\hat{f}_i = -\frac{1}{2}\nabla_i^2 - \sum_{A}^{M} \frac{Z_A}{r_{iA}} + V_{HF}(i)$$

Equation 3.13

The first term accounts for the kinetic energy and the second term the potential energy arising from nucleus-electron attraction. To solve Equation 3.13, the molecular orbitals are represented as combinations of simpler functions, termed basis functions $\phi(r)$:

$$\chi_i(r) = \sum_{j=1}^{n_{basis}} c_{ij}\phi_j(r) \qquad \textbf{Equation 3.14}$$

Basis functions (n_{basis}) are chosen to resemble the occupied atomic orbitals of each atom in the molecular system, and the set chosen is termed the basis set. Now the functions are fixed, and the coefficients (c_{ij}), which determine the contribution of each basis function to the molecular orbital, need solved. In order to solve for the coefficients and obtain the energies, an initial set of guess coefficients are applied to yield a set of orbitals. These orbitals are then used to calculate a new Fock operator, and the new Fock equations are solved to yield a new set of coefficients. This process is repeated until the orbitals used to construct the Fock operator become consistent with those obtained by solving it, this method is therefore commonly known as the self-consistent field (SCF) method.

Spin orbitals utilised for Hartree-Fock theory are a product of a spatial and spin function, as previously described. When a molecule has an equal number of spin-up and spin-down (α and β) electrons, which are paired in the spatial orbitals according to the Pauli principle (therefore an α paired with a β), it is termed a closed-shell system. When molecules are known to adopt this electronic structure, it can be used to simplify the process of solving the Fock equations since coefficients only need to be calculated for the different spatial orbitals. This type of calculation is referred to as a restricted Hartree-Fock calculation. On the other hand, when a molecule has an odd number of electrons or has unpaired electrons, there are two possible approaches in Hartree-Fock theory. First, it could be assumed that all electrons except one are paired, this would lead to a set of doubly occupied spatial orbitals with one α and one β electron, then a final spatial orbital containing the unpaired electron. This approach is termed a restricted open-shell Hartree-Fock calculation.

The second method assigns spin orbitals to each of the electrons, with an odd number being spin-up (α) and an even number being spin-down (β). For example, in a system with 9 electrons, there would be five α spin orbitals and four β spin orbitals each with an associated spatial orbital. The spin orbitals must be orthogonal to each other; however,

no such restriction is imposed on the spatial component of the α and β orbitals. This approach is termed an unrestricted Hartree-Fock calculation.

3.1.3 Electron Correlation

Hartree-Fock theory provides an approximate solution to the electronic Schrödinger equation by approximating the wavefunction through use of the Slater determinant. However, the variational principle states the H-F energy (E_{HF}) is always greater than the true ground state energy (E_0); the difference between these two values is called the correlation energy, E_C. The correlation energy arises from the fact that the positions of electrons are correlated, *i.e.*, the probability of an electron being in a particular place is dependent upon the location of other electrons. In H-F theory, electron-electron repulsion is dealt with in an average manner through the V_{HF} potential, this leads to electrons coming too close to each other at times, causing E_{HF} to be greater than E_0, as such E_C is always negative.

Wavefunction methods which account for electron correlation exist, however these will not be discussed here. Instead we will now focus on the theory behind the methods utilised within this work, Density Functional Theory (DFT).

3.2 Density Functional Theory

Whilst the previously discussed Hartree-Fock method sought to solve the Schrödinger equation by constructing an approximate many-electron wavefunction, DFT instead utilises the electron density, $\rho(r)$. The electron density is derived from the physical interpretation of the wavefunction (*i.e.*, $\int \Psi^2\, dr$):

$$\rho(r) = N \int \dots \int |\Psi(x_1, x_2, \dots, x_N)|^2 dx_1, dx_2, \dots, dx_N \qquad \textbf{Equation 3.15}$$

This is the probability of finding any of the electrons within a defined volume $d(r)$, since it is the probability of finding any one electron in the system multiplied by N. The electron density is an experimental observable which can be measured by X-ray diffraction.

The Hohenberg-Kohn (H-K) theorems demonstrated that the ground state electronic energy E_0 of a system could be calculated as a functional of its electron density, $E[\rho(r)]$. An expression for the ground state electronic energy could therefore be written:

$$E_0[\rho_0] = T[\rho_0] + E_{ee}[\rho_0] + E_{Ne}[\rho_0] \qquad \textbf{Equation 3.16}$$

Where T is the kinetic energy of the electrons, E_{ee} is potential energy due to electron-electron repulsion and E_{Ne} is the potential energy due to electron-nuclei attraction. The second H-K theorem also showed that the variational principle applied to the electron density, such that an approximate density, ρ', would return a higher energy than the true ground state density would, $E[\rho'] > E[\rho]$.

A method to solve the functional (explicitly the kinetic energy and electron-electron repulsion potential energy) was not presented in the original paper by Hohenberg and Kohn,[64] and this remains elusive today.

Approximate functionals have instead been developed to approximate the kinetic energy term and the potential energy term due to electron-electron repulsion. Early examples utilised simply the electron density as an input, but these struggled to approximate the kinetic energy accurately.

Kohn and Sham replaced the electron density with a sum of densities from a set of N non-interacting molecular orbitals (the Kohn-Sham orbitals).[65]

$$\rho(r) = \sum_i^N \psi_i^2(r)$$

The Kohn-Sham orbitals can be determined in a manner similar to the Hartree-Fock spin orbitals, by solving a set of equations similar in form to the Fock equations. This is done iteratively, as in Hartree-Fock theory, until the orbitals converge.

This approach allows calculation of the kinetic energy of the non-interacting N electron system, T_S, which is an approximation for the corresponding interacting system. The overall energy can thus be expressed as:

$$E[\rho(r)] = \frac{1}{2}\iint \frac{\rho(r_1)\rho(r_2)}{r_{12}} dr_1 r_2 + T_s[\rho(r)] - \sum_J \left(\int \frac{\rho(r)Z_J}{r_J} dr \right)$$
$$+ V_{XC}[\rho(r)]$$

Where the first term represents the Coulombic energy due to repulsion between electrons, the second term is the kinetic energy of the N-electron non-interacting system and the third term is the Coulombic energy due to attraction between the electron density and the nuclei (Z_J is the nuclear charge on nucleus J). The final term is termed the exchange-correlation functional, and this contains all the unknown parts of the exact density functional including the difference in kinetic energy between the N-electron non-interacting system and its corresponding interacting system.

The exact exchange-correlation functional to date remains unknown, it must therefore be approximated and methods to this end will be discussed in the next section.

3.2.1 The Exchange-Correlation Functional

As described above, the exchange-correlation (XC) functional ($V_{XC}[\rho(r)]$) contains the unknown contributions to the electronic energy of a system and must therefore be approximated. The accuracy of a DFT method is therefore reliant upon the XC functional utilised.

3.2.1.1 Local Density Approximation

One of the most widespread approximations for the XC functional is the local density approximation (LDA). This method is based on a uniform electron gas, where electrons move on a uniform background of positive nuclei, in a neutral system. The electron density (ρ) is therefore calculated as the number of electrons (N) divided by the volume (V) and is therefore constant everywhere.

$$\rho = \frac{N}{V}$$

Equation 3.19

The LDA is an XC functional used for systems where all the electrons are delocalised.

$$E_{XC}^{LDA}[\rho] = \int \rho(r)\varepsilon_{XC}(\rho(r))dr$$

Equation 3.20

Where $\varepsilon_{XC}(\rho(r))$ is the exchange-correlation energy per particle in the uniform electron gas with density $(\rho(r))$. By weighting this with the probability of finding an electron at a position in space, the energy per particle becomes energy per electron. A variant of the LDA comes from utilising spin densities as the input in place of the electron density, where the spin densities are related to the electron density by:

$$\rho(r) = \rho_\alpha(r) + \rho_\beta(r)$$

Equation 3.21

This method can deal with systems which have an odd number of electrons or have unpaired electrons and is therefore an open-shell functional. The functional is termed the Local Spin-Density Approximation (LSDA):

$$E_{XC}^{LSDA}[\rho_\alpha, \rho_\beta] = \int \rho(r)\varepsilon_{XC}(\rho_\alpha(r), \rho_\beta(r))dr$$

Equation 3.22

The VWN and VWN5 functionals of Vosko, Wilk and Nusair[66] are of the LSDA type and have commonly been used in solid state chemistry. The performance of the VWN functional was recently compared to a range of other density functionals for transition metal surface properties, where it was found to perform best for the prediction of surface energies.[67]

3.2.1.2 Generalised Gradient Approximation

In order to improve the XC functional approximation over the LDA, the generalised gradient approximation (GGA) utilises the gradient of the density, $\nabla\rho(r)$, as it is a better model for systems which do not have a uniform electron density. The general form of a GGA functional is:

$$E_{XC}^{GGA}[\rho_\alpha,\rho_\beta] = \int f(\rho_\alpha,\rho_\beta,\nabla\rho_\alpha,\nabla\rho_\beta)dr \qquad \textbf{Equation 3.23}$$

The exchange and correlation contributions tend to be approximated individually:

$$E_{XC}^{GGA} = E_X^{GGA} + E_C^{GGA} \qquad \textbf{Equation 3.24}$$

The exchange energy can therefore be represented by the gradient-corrected LDA approximation:

$$E_X^{GGA} = E_X^{LDA} - \sum_\sigma \int F(s_\sigma)\,\rho_\sigma^{\frac{4}{3}}(r)\,dr \qquad \textbf{Equation 3.25}$$

Where F is the reduced density gradient of the spin, defined as:

$$s_\sigma(r) = \frac{|\nabla\rho_\sigma(r)|}{\rho_\sigma^{\frac{4}{3}}(r)} \qquad \textbf{Equation 3.26}$$

The inclusion of the spin term ensures the system remains inhomogeneous by having large values for large gradients, but also for areas with small density. For small gradients small values of the spin term are found; this also applies for areas with large density.

The correlation energy functionals will not be discussed in detail here due to the complexity of their form.

3.2.1.3 Hybrid Functionals

A further class of functionals are the hybrid functionals which combine a pure density functional with Hartree-Fock exchange to account for the exchange energy. These functionals contain weighted combinations of other functionals to approximate the exchange and correlation energies.

Perhaps the longest standing and most widely utilised functional of the hybrid type is the B3LYP functional,[68] which has the following form:

$$E_{XC}^{B3LYP} = (1 - a_0)E_X^{LSDA} + a_0 E_X^{HF} + a_X \Delta E_X^{B88} + a_C \Delta E_C^{LYP} +$$
$$(1 - a_C)\Delta E_C^{VWN}$$

Equation 3.27

Where a_0, a_X and a_C are semiempirical coefficients that were determined through fitting to experimental data by Becke,[69] E_X^{HF} is the exact Hartree-Fock exchange, ΔE_X^{B88} is Becke's gradient correction to the exchange functional, ΔE_C^{LYP} is the gradient corrected Lee-Yang-Parr correlation functional[70] and ΔE_C^{VWN} is the local correlation functional of Vosko, Wilk and Nusair.[66]

The M06 suite of density functionals developed by Truhlar *et al*. also includes two widely utilised hybrid functionals, the M06 and M06-2X functionals.[71] These have the following general form:

$$E_{XC}^{Hybrid} = \frac{X}{100}E_X^{HF} + \left(1 - \frac{X}{100}\right)E_X^{DFT} + E_C^{DFT}$$

Equation 3.28

Where E_X^{HF} is the exact Hartree-Fock exchange energy, X is the percentage of Hartree-Fock exchange in the hybrid functional, E_X^{DFT} is the local DFT exchange energy and E_C^{DFT} is the local DFT correlation energy. For the M06 functional, the percentage of Hartree-Fock exchange (X) is 27% whilst the M06-2X has double this at 54%. The remaining contribution to the exchange energy is determined by the approximate density functional; as such the issue of double counting exchange occurs since it is not known how much of the real exchange is captured by the approximate density functional. The M06-2X functional performs better than the M06 functional for systems which contain unpaired electrons since the higher percentage of exact exchange helps negate the effects of self-interaction on the energy. The M06-2X functional has also been shown to perform well

compared to other hybrid functionals for main group thermochemistry, kinetics and non-covalent interactions.[72-73]

3.2.2 Basis Sets

As mentioned previously, for Hartree-Fock and DFT methods a set of basis functions are utilised to approximate the molecular orbitals of the system being studied, and thus calculate the wavefunction. There are two main types of functions utilised as basis functions: Slater type orbitals (STOs) and Gaussian type orbitals (GTOs), this is due to them being atomic orbital-like functions.

Slater type orbitals represent exact atomic orbital functions, accessed from the analytical solution to the Schrödinger equation for relatively simple one-electron systems (hydrogen atom, He^+, Li^{2+}, *etc.*). They have the general form:

$$\phi_{nlm}(r, \theta, \varphi) = NY_{lm}(\theta, \varphi)P(r)e^{-\zeta r} \qquad \textbf{Equation 3.29}$$

Where n, l and m are the principal, angular and magnetic quantum numbers; r, θ, φ are spherical polar coordinates with respect to the nucleus; N is a normalisation constant (such that $\int \phi^*(r)\phi(r)dr = 1$); Y_{LM} is a spherical harmonic function; $P(r)$ is a polynomial function and ζ defines how steeply the function decreases moving away from the nucleus. STOs are computationally costly and are therefore rarely used in quantum chemical calculations. The GTOs however are less computationally demanding and are therefore the most commonly used:

$$\phi_{nlm}(r, \theta, \varphi) = NY_{lm}(\theta, \varphi)P(r)e^{-\zeta r^2} \qquad \textbf{Equation 3.30}$$

Simply changing to a square within the exponential significantly changes the shape of the function, with the GTO not displaying the correct cusp behaviour (as $r \to 0$ the gradient tends to zero) and dropping too quickly to zero as $r\to\infty$.

GTOs offer a further improvement in computational cost when each basis function is itself a combination of primitive Gaussian functions, these combinations are termed contracted Gaussian basis functions.

$$\phi = \sum_i^{n_{contr}} d_i G_i(\zeta_i) \qquad \textbf{Equation 3.31}$$

Where each primitive is weighted by a coefficient *d*, which can be altered to make the contracted Gaussian basis function more similar in shape to a STO.

A basis set can be constructed with any number of basis functions, as the number of basis functions is increased, the representation of the orbital becomes more accurate; however, the computational cost also increases. A minimal basis set utilises one basis function per atomic orbital and is therefore the least accurate. When this is increased to two basis functions per atomic orbital, the basis set is termed double-ζ, for three basis functions the basis set is termed triple-ζ, *etc*. The basis set can be split, to utilise a minimal basis set for the core atomic orbitals/electrons whilst using an increased level of accuracy for the valence orbitals/electrons. An example of such a split-valence basis set would be the 6-31G basis set developed by Pople *et al.*,[74] where the 6 states that 6 primitive Gaussian functions are used to represent the core electrons; the valence electrons are then represented by two GTOs made up of 3 and 1 primitive Gaussian functions, respectively.

Basis sets can be further extended by the inclusion of polarisation and/or diffuse functions. Polarisation functions are basis functions with larger angular momentum quantum number than those normally found in the atom, *e.g.*, the addition of p-functions on hydrogen atoms. The addition of polarisation functions adds flexibility to the orbitals, allowing distortion during bond making and bond breaking.[75] In Pople-type basis sets this is represented by noting the polarisation functions in brackets with the polarisation functions for heavy atoms followed by those for hydrogen atoms, *e.g.*, 6-31G(d,p). Diffuse functions can be added to the basis set to allow better representation of anionic species which exhibit very diffuse electron density, this is represented in Pople-type basis sets by the addition of a '+' for diffuse functions on heavy atoms and a second '+' for diffuse functions on hydrogen atoms.[76]

3.2.3 Implicit Solvation Models

In order to 'place' a solute into a solvent three steps must be carried out: creation of a cavity in the solvent, insertion of the solute molecule into the cavity with only vdW interactions present and finally turning on electrostatic interactions. This means the solvation free energy in an implicit continuum model is given by:

$$\Delta G_{solv} = \Delta G_{cav} + \Delta G_{vdW} + \Delta G_{elec}$$

Equation 3.32

Where ΔG_{cav} is the free energy required to form a cavity in the solvent (a positive contribution due to work done against the solvent and entropic penalty from reorganizing solvent molecules around the solute), ΔG_{vdW} is the contribution from vdW interactions between solute and solvent (often split into ΔG_{rep} and ΔG_{disp}), and ΔG_{elec} is the contribution from polarisation of the solvent by polar or charged solutes. There exist different methods to approximate the free energy contribution arising from the electrostatic and non-electrostatic components of the solvation free energy.

The free energy of cavitation is, in general, calculated using a surface formed from one of the following methods:

- an ideal cavity of spherical or ellipsoidal shape around the whole solute molecule
- overlapping spheres (with radii corresponding to the vdW radii, in some instance multiplied by a constant factor) centred on the solute atoms/groups of atoms (for example, inclusion of hydrogen atoms in the sphere of a heavy atom)

ΔG_{cav} can then be calculated from an equation such as:[77]

$$\Delta G_{cav} = \sum_{i}^{spheres} \frac{A_i}{4\pi R_i^2} G_i^{HS}$$

Equation 3.33

Where, R_i is the radius of the ith sphere, A_i is the solvent exposed surface of sphere i, G_i^{HS} is the cavitation energy of a sphere with radius i in a fluid of hard spheres using Pierotti's equation.[78]

The vdW free energy has been calculated in a number of ways such as: utilising known intermolecular potentials,[79] making a uniform approximation for the solvent,[80] utilising molecular polarisability data for the solvent,[81] or using solvent accessible surface areas.[82]

A number of methods for calculating the contribution of ΔG_{elec} have been published. Two of the most common and widely applied methods are based on Generalised Born Equations and the Poisson Equation.

Continuum models based on the Generalised Born model utilise spherical or ellipsoidal cavities to house the solute molecule, **S**, in the reaction field (Figure 3.1).
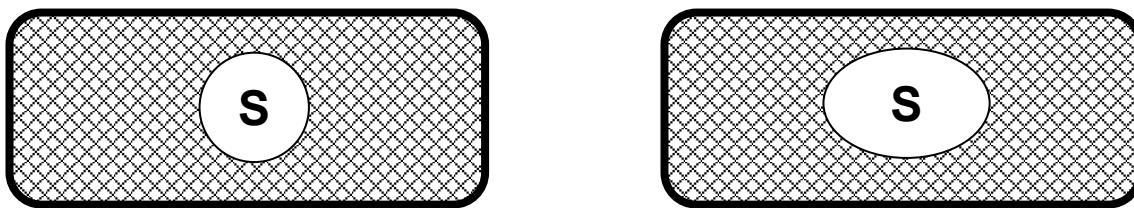
Figure 3.1. Reaction Field mode for a spherical or ellipsoidal cavity.

Another type of continuum model is based on the Poisson Equation, which allows the electrostatic potential to be expressed as a function of the charge density and dielectric constant:

$$\nabla^2 \Phi(r) = -\frac{4\pi\rho(r)}{\varepsilon}$$

Equation 3.34

Where $\nabla^2 \Phi(r)$ is the electrostatic potential, ε is the dielectric constant and $\rho(r)$ is the charge density.

Due to cavitation, the solute charge distribution can be thought of as being inside a cavity which displaces the homogeneous dielectric medium creating two regions: inside the cavity and outside the cavity. Thus, the Poisson Equation becomes:

$$\nabla\varepsilon(r).\nabla^2 \Phi(r) = -4\pi\rho(r)$$

Equation 3.35

The method of Miertus, Scrocco and Tomasi,[83] the polarisable continuum model (PCM) is a popular method based on the Poisson equation. The PCM model creates cavities from overlapping atomic spheres which have radii 20% larger than the van der Waals radii, Figure 3.2, and a distinction between 'polar' and 'non-polar' hydrogen atoms in molecules. A development of the PCM model is the conductor-like polarisable continuum model (CPCM)[84] which deals with the problem of the solute electron cloud sitting outwith the cavity and interacting with the dielectric medium.
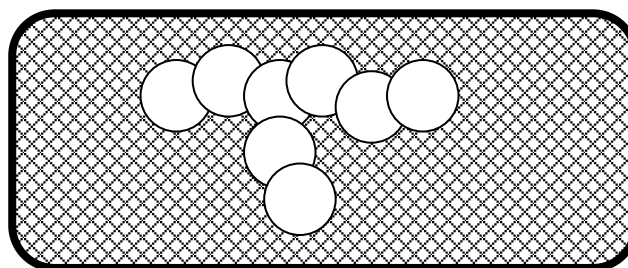

Figure 3.2. PCM type cavity in the reaction field.

3.3 Transition State Theory

When considering a chemical reaction, we may think of the reactants and products connected through the lowest energy pathway *via* a transition state. This can be represented in terms of a potential energy surface (PES), where the reactants and products represent minima on the surface and the transition state is a first order saddle point: a maximum with respect to the reaction coordinate and a minimum with respect to all remaining coordinates. This is often best described by visualisation, Figure 3.3 (Left), where it can be seen that the reactants, products and transition state also exist in discrete minima of their own (better visualised in the 3D plot, Figure 3.3 (Right)).
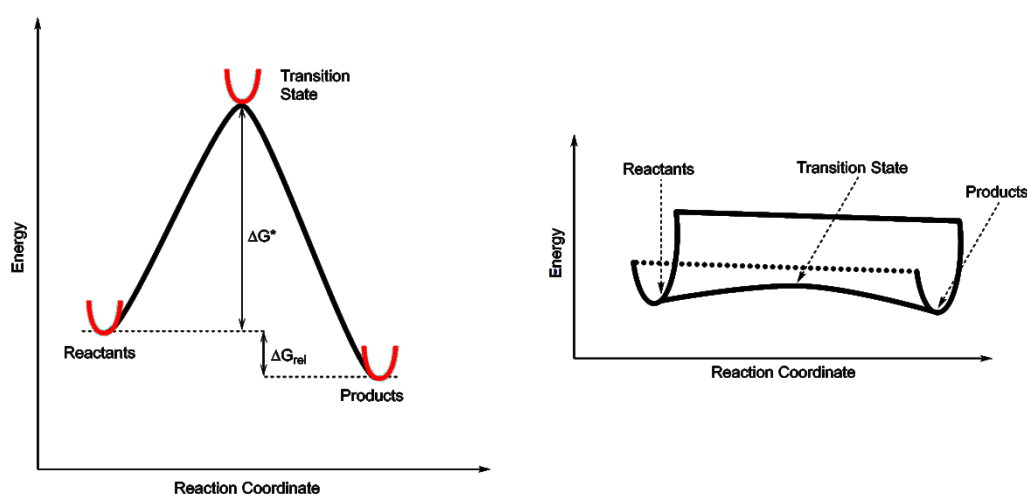

Figure 3.3: Left) Simple 2D PES, **Right)** 3D representation of a simple reaction coordinate.

Within transition state theory, first formulated by Henry Eyring,[85] it is assumed that the transition state (or activated complex) is in quasi-equilibrium with the reactants. Thus, allowing determination of the rate constant (k) from:

$$k = \frac{K_B T}{h} \; e^{-\frac{\Delta G^*}{RT}}$$
<div align="right">**Equation 3.36**</div>

Where K_B is the Boltzmann Constant, T is temperature in Kelvin, h is Planck's constant, ΔG^* is the Gibbs free energy of activation and R is the gas constant.

In order to determine ∆G* an optimised transition state geometry must be obtained, this can be achieved by a number of approaches. Within this work, transition state geometries were obtained by two methods: i) optimisation of a best guess starting geometry for the transition state based on chemical intuition or ii) by performing a bond scan of the key atom movement to obtain an improved starting point for the transition

state optimisation. Following a transition state optimisation, a frequency calculation was performed in order to determine if only one imaginary frequency, which corresponded to the desired transition state, was obtained. With a transition state geometry in hand, intrinsic reaction coordinate (IRC) calculations, where the imaginary frequency was followed both in the forward and reverse direction, were performed in order to access starting geometries of reactant and product complexes. These geometries were then optimised to obtain optimised geometries of the reactant and product complexes.

3.4 Marcus Theory of Electron Transfer

The ability to investigate electron transfer reactions using computational methods follows from the pioneering and Nobel Prize winning work on electron transfer theory by Rudolph A. Marcus.[86-87] Marcus' theory allows calculation of the activation free energy, of electron transfer reactions, based on the total reorganisation energy of the system, λ, and the relative free energy, ΔG_{rel}:

$$\Delta G^* = \frac{\lambda}{4}\left(1 + \frac{\Delta G_{rel}}{\lambda}\right)^2$$
Equation 3.37

To describe electron transfer Marcus Theory utilises two parabolas on the potential energy surface, which represent the motion of the nuclei of the reactant and the product, Figure 3.4. The intersection of the parabola represents the activation free energy, ΔG^*, and the relative free energy is the difference between the reactant and product minima, ΔG_{rel}. The reorganisation energy can be described as the energy required to reorganise the nuclei without transferring an electron, λ.
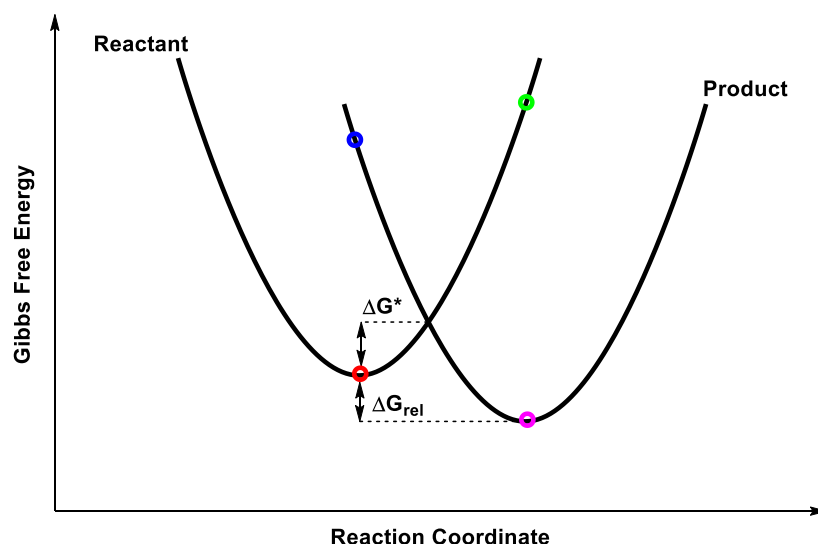
Figure 3.4: PES for electron transfer according to Marcus Theory. Legend: Red Circle = $E_s(R_s)$, Blue Circle = $E_p(R_s)$, Purple Circle = $E_p(R_p)$ and Green Circle = $E_s(R_p)$.

The total reorganisation energy, λ, is the sum of the internal reorganisation energy (λ_i) due to the electron donor and acceptor molecules, and the external reorganisation energy (λ_o) due to solvent reorganisation. It has been found that the internal reorganisation energy is the most significant contribution to the total reorganisation energy, for systems of relevance to those studied here,[88-91] therefore Equation 3.37 can be reduced to:

$$\Delta G^* = \frac{\lambda_i}{4}\left(1 + \frac{\Delta G_{rel}}{\lambda_i}\right)^2 \qquad \textbf{Equation 3.38}$$

The internal reorganisation energy λ_i is calculated as:

$$\lambda_i = \frac{\lambda_i(D) + \lambda_i(A)}{2} \qquad \textbf{Equation 3.39}$$

where $\lambda_i(D)$ and $\lambda_i(A)$ are the internal reorganisation energies for the donor and acceptor respectively. This is calculated using the Nelsen four-point method,[92] where $\lambda_i(D)$ (or similarly $\lambda_i(A)$) is calculated as follows:

$$\lambda_i(D) = \left(E_s\left(R_p\right) - E_s(R_s)\right) + \left(E_p(R_s) - E_p(R_p)\right) \qquad \textbf{Equation 3.40}$$

$E_s(R_p)$ is the single point energy of the optimised product with the starting electronic configuration; $E_s(R_s)$ is the energy of the optimised reactant; $E_p(R_s)$ is the single point energy of the optimised reactant with the product electronic configuration and $E_p(R_p)$ is the energy of the optimised product (these can be viewed in Figure 3.4).

A more accurate method for calculating the internal reorganisation energy, λ_i was presented recently by Tuttle, Murphy and co-workers.[93] Here, the donor and acceptor species are treated as a complex, as opposed to the separate species of the Nelsen method, and counter-ions are also utilised to balance charge. This reduces Equation 3.39 to simply:

$$\lambda_i = \lambda_i(DA)$$

Equation 3.41

Where $\lambda_i(DA)$ is given by Equation 3.42:

$$\lambda_i(DA) = \left(E_s(R_p) - E_s(R_s)\right) + \left(E_p(R_s) - E_p(R_p)\right)$$

**Equation 3.42**

4. Bad Leaving Groups

4.1 Background

When chemical reactions involving leaving groups occur, chemists tend to use the general rule of thumb that leaving groups perform better if they are weak bases (their conjugate acid has a small pK_a value). Therefore, iodide, bromide and chloride would be good leaving groups, whilst hydride, amides, alkyl anions or aryl anions would be regarded as poor leaving groups. This poses the question: do only the so called 'good' leaving groups take part in elimination or substitution reactions?

The Murphy and Tuttle groups first became aware of reactions involving so called 'bad leaving groups' in 2016 when Ghorai *et al.*[1] reported on their synthesis of 1,2,4-triarylbenzenes. The products were afforded after treating 1,3-diarylpropan-1-ones (**4.2**) or 1,3-diaryl-2-propen-1-ols (**4.1**) with potassium hydroxide (KOH) in DMSO at 100 °C under argon, Scheme 4.1.
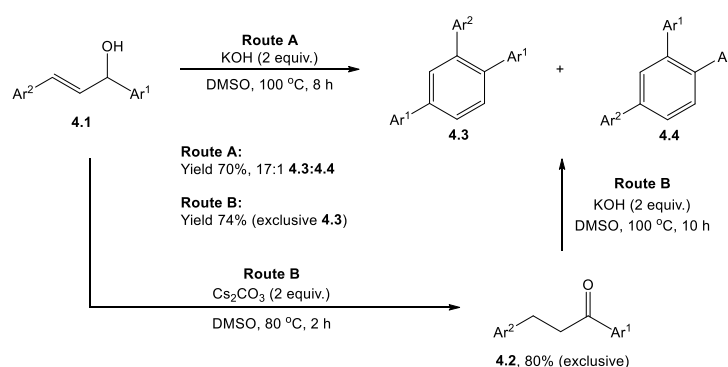

Scheme 4.1: Synthesis of 1,2,4-triarylbenzenes as reported by Ghorai *et al.*[1] in 2016.

This was a somewhat remarkable reaction whereby relatively simple and accessible starting materials were transformed selectively into a new aryl motif. The most interesting feature of the reaction for the Murphy and Tuttle groups was the selective loss of an aryl group required to afford the product. Indeed, Ghorai *et al.*[1] were equally as intrigued by this and conducted some additional reactions in order to ascertain the fate of the aryl leaving group. First, they treated 1,3-diphenyl-2-propen-1-ol with KOH in DMSO for 4 hours at 100 °C to form 1,2,4-triphenylbenzene, and did not observe any dimerisation of the phenyl leaving groups. Following this, biphenyl-containing substrate **4.7** was subjected to the same conditions as above and yielded the expected product **4.8** in 80% yield, whilst biphenyl (**4.9**) was also isolated in 42% yield. Biphenyl would be expected to form following loss of the aryl group from the 3-position of the allylic alcohol.
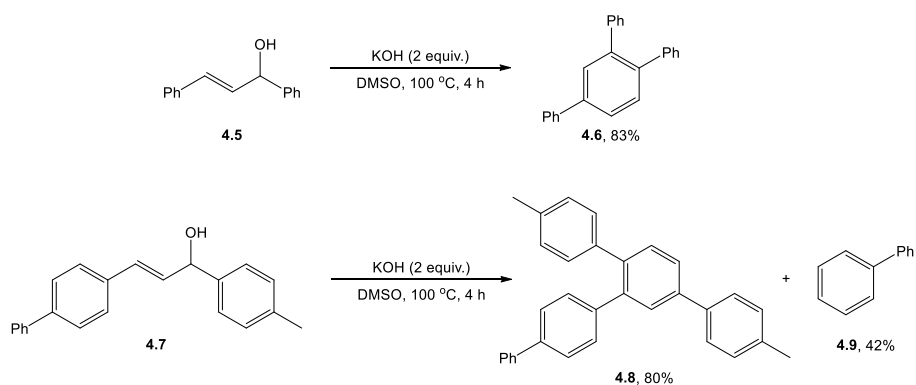
Scheme 4.2: Substrates tested by Ghorai *et al.* in an attempt to detect the aryl moiety which is lost during formation of 1,2,4-triarylbenzene.

With their results in hand, Ghorai *et al.* proposed a mechanism for their reaction, Scheme 4.3, starting from either the allylic alcohol or ketone.
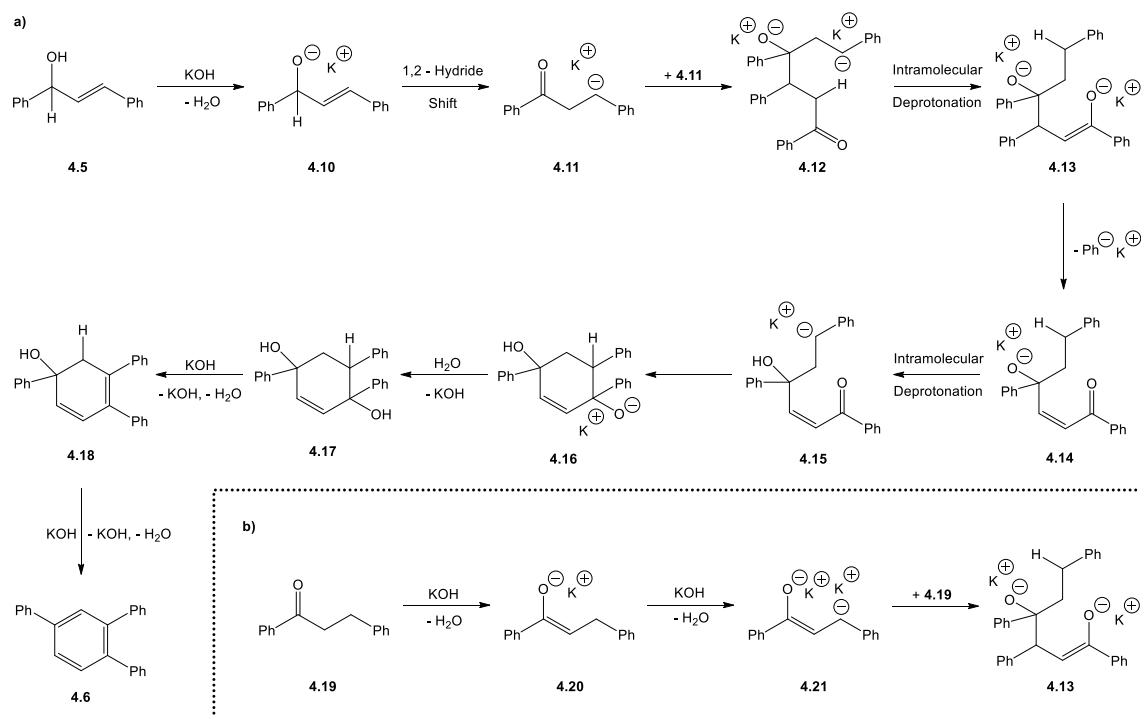

Scheme 4.3: Proposed mechanism for formation of 1,2,4-triarylbenzene (phenyl used for illustration) from **a)** allylic alcohol or **b)** ketone.

Starting from allylic alcohol (**4.5**) they proposed a deprotonation of the alcohol to yield alkoxide **4.10**, which was then proposed to undergo 1,2-hydride shift. Such a 1,2-hydride shift has been proposed before for base-promoted isomerisation of a similar substrate by Schmid and Borschberg,[94] however during a reaction with a deuterium-labelled substrate they observed products from both a 1,2- and 1,3-hydride shift, with the 1,3-product being the major component.
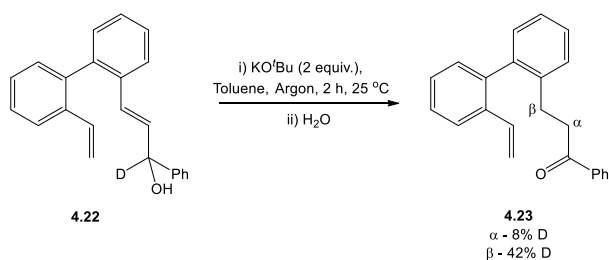
Scheme 4.4: Deuterium labelled substrate isomerised by Schmid and Borschberg after treatment with KO^{t}Bu.

More recently, isomerisation of 1,3-diaryl-2-propen-1-ols (**4.24**) to 1,3-diarylpropen-1-ones (**4.30**) using 1,10-phenanthroline and NaO^{t}Bu has been reported by Tang *et al*.[95] In keeping with previous literature on the combination of 1,10-phenanthroline and *tert*-butoxide, Tang *et al*. proposed that their isomerisation reaction was occurring *via* a single electron transfer initiated mechanism as depicted in Scheme 4.5. With dimsyl anion having been previously shown to act as an electron donor,[47] the mechanism of Tang *et al*. could point to an alternative radical-based mechanism for the reaction carried out by Ghorai *et al*.
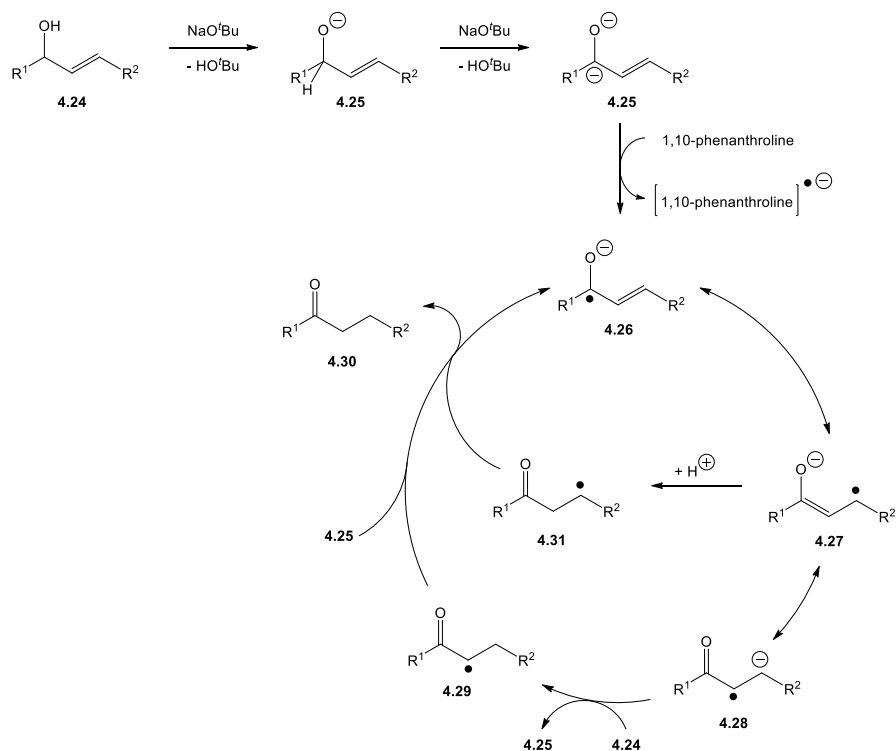
**Scheme 4.5:** Single electron transfer initiated isomerisation mechanism proposed by Tang *et al*.

Suchand and Satyanarayana[96] have also performed a domino isomerisation and functionalisation of aryl allylic alcohols under basic conditions (KO^{t}Bu), which was

postulated to proceed *via* a radical mechanism, Scheme 4.6. Deprotonation of the alcohol, followed by electron transfer from KO*t*Bu to the enolate (**4.33**) is proposed to form a ketyl radical anion (**4.34**), which upon protonation could add to styrene in order to access the functionalised product (**4.39**). This would be further reason to investigate the possibility of an electron transfer initiated radical mechanism for the formation of 1,2,4-triarylbenzenes, in contrast to the author's original proposed mechanism.
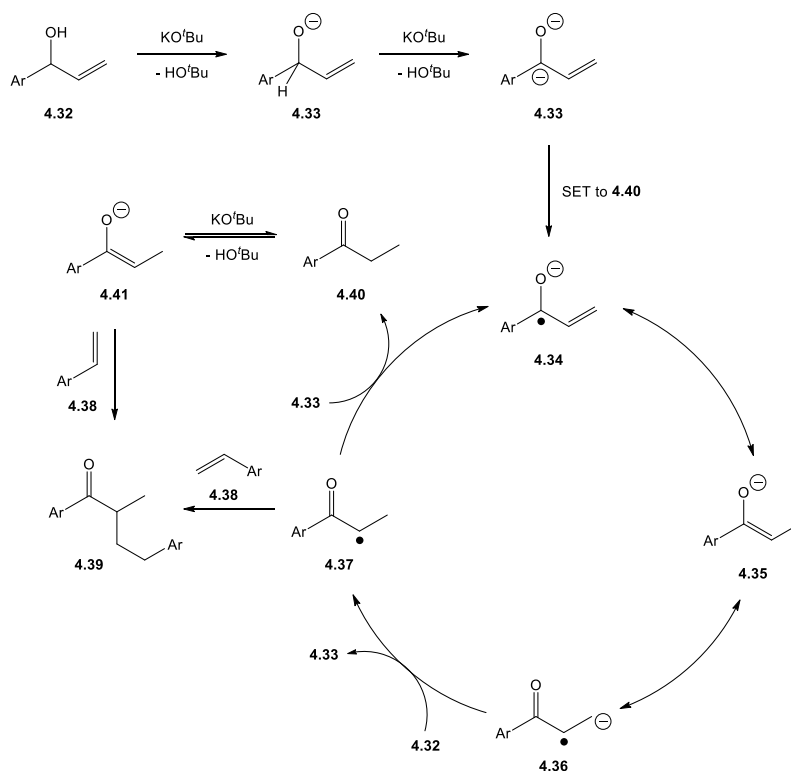
Scheme 4.6: Mechanism proposed by Suchand and Satyanarayana for their domino isomerisation and functionalisation of aryl-substituted allylic alcohols.

Another alternative to the 1,2-hydride shift, would be double deprotonation of the allylic alcohol to yield a dianion which could preferentially react *via* the 3-position first. Indeed, the work of Cook *et al*.[97] shows just that; taking deuterated **4.42** and treating with sodium hydride (NaH) followed by an electrophile (E) leads to exclusive formation of the α-substituted product. This suggests that the β-position could perform the deprotonation of a second molecule of allylic alcohol (**4.44** - **4.45**), forming enolate **4.45** which would further react at the α-position.
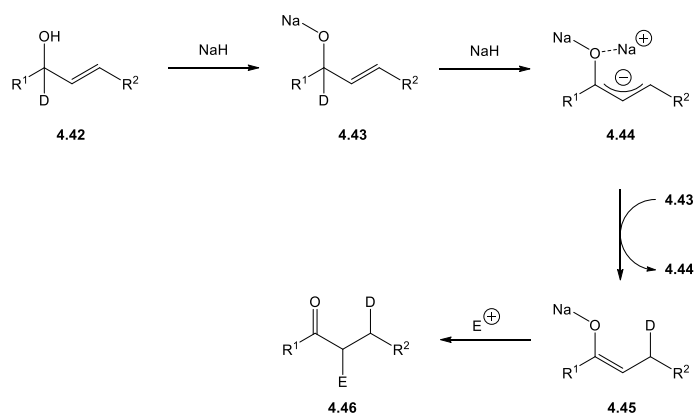
Scheme 4.7: Tandem isomerisation and functionalisation of allylic alcohol **4.42** carried out by Cook *et al.*, use of deuterated substrate highlighted the double deprotonation mechanism.

Looking beyond the early steps in the proposed mechanism of Ghorai *et al.*, Scheme 4.3, step (**4.13** - **4.14**) involving loss of an aryl anion, was interesting - with the driving force solely being formation of an α,β-unsaturated carbonyl. Expulsion of such a poor leaving group, the aryl anion, would likely require a stronger driving force – perhaps the gain of aromaticity following expulsion of the aryl anion from a cyclohexadiene type intermediate. A search of the literature for reactions which involved 'bad leaving groups,' produced several interesting results.

In 1964, Schriesheim *et al.*[98] studied the reaction between 1,3-cyclohexadiene and KO^{t}Bu in DMSO at 55 °C and found quantitative conversion to benzene and cyclohexene. Through kinetics experiments they were able to calculate an activation energy of 13.5 kcal/mol for this reaction, with the kinetics second order in cyclohexadiene concentration.[98] This led the authors to propose an initial deprotonation of 1,3-cyclohexadiene followed by rate-limiting hydride transfer to a second molecule of cyclohexadiene. Hydride transfer to other hydride acceptors, such as naphthalene and anthracene was also reported alongside the near complete exclusion of cyclohexene, thus supporting the proposed mechanism. Loss of a hydride at first appears odd, given that the pK_a of hydrogen is ~36, however the loss of hydride from the cyclohexadienyl anion **4.49** leads to the formation of an aromatic system (**4.51**), which provides a rationale for the observed reactivity. Similar results were also later observed by Venkatasubramanian and Siegel[99] for aromatisation of 1,3- or 1,4-cyclohexadiene when treated with potassium 3-aminopropylamide.
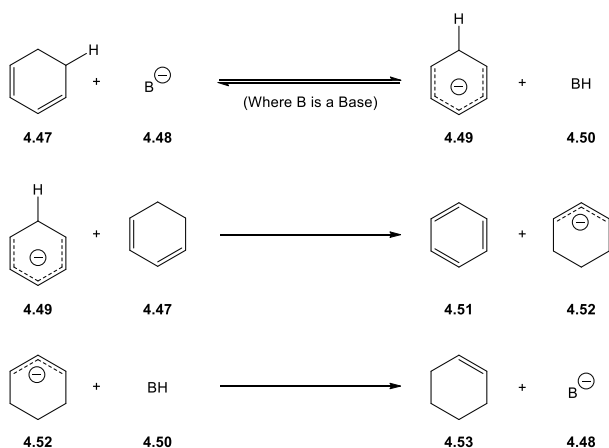
Scheme 4.8: Mechanism proposed by Schriesheim *et al*.[98] for the disproportionation of cyclohexadiene to benzene and cyclohexene.

Staley and Erdman[100] followed the work of Schriesheim *et al*. by treating 6-methyl,6-phenyl-1,3-cyclohexadiene with potassium amide in liquid ammonia at 25 °C, in order to assess whether methyl or phenyl anion could act as a leaving group. In fact, what was observed from this reaction were 8 different products in a combined yield of 75 - 90%, Scheme 4.9.
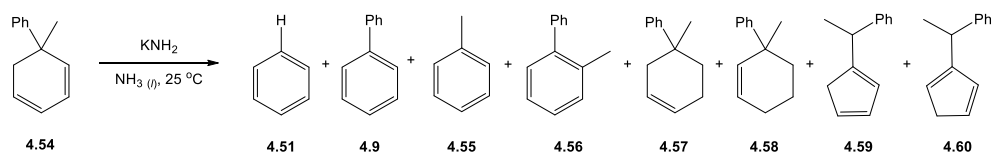
Scheme 4.9: Products formed following deprotonation of **4.54** by potassium amide, conducted by Staley and Erdman.

Each product was explained following an initial deprotonation of **4.54**, to yield **4.61**. A disrotatory electrocyclic ring closure of **4.61**, followed by cleavage of the cyclopropyl ring then protonation would yield either **4.59** or **4.60**. Alternatively, **4.61** could undergo 1,2-phenyl migration to form **4.65** which could then lose potassium hydride to yield **4.56**, or the hydride could be delivered to another molecule of **4.54** to yield one molecule of **4.56**, and one of **4.57** or **4.58**. This was supported by experiments where **4.54** was used in excess instead of potassium amide and the observed yields of **4.56**, **4.57** and **4.58** were found to be increased. Such a hydride transfer is also supported by the findings of Schriesheim *et al*.[98] discussed above. Finally, the formation of benzene, toluene and biphenyl can be explained by loss of phenylpotassium and methylpotassium from **4.61**, respectively.
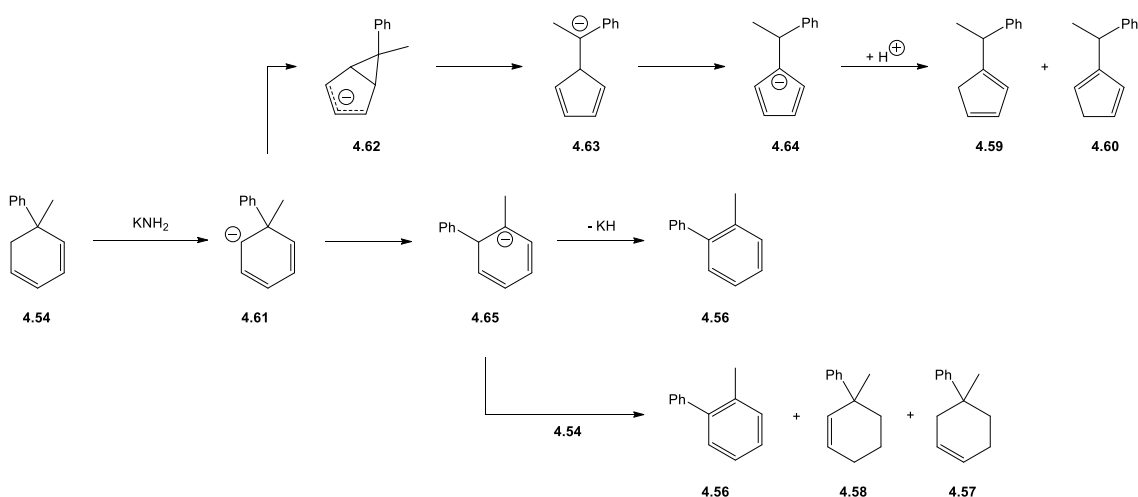
Scheme 4.10: Mechanisms proposed by Staley and Erdman for formation of products **4.56** - **4.60**.

This was the first report in the literature of phenyl and methyl anions acting as leaving groups, a somewhat surprising result given the pK_a of benzene is 43 and of methane is 48 and as such are classified as very poor leaving groups. Subsequently, there have been a handful of reports in the literature detailing reactions involving similarly 'bad leaving groups.'

Collins *et al.*[101] exposed the benzyl anion as a leaving group in 1981 in their report of *ipso*-aromatic substitution when reacting diphenylmethane with sodium-potassium alloy (NaK). Toluene (**4.55**) and 3-benzyl-1,1'-biphenyl (**4.57**) were the products isolated following the reaction, Scheme 4.11. They also showed that reacting benzene and diphenylmethane with NaK yielded toluene (**4.55**), biphenyl (**4.9**) and hydrogenated biphenyls; showing again that benzyl anion was acting as a leaving group.
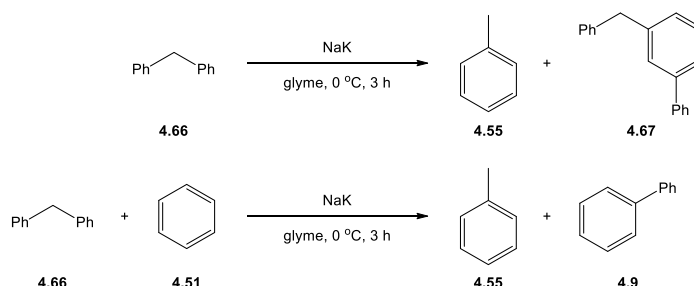
Scheme 4.11: *Ipso* aromatic substitution carried out by Collins *et al.* which involved benzyl anion as leaving group.

It was proposed that diphenylmethane received an electron from the highly reducing NaK generating the radical anion which then acts as a nucleophile towards the *ipso* position of a second molecule of diphenylmethane, with the leaving group being benzyl anion.

Interestingly, as part of their mechanistic discussions for this reaction, Collins *et al.* also mention that hydride acts as a leaving group following the *ipso* aromatic substitution in order to restore aromaticity, Scheme 4.12. This work highlights that so called 'bad leaving groups' are in fact competent leaving groups under highly reducing conditions.
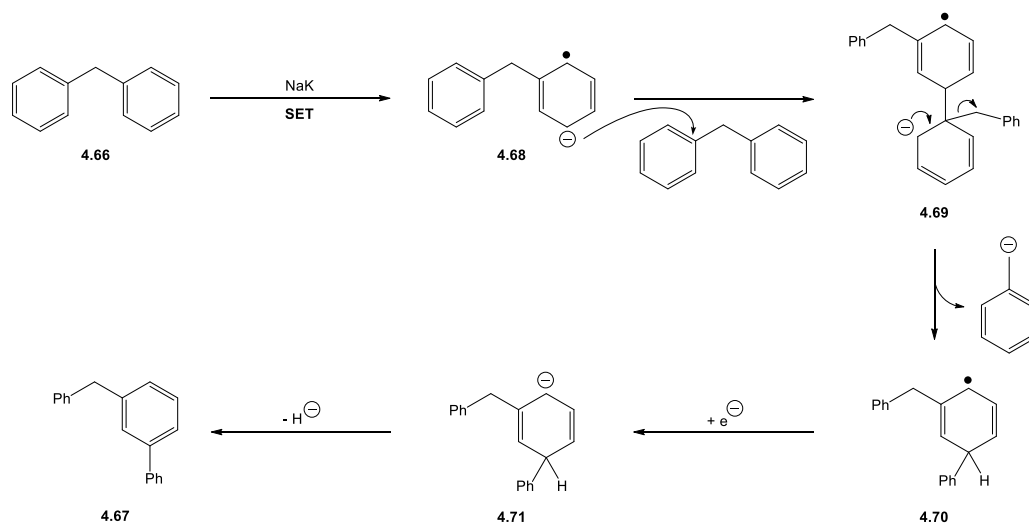
Scheme 4.12: Mechanism proposed by Collins *et al.* for *ipso* aromatic substitution involving loss of benzyl anion and hydride as leaving groups under highly reducing conditions (NaK).

Loss of benzyl anion has also been shown more recently by Trofimov *et al.*[102] in their dimerisation of γ-aryl-β,γ-enones (**4.72**) to acylated terphenyls (**4.78**) catalysed by KO*t*Bu in DMSO. Their proposed mechanism is depicted in Scheme 4.13, and the final stage of this is loss of benzyl anion in an E1cB reaction.
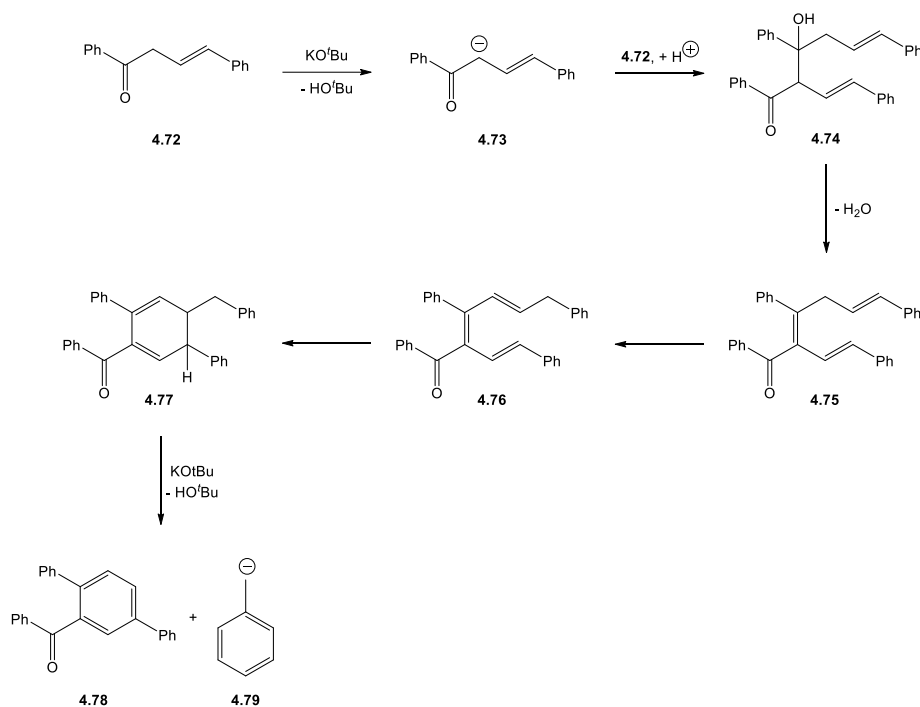
Scheme 4.13: Mechanism proposed by Trofimov *et al*. for the KO*t*Bu-catalysed dimerisation of γ-aryl-β,γ-enones (**4.72**) to acylated terphenyls (**4.78**), involving a benzyl anion leaving group.

A similar type of 'bad leaving group,' the allyl anion, has also been demonstrated to be an effective leaving group by Maldonado *et al*.[103] during their attempts to conduct a Birch reduction-allylation reaction. Whilst attempting to form 1,4-diallyl product **4.81**, by treating **4.80** with sodium followed by allyl bromide, they observed formation of mono-allylated product **4.82** and 3,5-dimethoxybenzoic acid (**4.80**). To determine whether 3,5-dimethoxybenzoic acid was present due to an incomplete Birch reduction, **4.82** was treated with *n*-butyllithium (*n*BuLi) followed by allyl bromide and this yielded solely 3,5-dimethoxybenzoic acid. Therefore, it was proposed that **4.82** was being deprotonated by the *n*BuLi and the resulting cyclohexadienyl anion was undergoing rearomatisation by loss of an allyl anion.
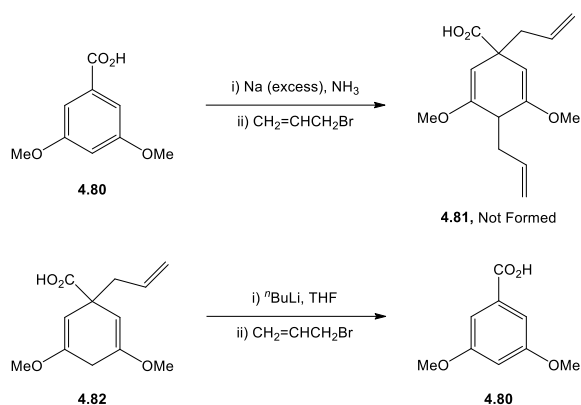
Scheme 4.14: Loss of an allyl anion, as observed by Maldonado *et al*. during their attempts to form 1,4-diallylated product **4.81**.

With a more thorough understanding of the literature, DFT calculations were used to probe the validity of the mechanism proposed by Ghorai *et al*.[1]

4.2 Computational Methods

DFT calculations in this chapter were run using the M06-2X functional[71-72] and 6-31++G(d,p)[74-75, 104-110] basis set on all atoms. Solvation was modelled implicitly using the CPCM model[84] with parameters for dimethylsulfoxide as solvent. All calculations were carried out in Gaussian09.[111]

Calculated ΔG_{rel} and $\Delta G^{\ddagger}$ are relative to the reactants for each step and include the formation of reactant complexes and dissociation of product complexes where appropriate.

4.3 DFT Study of 1,2,4-Triarylbenzene Formation

As discussed in the introduction, there exists a range of mechanistic possibilities for the formation of 1,2,4-triarylbenzenes from either 1,3-diarylpropan-1-ones or 1,3-diaryl-2-propen-1-ols. First, the mechanism proposed by Ghorai *et al.*[1] in their original publication warrants investigation to understand whether a number of key steps would be possible. Should these indeed not be feasible at the reaction conditions, alternative mechanistic steps should be investigated. Namely, double deprotonation of the allylic alcohol starting material and elimination of aryl anions from a cyclohexadienyl anion intermediate.

4.3.1 The Ghorai Mechanism

The mechanism proposed by Ghorai *et al.*[1] was not studied in full by DFT calculations, instead the relative free energies and activation free energies were determined until **4.14**. This choice was made based on the hypothesis that the loss of phenyl anion from **4.13** would be highly endergonic and exhibit a large free energy of activation. Understanding the preceding steps was also vital to understanding the process of dimerisation of two allylic alcohol (**4.5**) or ketone (**4.19**) molecules.
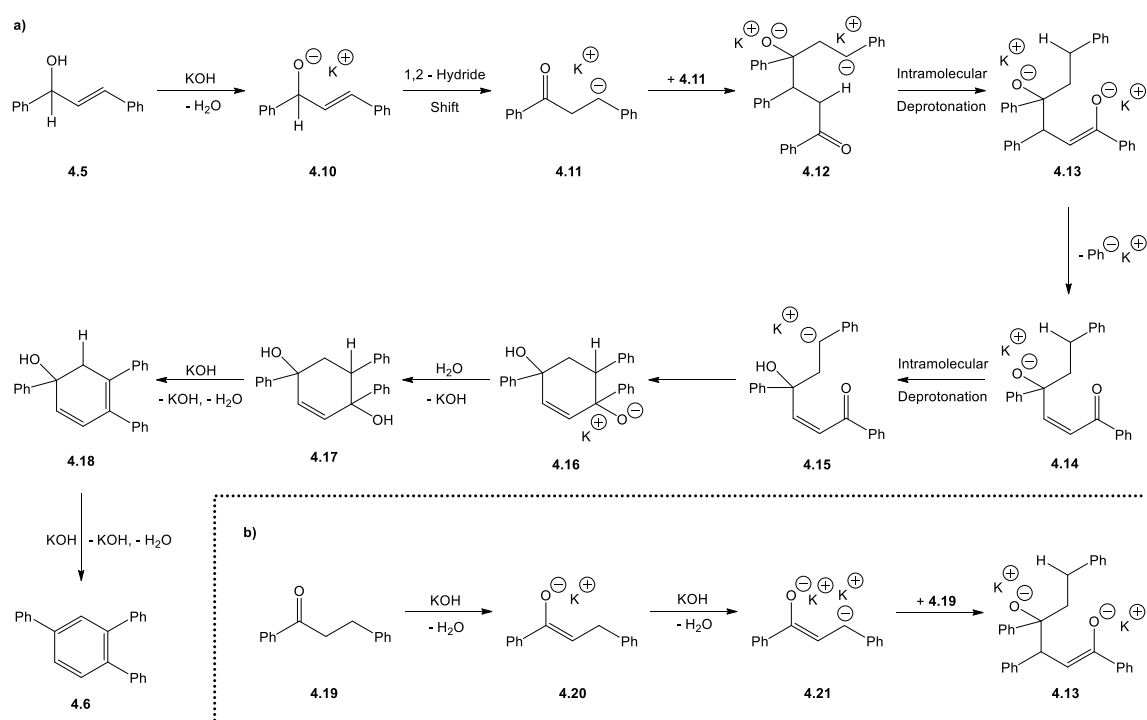
Scheme 4.15: Proposed mechanism for formation of 1,2,4-triarylbenzene (phenyl used for calculations) from **a)** allylic alcohol or **b)** ketone.
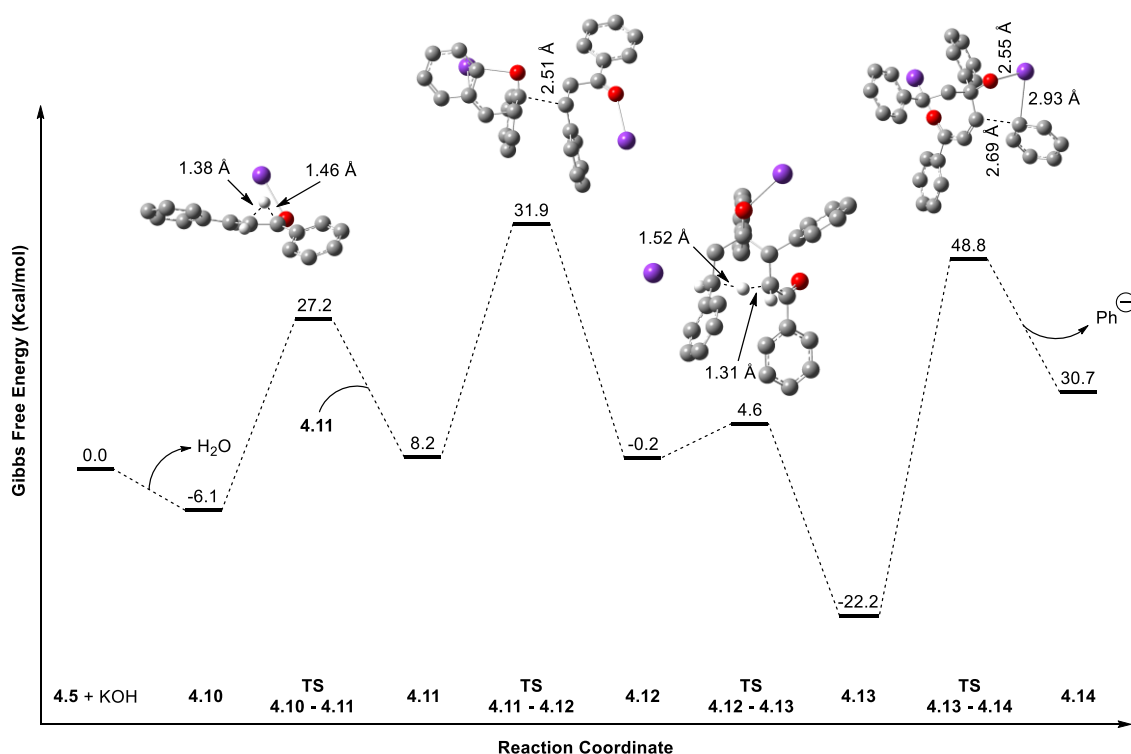
Figure 4.1: Calculated potential energy surface of the initial section (**4.5** to **4.14**) of the mechanism proposed by Ghorai *et al.* (Hydrogen atoms not involved at the reaction centre omitted from images of optimised transition state geometries for clarity).

Attempts to optimise a transition state for the deprotonation of **4.5** proved unsuccessful, however, the reaction was exergonic and favoured. 1,2-Hydride shift from **4.10** was found to be endergonic and had an accessible barrier of 27.2 kcal/mol, subsequent dimerisation of two molecules of **4.11** was found to be almost thermoneutral whilst having a free energy barrier of 31.9 kcal/mol. This free energy barrier would be at the limit of accessibility for a reaction conducted at 100 °C, since the reaction rate would be extremely slow. Considering the previous step being endergonic by 8.4 kcal/mol, this would make the energy span for the overall conversion of **4.10** to **4.12** to 40.3 kcal/mol making it inaccessible at the reaction conditions. Upon taking into account only the enthalpic contributions to reaction **4.11** to **4.12** the reaction was found to be exothermic by 18.9 kcal/mol, with an associated activation energy of 15.3 kcal/mol. Considering the known problems of entropy calculations within DFT due to the solution phase entropy being estimated from gas-phase calculations,[112] the free energy barrier determined above may in fact be overestimated. This would require higher level calculations or experimental data however to confirm, so we therefore maintain the current conclusion.

Despite being able to rule out this mechanism at this stage, the loss of a phenyl anion from **4.13** to **4.14** was still of interest. This reaction has a calculated activation free

energy of 48.8 kcal/mol alone, indicating this would not proceed at the reaction conditions - as had been predicted based on the poor driving force for this reaction.
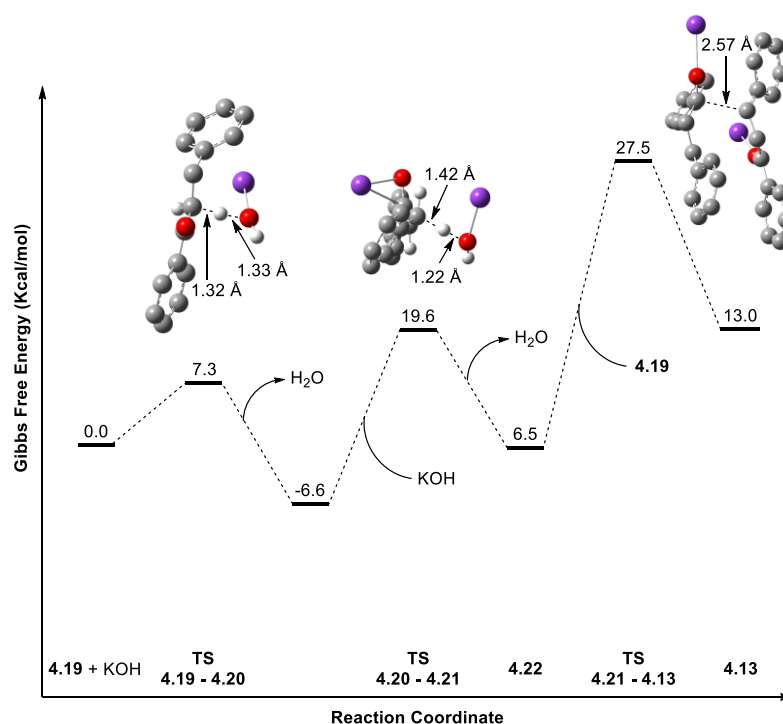

Figure 4.2: Calculated potential energy surface of the initial section (**4.19** to **4.13**) of the mechanism proposed by Ghorai *et al.* (Hydrogen atoms not involved at the reaction centre omitted from images of optimised transition state geometries for clarity).

Examining the proposed mechanism with **4.19** as substrate, Figure 4.2, an initial deprotonation would occur to form enolate **4.20**. A subsequent deprotonation has an accessible free energy barrier however is endergonic, so the equilibrium would lie in favour of the enolate. There would likely be sufficient **4.21** to undergo further reaction with another molecule of **4.19**, and this has an associated free energy barrier of 27.5 kcal/mol, however the reaction was endergonic by 13.0 kcal/mol. The mechanism from **4.19** to **4.13** was therefore endergonic by around 13 kcal/mol, meaning that the subsequent steps in the mechanism would determine if this could be a productive route.

Since Ghorai *et al.* observed formation of ketone **4.19** as a by-product in the formation of 1,2,4-triarylbenzenes, and were also able to perform the reaction using **4.19** as a starting material, there must be a mechanism for conversion between allylic alcohol and ketone. Protonation of **4.11** may explain the observed formation of ketone from allylic alcohol, however deprotonation of **4.10** to yield **4.21** was also investigated.

Table 4.1: Deprotonation of **4.10** to yield **4.21**, an alternative route to convert allylic alcohol **4.5** to ketone **4.19**.
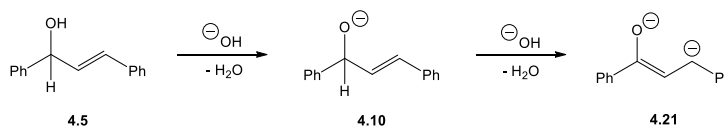
Reaction Step	$\Delta G^{\ddagger}$ (kcal/mol)	ΔG_{rel} (kcal/mol)
4.10 - 4.21	11.2	-9.5

This deprotonation has a small barrier of 11.2 kcal/mol and is exergonic, this deprotonation step would therefore be favoured over the 1,2-hydride shift proposed by Ghorai *et al*. and shift the mechanism to that proceeding *via* **4.21**.

4.3.2 Alternative Mechanism

As demonstrated in the previous section a number of key steps in the original mechanistic proposal by Ghorai *et al*. were thermodynamically and kinetically unfavourable. As such a revised mechanism was proposed, where **4.12** cyclised directly to form **4.83**, this could then be protonated to form diol **4.84**. An elimination of water from **4.84** would yield alkene **4.85** which would undergo further elimination to access either a 1,3- or 1,4-cyclohexadiene intermediate. Upon deprotonation, only the 1,3-cyclohexadiene depicted would lead to the experimentally observed selective aryl anion loss. Were the 1,4-cyclohexadiene intermediate to be formed, the site of deprotonation would be influenced by the aryl ring substituents, an affect which is not observed experimentally.
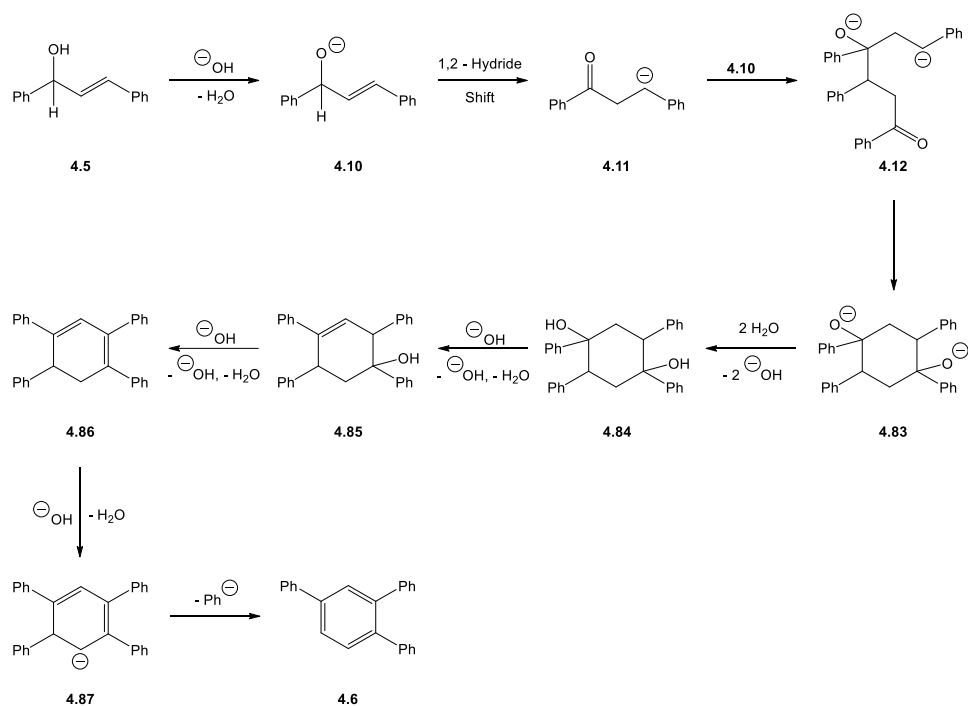
Scheme 4.16: Alternative mechanism for formation of 1,2,4-triarylbenzene *via* loss of phenyl anion from a cyclohexadienyl anion intermediate.

The results for **4.5** to **4.12** have been discussed in the previous section and will therefore not be discussed further, however we note that formation of **4.12** was previously concluded to be energetically unfavoured. In order to investigate the formation of cyclohexadiene intermediates and elimination reactions from these we chose to proceed from intermediate **4.12** regardless. Cyclisation of **4.12** would readily occur to yield **4.83**, the subsequent protonation of **4.83** to yield diol **4.84** is slightly endergonic however the equilibrium would lead to significant formation of **4.84**. Subsequent elimination of two molecules of water was found to be exergonic by 23.3 kcal/mol, indicating that **4.86** would be readily formed.
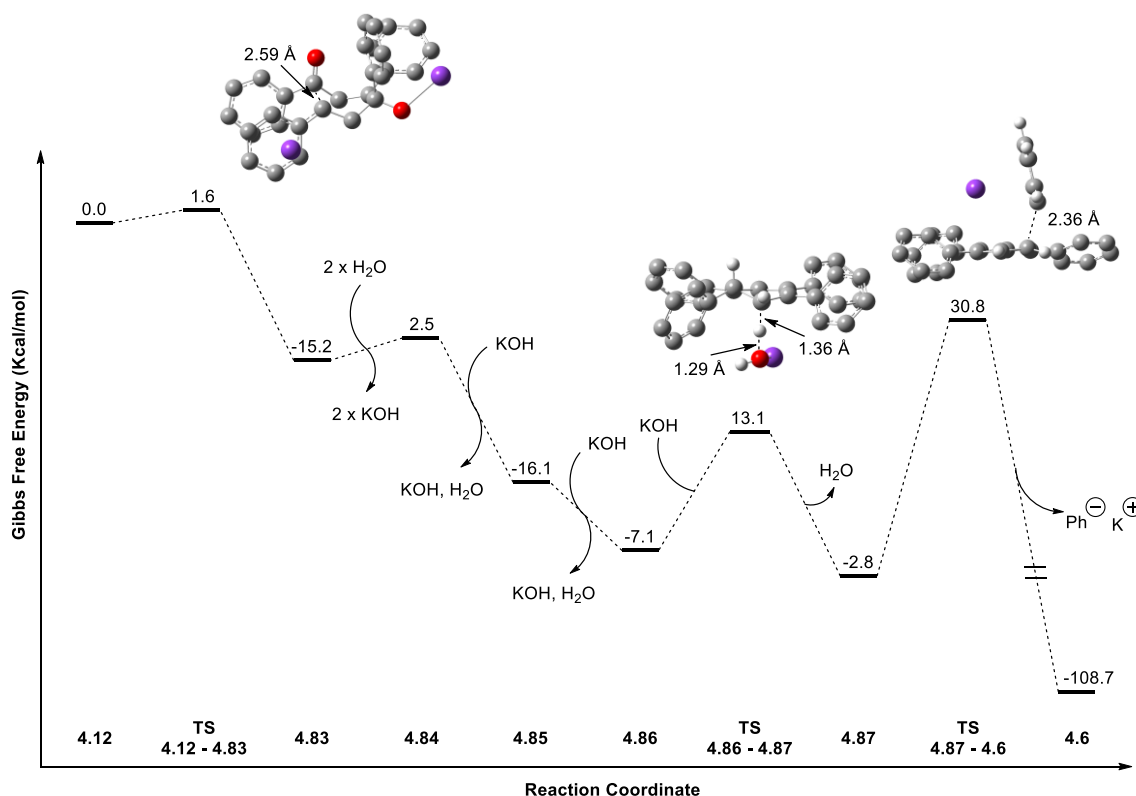
Figure 4.3: Calculated potential energy surface for the later stages of the proposed alternative mechanism. (Hydrogen atoms omitted for clarity unless involved at reaction centre).

Intermediate **4.84** resides in a boat conformation (Figure 4.4) where elimination of water could occur in only one way, due to the presence of one anti-periplanar relationship between a proton and hydroxyl group. Deprotonation of **4.86** to **4.87** would reside in an equilibrium slightly favouring **4.87** (ΔG_{rel} = -2.8 kcal/mol), thus allowing the possibility for aromatisation by elimination of a hydride or phenyl anion. Interestingly, elimination of hydride anion to form KH and 1,2,4,5-tetraphenylbenzene would be unfavourable, whilst the elimination of a phenyl anion is extremely exergonic (ΔG_{rel} = -108.7 kcal/mol). This demonstrates that phenyl anion has a superior leaving group ability than hydride, for this substrate.

Figure 4.4: Optimised geometry of **4.84** in the boat conformation.

4.4 Conclusions

Through the use of DFT calculations, the mechanism proposed by Ghorai *et al.*[1] for the formation of 1,2,4-triarylbenzenes from 1,3-diaryl-2-propen-1-ols has been interrogated in search of mechanistic insights. Results of DFT calculations have demonstrated that several aspects of the proposed mechanism suffer from unfavourable energetics. Taking into account the early steps of th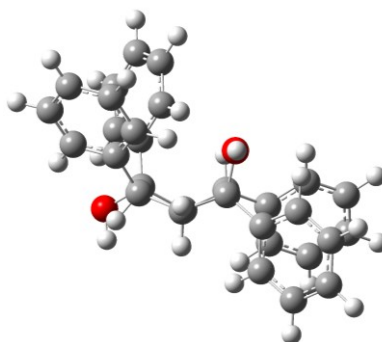e proposed Ghorai mechanism (**4.5** to **4.12**) the calculated energies put into doubt the feasibility of the mechanism.

A further key step of the proposed mechanism was loss of an aryl anion from **4.13** to **4.14**, this was found to exhibit an extremely large free energy barrier (48.8 kcal/mol) whilst also being extremely endergonic (30.7 kcal/mol). Upon initial viewing of this mechanistic proposal, the driving force for this reaction - formation of an α,β-unsaturated ketone - was thought to be insufficient to enable such a reaction to occur, a hypothesis confirmed by this DFT result. In order to enable the loss of an aryl anion, the driving force would therefore need to be extremely strong and would also have to allow the loss to occur in a selective manner to explain the experimentally observed major product.

Despite the concerns raised previously about the accessibility of **4.12**, a proposed alternative mechanism forward from **4.12** has been shown to allow access to **4.83** which in turn may form 1,3-cyclohexadiene intermediate **4.86**. It was then demonstrated that a deprotonation of **4.86** to form a cyclohexadienyl anion (**4.87**) could occur ($\Delta G^{\ddagger}$ = 13.1 kcal/mol and ΔG_{rel} = -2.8 kcal/mol) which would allow access to an intermediate where selective loss of an aryl anion may occur. From **4.87**, loss of either hydride or aryl anion would be possible - indeed both transition states have a very similar barrier at ~31 kcal/mol. It was found though, that loss of an aryl anion led to a highly exergonic reaction, whilst loss of hydride anion was slightly endergonic.

The search for mechanistic insights for the reaction published by Ghorai *et al.*[1] has been at the heart of this chapter, however this search has proven to be a complicated one. It has been difficult to improve upon the earliest mechanistic steps proposed by Ghorai *et al.* regarding access to a dimer of the starting material. Whereas, one important insight has been uncovered with the determination that the loss of an aryl anion occurs following deprotonation of a 1,3-cyclohexadiene intermediate. These results should serve to highlight the abilities of groups such as aryl anions to act as leaving groups under the driving force of aromatisation, something previously highlighted in the 1960's and 70's.

4.5 Future Work

Whilst the conclusions yielded from the DFT calculations herein provide a somewhat improved mechanistic proposal; in order to further understand the mechanism of the Ghorai *et al*. reaction and more generally the concept of 'bad leaving groups' made good, experimental studies and evidence would add further weight.

Although this work was unable to invest time to study the potential for a SET initiated mechanism, with dimsyl anion acting as an electron donor, this should be considered for future studies of the reaction reported by Ghorai *et al*. and other reactions involving bad leaving groups.

In order to fully probe finer mechanistic details, substrates with a cyclohexadiene core bearing 'bad leaving group' substituents on the sp^3 carbons would need to be synthesised. Inherently many cyclohexadiene substrates are highly reactive even in air, undergoing oxidation to afford aromatic systems. For this reason, it may prove difficult to access substrates which could provide valuable mechanistic information in terms of the abilities of 'bad leaving groups.' That said, a range of substrates which have reported syntheses are shown below and could provide evidence for the loss of 'bad leaving groups' when treated with KOH in DMSO. Substrates **4.89** - **4.92** would provide experimental evidence for the leaving group abilities of hydride *vs* phenyl anion where the steric environment around the forming benzene ring would be less bulky. Substrate **4.92** having more steric bulk around the site of elimination would provide further evidence as to the effects of sterics on the preference for hydride or phenyl anion to act as leaving group. Substrate **4.88** would directly test the ability of phenyl anion to act as a leaving group in competition with the allyl group, further substrates such as this could be envisaged to enable similar direct comparison of leaving group ability.
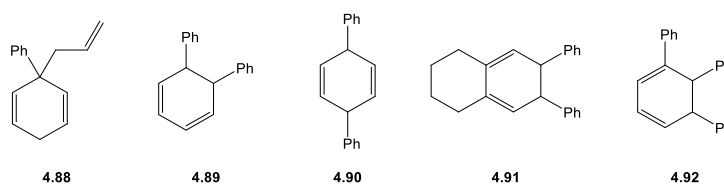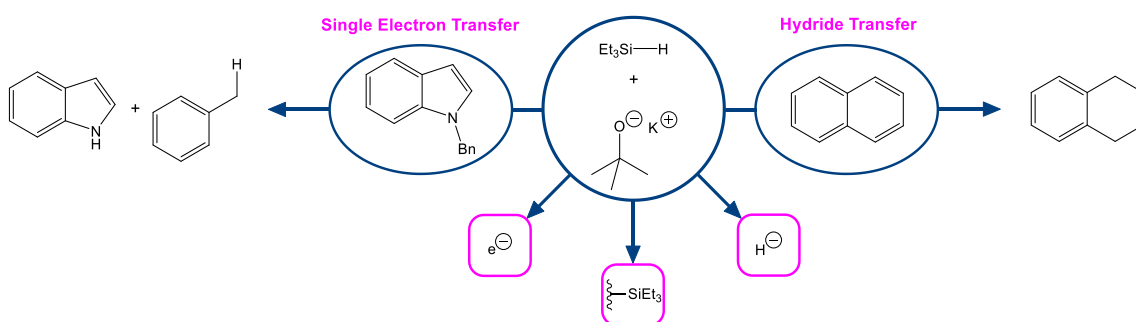

Figure 4.5: Substrates, with literature reported synthesis, for experimental testing of leaving group ability.

5. Computational Investigation of the Stoltz-Grubbs Reducing System

(NB: Experimental work discussed in this chapter was carried out by Andrew J. Smith, Simon Rohrbach, Jude Norman Arokianathar, Erin F. O'Connor and Hong-Shuang Wang)

5.1 Background

The combination of KO^{t}Bu plus a range of small molecules has been shown to lead to the formation of highly reactive intermediates, as described in Section 2. These intermediates have typically been found to be highly reducing in nature and have been applied for the initiation of BHAS type reactions. More recently, Grubbs *et al.* have shown that the combination of KO^{t}Bu plus Et$_3$SiH produced triethylsilyl radicals capable of leading to cleavage of C-O[56] and C-S[60] bonds, as well as the C2 selective silylation of N-substituted indoles.[57]

A hidden gem amongst these publications was the divulgence of information that the KO^{t}Bu/Et$_3$SiH system was also capable of affording reduction in a number of substrates (see Scheme 2.43). Due to the low yields of these reduced products, they were not the focus of the publications by Grubbs *et al.*, however these reductive transformations could be further elaborated to provide another facet to the reactivity of the KO^{t}Bu/Et$_3$SiH mixture.

Indeed, this is what the Murphy Group sought to do by applying their previous knowledge of *in situ* generated electron donor species by the action of KO^{t}Bu on small organic molecules. In fact, the mechanistic studies of Grubbs *et al.*[58-59] discussed earlier mention that the Et$_3$SiO^{t}Bu radical anion (**2.194**) as a possible intermediate formed during the action of KO^{t}Bu on Et$_3$SiH. Radical anion **2.194** would potentially be a very potent electron donor, as such the Murphy group set out to apply the KO^{t}Bu/Et$_3$SiH system to carry out challenging reduction reactions found in the literature. The first substrate type utilised were N-benzylindoles, which have been previously shown to undergo reductive cleavage to indoles and toluene under electron transfer conditions. The first literature example utilised Birch reduction conditions (sodium in ammonia),[113] whilst the other example employed low-valent titanium reagents which were activated by iodine.[114] A range of N-benzylindoles (**5.1 - 5.8**) were synthesised by the Murphy group and subjected to the KO^{t}Bu/Et$_3$SiH system. Cleavage of the benzyl group was observed with each substrate yielding the corresponding indoles in moderate to high yields, whilst the benzyl fragment yielded volatile products which were not isolated. Blank reactions, in the absence of silane, were conducted for each substrate and led to excellent recovery of starting material.

Table 5.1: Results of N-benzylindole cleavages upon treatment with the KO^{t}Bu/Et$_3$SiH system.
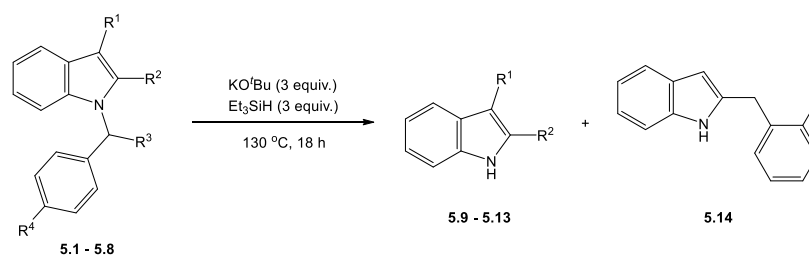
Entry	Substrate	R^1	R^2	R^3	R^4	Yield (%)
1	**5.1**	H	H	H	H	**5.9** (29)
2	**5.2**	H	Me	H	H	**5.10** (49) **5.14** (15)
3	**5.3**	Me	H	H	H	**5.11** (73)
4	**5.4**	Me	H	H	OMe	**5.11** (76)
5	**5.5**	Me	H	H	Me	**5.11** (63)
6	**5.6**	Me	H	Me	H	**5.11** (47)
7	**5.7**	Ph	H	H	H	**5.12** (80)
8	**5.8**	(CH=CH)$_2$	(CH=CH)$_2$	H	H	**5.13** (57)

Further to the N-benzylindoles, N-allylindoles **5.15** and **5.17** were cleaved to their corresponding indoles (**5.11** & **5.18**) in moderate yields of 35 % and 33 %, respectively, whilst **5.15** also afforded 18 % of *o*-isopropylaniline, **5.16**. In order to further test the reducing abilities of the KO^{t}Bu/Et$_3$SiH system, the Murphy Group prepared benzyl methyl ether **5.19** and nitrile **5.21**. Following their reaction with KO^{t}Bu/Et$_3$SiH, cleavage of the methoxy group was observed in 52 % yield, whilst the nitrile was cleaved with a 43 % yield, results which were indicative of electron transfer having occurred. A closely related methyl benzyl ether having been previously shown to require double electron transfer to afford loss of methoxide.[115]
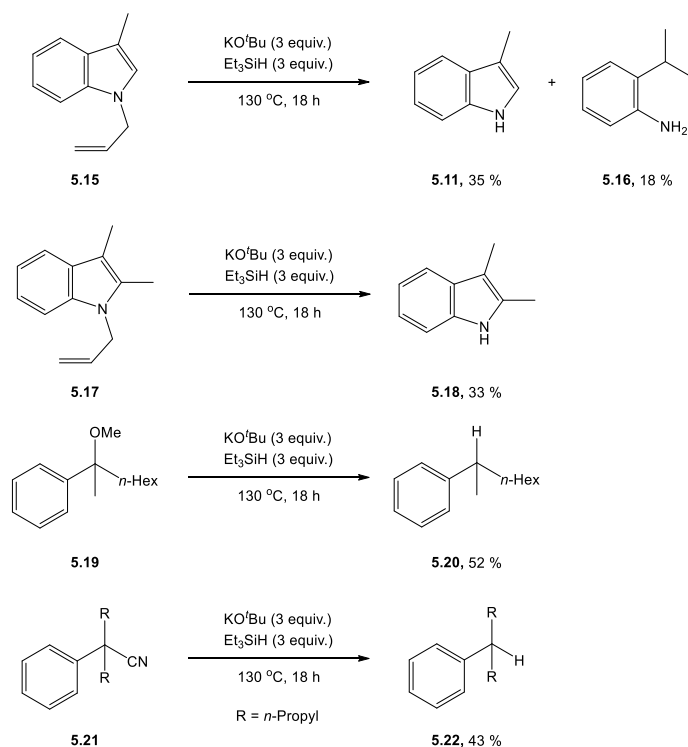
Scheme 5.1: N-allylindoles, methyl benzyl ether and nitrile substrates cleaved by the Murphy Group under KO^{t}Bu/Et$_3$SiH conditions.

Finally, the Murphy Group took the chance to further probe the observations of Grubbs *et al.*[60] who had recovered small quantities (<5 %) of 1,2,3,4-tetrahydronaphthalene during their desulfurisation of 2-naphthalenethiol. They therefore treated naphthalene, phenanthrene and anthracene with 30 equivalents of both KO^{t}Bu and Et$_3$SiH and pleasingly observed the corresponding dihydro compounds in 31 %, 21 % and 85 % yields, respectively.
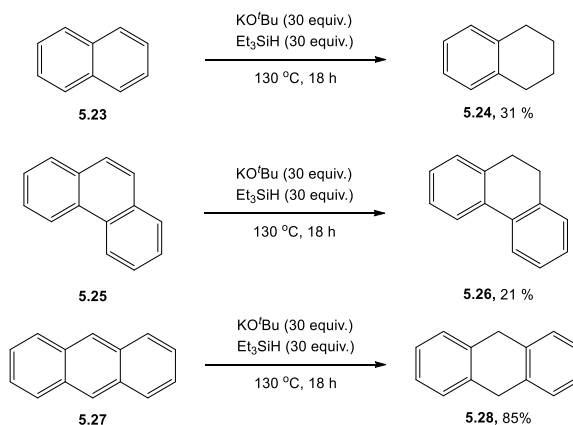
Scheme 5.2: Reduction of arenes by KO^{t}Bu/Et$_3$SiH system carried out by the Murphy Group.

Revisiting the interesting formation of *o*-isopropylaniline (**5.16**) from **5.15**, the Murphy Group sought further substrates where ring-opening of the indole may be observable. They therefore looked to the recent work of Studer *et al.*[116] who had demonstrated ring-opening of N-arylindoles, such as **5.29**, using silyl anions to form *E*-vinylsilanes, such as **5.30**, in good to excellent yields.
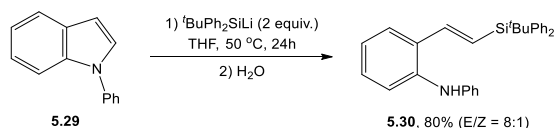
Scheme 5.3: Example of N-phenylindole cleavage by a silyl anion to yield *E*-vinylsilane, as reported by Studer *et al.*[116]

Table 5.2: Rearrangement of N-arylindoles to dihydroacridines when subjected to KO^{t}Bu and Et$_3$SiH, as observed by the Murphy Group.

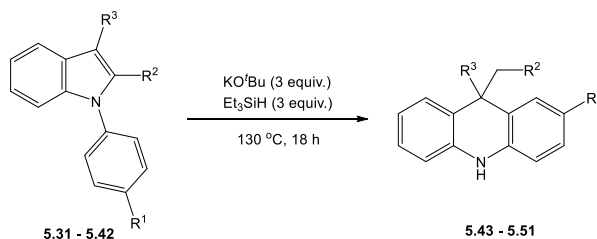| Entry	Substrate	Product	Yield (%)
1	**5.31** R^1=R^2=R^3=H	**5.43** R^1=R^2=R^3=H	58
2	**5.32** R^1=R^2=H, R^3=Me	**5.44** R^1=R^2=H, R^3=Me	77
3	**5.33** R^1=R^2=H, R^3=Et	**5.45** R^1=R^2=H, R^3=Et	66
4	**5.34** R^1=H, R^2=R^3=Me	**5.45** R^1=R^2=H, R^3=Et	53
5	**5.35** R^1=R^2=H, R^3=Ph	**5.46** R^1=R^2=H, R^3=Ph	92
6	**5.36** R^1=Me, R^2=R^3=H	**5.47** R^1=Me, R^2=R^3=H	38
7	**5.37** R^1=R^2=H, R^3=CH(CH$_2$)$_2$	**5.48**, R^1=R^2=H, R^3=CH(CH$_2$)$_2$ **5.49**, R^1=R^2=H, R^3=(CH$_2$)$_2$CH$_3$	12 30
8	**5.38** R^1=R^2=H, R^3=(CH$_2$)$_3$CH=CH$_2$	**5.43** R^1=R^2=R^3=H	12*
9	**5.39** R^1=R^2=H, R^3=(CH$_2$)$_2$CH=CH$_2$	**5.43** R^1=R^2=R^3=H	48*
10	**5.40** R^1=R^2=H, R^3=CH$_2$Ph	No reaction	-
11	**5.41** R^1=R^2=H, R^3=C$_8$H$_{17}$	**5.50** R^1=R^2=H, R^3=C$_8$H$_{17}$	55
12	**5.42** R^1=R^2=H, R^3=C$_4$H$_9$	**5.51** R^1=R^2=H, R^3=C$_4$H$_9$	71

* Isolated as corresponding acridines after oxidation in air

The Murphy Group synthesised a selection of N-arylindoles **5.31 - 5.42** and subjected these to the KO*t*Bu/Et₃SiH reaction conditions; unexpectedly, the indoles underwent conversion to dihydroacridines **5.43 - 5.51**. Conversion occurred with moderate to excellent yields of dihydroacridines, while substituents in the 2- and 3- position of the indole were tolerated as well as substituents on the N-aryl moiety (Table 5.2, entries 2 – 6). In order to gain some mechanistic insights, cyclopropyl substituted indole **5.37** was tested and afforded a mixture of the cyclopropyl substituted dihydroacridine as well as the product of reductive ring opening of the cyclopropane.
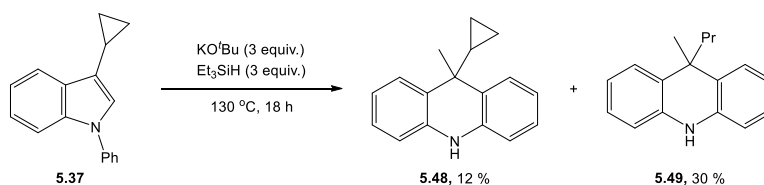
Scheme 5.4: Rearrangement of cyclopropyl substituted indole, with opening of the cyclopropyl ring.

A further radical probe substrate, **5.38**, was reacted under the KO*t*Bu/Et₃SiH conditions and yielded the dihydroacridine **5.43** following cleavage of the pentenyl side chain (Table 5.2, entry 8). In addition to **5.43**, cyclised products **5.52** and **5.53** were also formed. The similar substrate, **5.39**, bearing a butenyl group also yielded dihydroacridine **5.43** following loss of the butenyl side chain, however no cyclised products were formed (Table 5.2, entry 9).
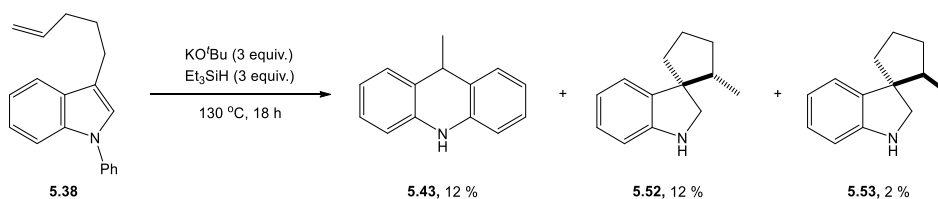
Scheme 5.5: Reaction of indole **5.38** under KO*t*Bu/Et₃SiH conditions yielded a mixture of rearranged products.

In order to obtain further insights into the above experimental observations, DFT calculations were then utilised to understand the energies associated with forming the postulated reactive intermediates. As well as this, the mechanism of reduction for the N-benzylindole and arene substrates was studied in order to clarify whether indeed single electron transfer chemistry was in operation or alternatively whether reduction was being afforded by hydride reactivity.

5.2 Computational Methods

DFT calculations in this chapter were run using the M06-2X functional[71-72] and 6-31++G(d,p)[74-75, 104-110] basis set on all atoms. Solvation was modelled implicitly using the CPCM model[84] with parameters for triethylamine as solvent. No silane (Me$_3$SiH or Et$_3$SiH) solvents were parameterised within Gaussian09, triethylamine was chosen as solvent since it has a similar dielectric constant (ε = 2.3832) to triethylsilane (ε = 2.323).[117] All calculations were carried out in Gaussian09.[111]

Calculated ΔG_{rel} and $\Delta G^{\ddagger}$ are relative to the reactants for each step and include the formation of reactant complexes and dissociation of product complexes where appropriate.

In order to model single electron transfer reactions computationally, Marcus-Hush Theory[87] was employed with the 4-point method of Nelsen et al.[92] or the complexation method of Tuttle, Murphy and co-workers[93] allowing calculation of the reorganisation energy (λ), ΔG_{rel} and ΔG^*. The Nelsen 4-point method requires optimisation of the individual electron donor and acceptor species, before and after single electron transfer. Single point energy calculations must then be performed on these optimised geometries using the charge and multiplicity of their other state in the electron transfer reaction. The complexation method requires optimisation of the electron donor and acceptor as a complex in both the reactant and product electronic states. Single point energy calculations must then be performed on these optimized geometries with the alternative electronic configuration.

Trimethylsilane was used in place of triethylsilane in order to reduce computational cost, the trimethylsilane has been shown to be representative of triethylsilane by Grubbs *et al*.[60]

In order to avoid complications with electron transfer calculations utilising the Nelsen 4-point methodology, potassium counter ions were not utilised throughout the work in this chapter. Use of naked *tert*-butoxide monomer has been shown by Murphy, Tuttle and co-workers to be a good representation of the tetrameric form of KO*t*Bu.[118] Grubbs *et al*. also utilised *tert*-butoxide anion within their calculations stating that naked *tert*-butoxide would be free following the formation of cation-π complexes between substrates and KO*t*Bu tetramer.[58]

5.3 Formation of Reactive Species from KO^{t}Bu/Et$_3$SiH

Given the Murphy and Tuttle groups knowledge and experience of working with KO^{t}Bu and electron donor chemistry, we proposed that an electron donor species was being formed *in situ* by reaction of KO^{t}Bu and Et$_3$SiH. In line with the literature discussed earlier regarding pentavalent silicates acting as electron donors, formation of such a species was investigated first. The pentavalent silicate **5.56** would exist in equilibrium with the separated species, with the latter existing in slightly higher concentrations since formation of the silicate was found to be endergonic.
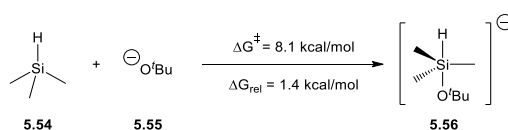
Scheme 5.6: Formation of pentavalent silicate **5.56** by addition of *tert*-butoxide to trimethylsilane.

As well as **5.56**, Grubbs *et al.*[59] also discussed the possibility of a silicate radical anion as a reactive intermediate, formation of **5.58** was therefore explored. Since Grubbs *et al.*[59] had already presented evidence for the intermediacy of trialkylsilyl radicals through their experimental studies, the trimethylsilyl radical was taken as the likely starting point for forming **5.58**. Coupling of a trimethylsilyl radical with *tert*-butoxide was found to be highly exergonic, as was abstraction of a hydrogen atom from **5.56** by trimethylsilyl radical.
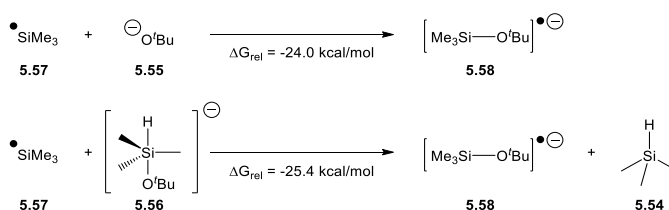
Scheme 5.7: Formation of silicate radical anion **5.58** by reaction with trimethylsilyl radical.

Finally, formation of the trimethylsilyl anion (**5.59**) by deprotonation **5.54** was investigated, as this could potentially act as an electron donor and simultaneously generate trimethylsilyl radicals. However, the deprotonation was significantly endergonic, with the resultant equilibrium lying heavily toward the reactants.
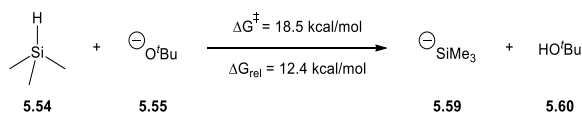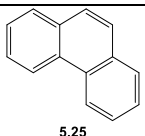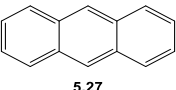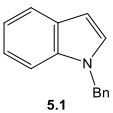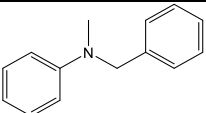
Scheme 5.8: Deprotonation of trimethysilane by *tert*-butoxide.

5.4 SET *vs* Hydride Reduction by KO*t*Bu/Et₃SiH

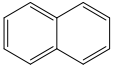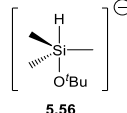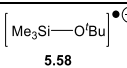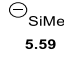As discussed in the background section, a range of substrates including polyaromatic hydrocarbons and N-benzylindole have been reduced by the KO*t*Bu and Et₃SiH reducing system. The first proposal for reduction of such substrates is by single electron transfer from a potential electron donor species, of which three have been postulated to form upon the reaction of KO*t*Bu with Et₃SiH (see section 5.3).

Table 5.3: Calculated reorganisation energy, relative free energy and predicted free energy of activation for single electron transfer from candidate electron donors to a range of substrates. (All energies calculated using the Nelsen 4-point method)

Substrate	Electron Donor	λ (kcal/mol)	ΔG_{rel} (kcal/mol)	ΔG^* (kcal/mol)
5.23	**5.56**	25.8	35.3	36.2
	5.58	3.4	-22.3	25.7
	5.59	15.9	24.6	25.8
5.25	**5.56**	26.3	32.5	32.9
	5.58	3.9	-25.0	28.3
	5.59	16.4	21.8	22.3
5.27	**5.56**	25.7	19.8	20.1
	5.58	3.3	-37.8	90.0
	5.59	15.8	9.1	9.8
5.1	**5.56**	27.8	49.4	53.6
	5.58	5.4	-8.1	0.3
	5.59	17.9	38.7	44.8
5.61	**5.56**	28.2	53.1	58.6
	5.58	5.8	-4.4	0.1
	5.59	18.3	42.4	50.4

Single electron transfer from trimethylsilyl anion (**5.59**) was found to be highly endergonic for each substrate (Table 5.3), which taken in conjunction with the poor thermodynamics for formation of **5.59**, allows it to be ruled out as a candidate electron donor within these reactions. The second candidate electron donor species of interest was the pentavalent silicate **5.56**, this was found to exhibit poorer thermodynamics than **5.59** with SET to

each substrate being highly endergonic. For both **5.56** and **5.59**, the free energies of activation predicted by Marcus theory were close in energy to the relative free energies, showing that SET would also be kinetically unfavourable. The final candidate electron donor studied was the silicate radical anion **5.58**, which was hypothesised to be a strong electron donor species. This was indeed found to be the case for both N-benzylindole (**5.1**) and N-methyl-N-benzylaniline (**5.61**). The single electron reduction of **5.1** was found to be exergonic (-8.1 kcal/mol) with a predicted free energy of activation of 0.3 kcal/mol, suggesting that electron transfer would occur rapidly. Upon accepting an electron, **5.1** becomes radical anion **5.62**, which would then have to undergo fragmentation to form **5.63**, which upon protonation would yield the observed product, **5.9**.
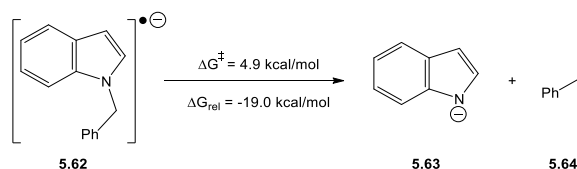
Scheme 5.9: Fragmentation of N-benzylindole radical anion to indole anion and tolyl radical.

Fragmentation of the N-benzylindole radical anion to indole anion and tolyl radical would occur readily with the reaction being highly exergonic and requiring only 4.9 kcal/mol to overcome the transition state. Therefore, **5.58** has the ability to reductively cleave N-benzylindole. Whilst it has been shown that reductive cleavage of **5.1** should occur readily upon reaction with **5.58**, the experimental yield for this reaction was only 29%. This could be due to formation of C2 and/or C3 silylated indoles similar to those observed by Grubbs *et al.* in their lower temperature reactions - indeed when the C2 or C3 position was substituted as in **5.2** - **5.8** higher yields were observed.

However, when **5.58** was utilised as an electron donor towards the polyaromatic hydrocarbons naphthalene (**5.23**), phenanthrene (**5.25**) and anthracene (**5.27**) an interesting trend was observed. The relative free energy for single electron reduction followed the expected trend, with anthracene being more exergonic than phenanthrene, which in turn was more exergonic than naphthalene. When examining the predicted free energies of activation however, naphthalene was found to be smallest (25.7 kcal/mol) with anthracene having the largest at 90.0 kcal/mol. Each of the polyaromatic hydrocarbons (PAHs) had a similar reorganisation energy (~3 kcal/mol) so this cannot explain the increased activation energies. Therefore it can be proposed that this is an example of the Marcus inverted region,[119] whereby substrates with similar reorganisation

energies, but which are increasingly exergonic display retarded electron transfer reactions. For this to be proven however a detailed experimental study would be required.

Table 5.4: Optimised geometries of candidate electron donors **5.56**, **5.58** and **5.59** (left) as well as the respective products following electron transfer (right).
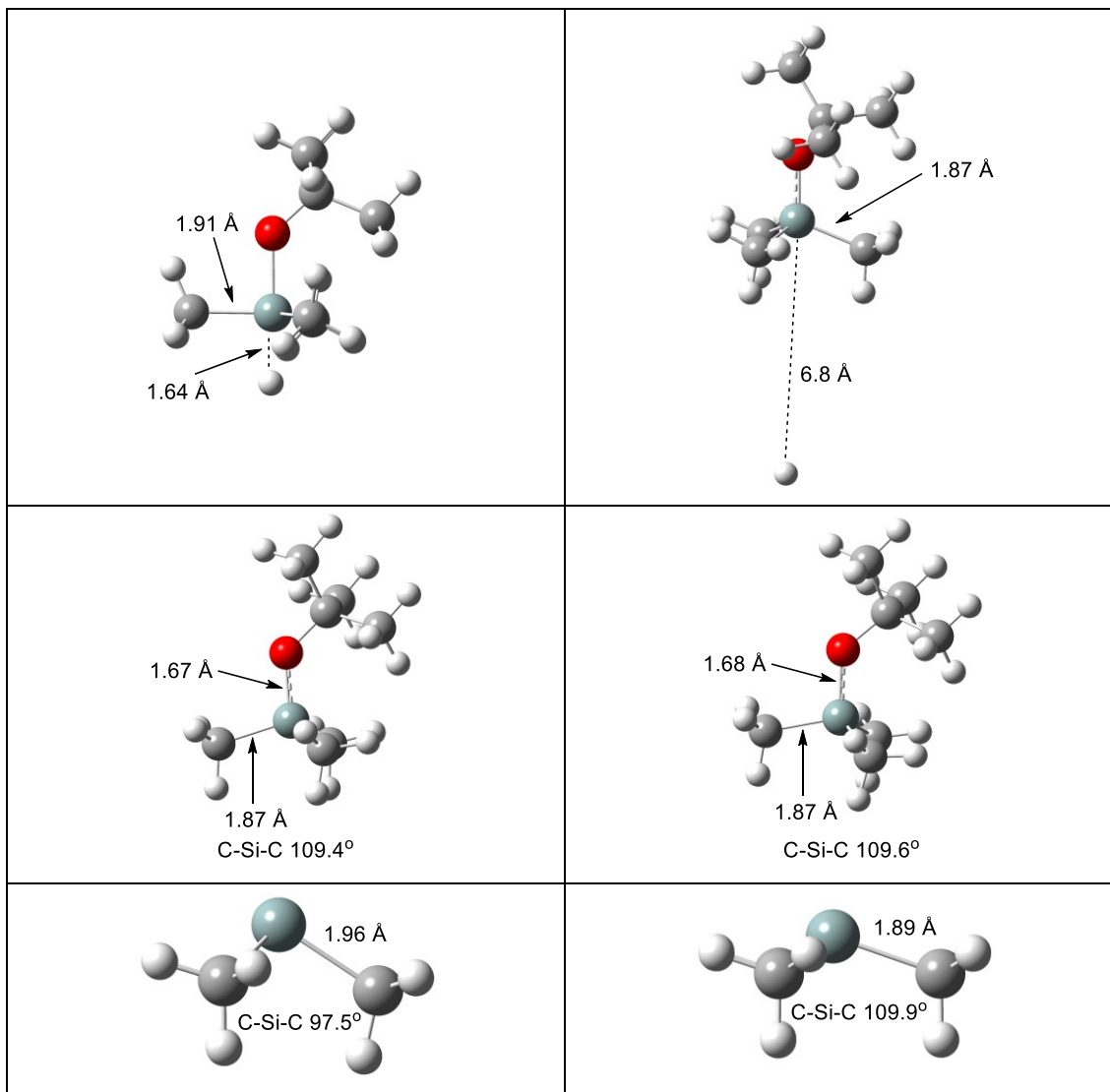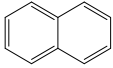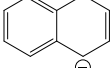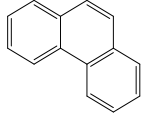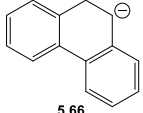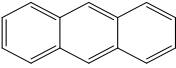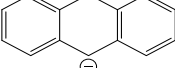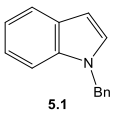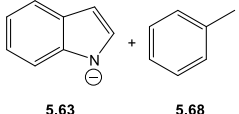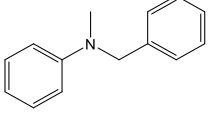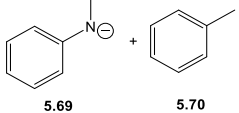
An important component for the prediction of ΔG^* for SET is the reorganisation energy, λ. The reorganisation energy was smallest for all substrates with the radical anion electron donor **5.58**, while **5.56** was always found to have the largest reorganisation energy. Upon investigation of the optimised geometries of the electron donor species before and after electron transfer, some key structural changes were noted (Table 5.4). For **5.58** (middle row) the structure of the neutral species formed after electron loss was found to be structural similar with very small changes in bond angles and lengths noted. On the other hand, for **5.59** (bottom row) the most significant structural change upon loss

of an electron was found to be the C-Si-C bond angle which become 109.9° in the Me₃Si radical, such a large change explains the much larger reorganisation energies for SET reactions with **5.59** as electron donor. Finally, the largest reorganisation energy, for **5.56**, can be explained by the dissociation of the hydrogen atom following electron transfer. Optimisation of Me₃HSiO^{t}Bu radical resulted in the lengthening of the Si-H distance to 6.8 Å from 1.64 Å in **5.56**, this was also coupled with a change in geometry to tetrahedral from trigonal bipyramidal.

In order to determine the mechanism for reduction of the PAHs, an alternative to SET had to be investigated. Taking the candidate electron donors studied above, it could also be hypothesised that **5.56** could act as a reducing agent by delivery of a hydride to a substrate. The hydride reduction of **5.23, 5.25, 5.27, 5.1** and **5.61** was therefore probed by DFT calculations to determine the free energy of activation and relative free energy.

Table 5.5: Calculated free energies for hydride transfer from pentavalent silicate **5.56** to a range of substrates.

Substrate	Product	$\Delta G^{\ddagger}$ (kcal/mol)	ΔG_{rel} (kcal/mol)
5.23	5.65	21.6	-13.2
5.25	5.66	20.0	-14.8
5.27	5.67	16.7	-29.4
5.1	5.63 + 5.68	36.9	-53.7
5.61	5.69 + 5.70	40.7	-41.2

In contrast to their SET reduction by **5.58**, **5.1** and **5.61** were found to have large free energies of activation which would rule out their reduction by delivery of hydride from **5.56**, despite the reactions overall being highly exergonic (Table 5.5). In contrast, the addition of hydride to the PAHs was found to be accessible and exergonic in all cases. Here, anthracene was found to have the lowest free energy of activation and was also

the most exergonic, with naphthalene having the largest free energy of activation and least exergonic.

Taking the results of single electron transfer alongside hydride transfer, it was clear that the PAHs were being reduced through a hydride transfer mechanism whereas N-benzylindole and N-methyl-N-benzylaniline were being reduced by SET.

5.5 Rearrangement of N-phenylindoles

Based on the experimental observations described in Section 5.1, we proposed an electron transfer based mechanism to explain the rearrangement of N-arylindoles to the corresponding dihydroacridines, Scheme 5.10. Single electron transfer to N-phenylindole, here from radical anion **5.58**, would generate radical anion **5.71** which could undergo C-C bond cleavage to generate **5.72**. Hydrogen atom abstraction from triethylsilane by the vinyl radical would generate styryl intermediate **5.73**. SET from **5.58** to **5.73** would afford radical dianion **5.74**, where, if the electron resides within the N-phenyl moiety could be protonated to yield cyclohexadienyl radical **5.75**. We then proposed that **5.75** would undergo 6-*exo*-trig cyclisation generating primary radical **5.76** which could abstract a hydrogen atom, intramolecularly. Protons adjacent to radicals have been shown to undergo a radical enhancement of deprotonation or "RED shift" making them highly acidic.[120] As such **5.77** should be readily deprotonated to afford radical dianion **5.78** which should readily donate an electron to another molecule of N-phenylindole, affording **5.79**. Intermediate **5.79** would afford the observed product upon aqueous work-up.
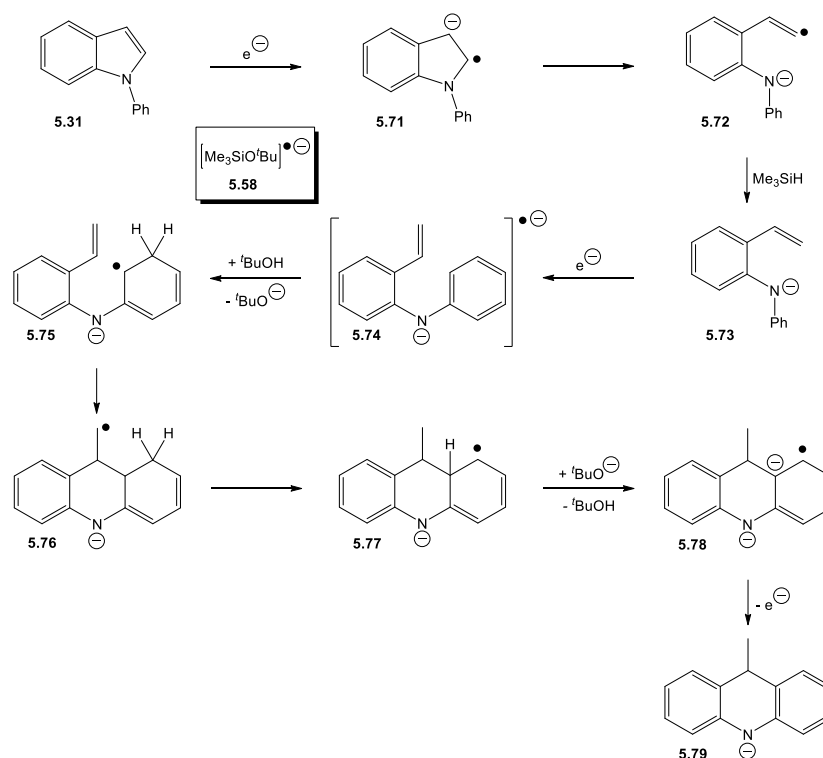
Scheme 5.10: Mechanism proposed by the Murphy and Tuttle Groups for rearrangement of N-phenylindole to 9-methyl-9,10-dihydroacridine.
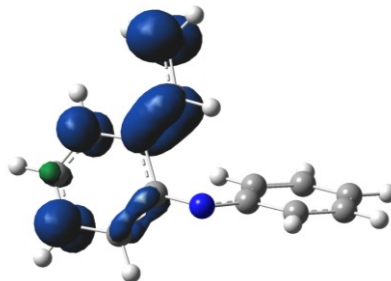
Figure 5.1: Spin density map for optimised geometry of **5.74**.

Following optimisation of **5.74**, the SOMO was examined to determine where the electron density was residing within the molecule. The SOMO was found to be residing on the styrene moiety, therefore the mechanism proposed in Scheme 5.10 could not be operative. An alternative mechanism (Scheme 5.11) was therefore proposed that considers the position of the SOMO.

The alternative mechanism follows the same initial steps as that proposed above, until radical dianion **5.74**, which could be protonated by *t*BuOH. This radical (**5.80**) could then undergo addition to the N-phenyl ring forming cyclohexadienyl radical **5.77**.
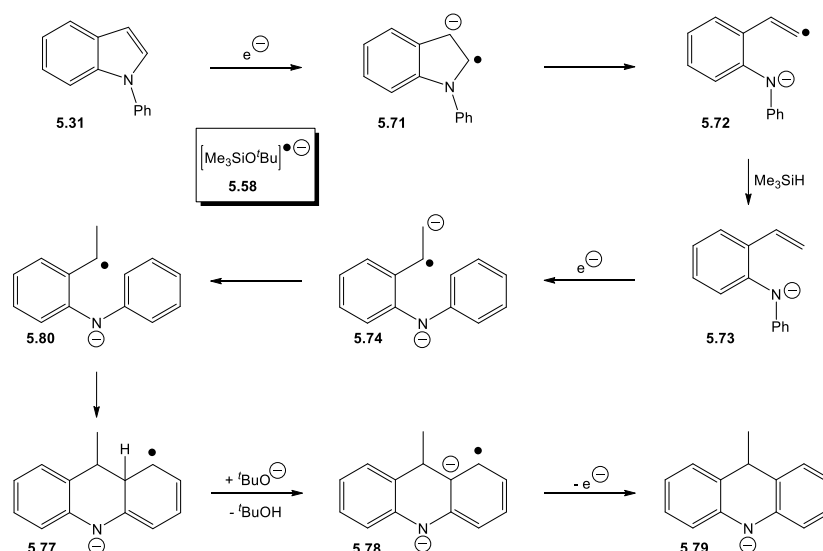
Scheme 5.11: Adapted mechanism for rearrangement of N-phenylindole to 9-methyl-9,10-dihydroacridine.

Investigation from the initial electron transfer between **5.58** and N-phenylindole showed that SET would be facile, with a small predicted free energy of activation (0.9 kcal/mol) and the reaction overall being exergonic (-11.5 kcal/mol). However, subsequent ring cleavage of N-phenylindole radical anion was highly endergonic (28.2 kcal/mol) and had an associated free energy barrier of 32.8 kcal/mol. Although if this step were coupled to a kinetically accessible exergonic process it could be productive, a new mechanistic proposal was sought which would be more thermodynamically accessible. Very recently Jeon *et al.*[121] published a report of hydrogen atom transfer to vinylarenes from the combination of KO^{t}Bu and a hydrosilane. They performed a wide ranging experimental and computational study of the reaction, and were able to determine that the pentavalent silicate, formed by addition of KO^{t}Bu to a hydrosilane, was acting as the source of hydrogen atoms. A simple example of this can be seen from their deuterosilylation of **5.81**, utilising deuterated diphenylsilane, where the deuterium atom is transferred to preferentially form the benzyl radical.
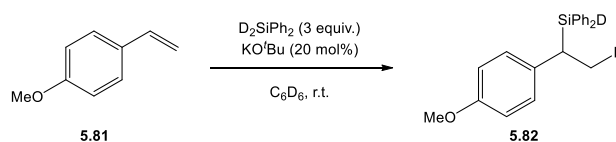
Scheme 5.12: Deuterosilylation of *p*-methoxystyrene by KO^{t}Bu and deuterated diphenylsilane, reported by Jeon *et al.*[121]

Understanding that pentavalent silicates such as **5.56** can act as hydrogen atom donors, allowed a new mechanism to be proposed for the rearrangement of N-phenylindole to 9-methyl-9,10-dihydroacridine, Scheme 5.13.
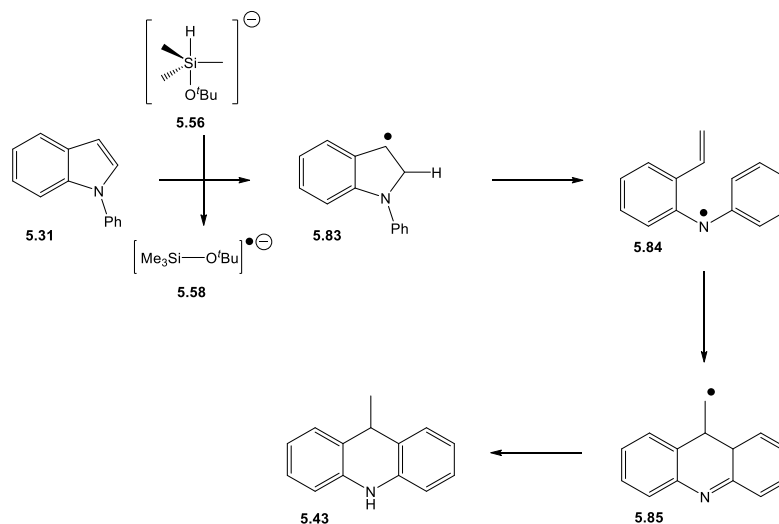
Scheme 5.13: Proposed mechanism for rearrangement of N-phenylindole initiated by hydrogen atom transfer from **5.56**.

Due to the biradical nature of the initial hydrogen atom transfer step, this could not be studied within this work. A simplified addition of a hydrogen atom only to N-phenylindole was however studied, in order to gauge the energies associated with this simplified hydrogen atom transfer. Hydrogen atom addition to the 2-position of N-phenylindole would occur readily, however the subsequent ring opening of **5.83** was found to be uphill by 12.6 kcal/mol. Likewise, the ring closure to afford **5.84** was uphill by 16.9 kcal/mol, two such thermodynamically unfavourable steps rules out this proposed mechanism.

Table 5.6: Calculated free energies for the mechanism proposed in Scheme 5.13.

Reaction Step	$\Delta G^{\ddagger}$ (kcal/mol)	ΔG_{rel} (kcal/mol)
5.31 - **5.83** (Using Hydrogen atom in place of **5.56**)	9.5	-21.9
5.83 - **5.84**	32.1	12.6
5.84 - **5.85**	32.1	16.9

5.6 Conclusions

Formation of the highly reducing Me$_3$SiO^{t}Bu radical anion by coupling of trimethylsilyl radical and *tert*-butoxide anion (ΔG_{rel} = -24.0 kcal/mol) or hydrogen atom abstraction from Me$_3$Si(H)O^{t}Bu anion by trimethylsilyl radical (ΔG_{rel} = -25.4 kcal/mol) has been shown to be favourable. Meanwhile, the formation of trimethysilyl anion by deprotonation of trimethylsilane by *tert*-butoxide was ruled out due to unfavourable energetics ($\Delta G^\ddagger$ = 18.5 kcal/mol and ΔG_{rel} = 12.4 kcal/mol). Grubbs *et al.*[57, 60] had already demonstrated that open-shell species (trimethylsilyl radical) were present upon the mixing of KO^{t}Bu and Et$_3$SiH, this work has demonstrated that this radical would undergo further transformation to yield a highly reducing species.

With a highly reducing species present in the reaction system, the single electron reduction of the experimentally studied substrates was probed utilising DFT calculations applying Marcus Theory. Here, it was found that N-benzylindole and N-methyl-N-phenylaniline would be reduced by **5.58**, whereas the polyaromatic hydrocarbons naphthalene, phenanthrene and anthracene were not able to undergo single electron reduction by **5.58**. Indeed, for these substrates the Marcus inverse region[119] appeared to have been entered, with electron transfer becoming more retarded (ΔG^*: anthracene > phenanthrene > naphthalene) as the reductions became more exergonic (ΔG_{rel}: anthracene > phenanthrene > naphthalene).

The reduction of anthracene, phenanthrene and naphthalene was instead shown to be occurring *via* hydride reduction, with the hydride being delivered from pentavalent silicate anion **5.56**. The similar reduction of N-benzylindole and N-methyl-N-phenylaniline was demonstrated to be inaccessible at the reaction conditions, lending further evidence that the single electron transfer reduction of these substrates was indeed taking place.

Following the observation of a rearranged product upon treatment of N-phenylindole with KO^{t}Bu and Et$_3$SiH, a range of mechanistic proposals were probed by DFT calculations in the search for mechanistic insights about this reaction. Despite single electron transfer from **5.58** to N-phenylindole being favourable, subsequent ring opening of N-phenylindole radical anion was shown to be an unproductive mechanistic route. In an alternative to single electron transfer, and following the novel work of Jeon *et al.*,[121] hydrogen atom transfer to the 2-position of the indole was demonstrated to be accessible and exergonic. However, in a similar manner to N-phenylindole radical anion, the ring opening of N-phenylindole radical had a large barrier ($\Delta G^\ddagger$ = 32.1 kcal/mol) and was

endergonic (ΔG_{rel} = 12.6 kcal/mol). Further to this the subsequent step of ring closure to form the dihydroacridine moiety exhibited both a similar barrier and relative energy, also leading this mechanism to be dismissed.

In this chapter, the search for mechanistic insights in the KO^{t}Bu and Et$_3$SiH system has been a tale of two sides: first it was shown that the reagents can form two competent reducing agents, namely the single electron reductant **5.58** and the hydride reductant **5.56**. However, mechanistic insights were not successfully obtained for the curious rearrangement of *N*-phenylindole upon its treatment with KO^{t}Bu and Et$_3$SiH - despite this, the computational efforts presented in this chapter have not been in vain. Instead, they have guided further proposals as to the mechanism of this reaction as well as having guided the work of experimental colleagues in the design of experiments to further the search for mechanistic insights.

5.7 Future Work

Within the literature and throughout this chapter the diversity of reactions which have been found to occur upon treating substrates with the combination of KO^{t}Bu and a hydrosilane has been wide. Therefore, testing the KO^{t}Bu and hydrosilane reagents in reactions with a wide variety of substrates not already reported would be beneficial. This could yield important information about the reactivity exhibited for specific classes of substrate. For example, could the work of Jeon *et al*. with hydrosilylation of styrenes be extended to other alkenes or alkynes? Or would this result in reduction of these substrates to alkanes? Investigating a diverse catalogue of substrates could allow trends in the observed reactivity towards substrate classes to be categorised, this would therefore allow further investigation by experimental and computational means to elucidate whether hydrogen atom transfer, electron transfer, silyl radical addition or hydride transfer pathways were operating.

Perhaps the most impactful future work would be the experimental investigation of the observed Marcus inverse region for the polyaromatic hydrocarbons anthracene, phenanthrene and naphthalene. Could this be confirmed by experimental methods it would provide a further example of the Marcus inverse region, 35 years on from the first experimental evidence proving its existence.[122]

In addition, further experimental and computational efforts should be directed towards investigating the intriguing rearrangement of N-phenylindole to 9-methyl-9,10-

dihydroacridine. Key experimental evidence may be gained by carrying out the reaction with deuterated silanes in order to assess whether a hydrogen atom transfer type mechanism could be initiating the rearrangement. Should this be the case, it might be expected that deuterium would be observed on the 9-methyl group, if a similar hydrogen atom transfer to that reported by Jeon *et al*. towards styrenes was taking place.

6. Reduction of Benzophenone by KO*^t*Bu Under Visible Light Irradiation

(NB: Experimental work discussed in this chapter was carried out by Giuseppe Nocera)

KO*t*Bu-Benzophenone Complex
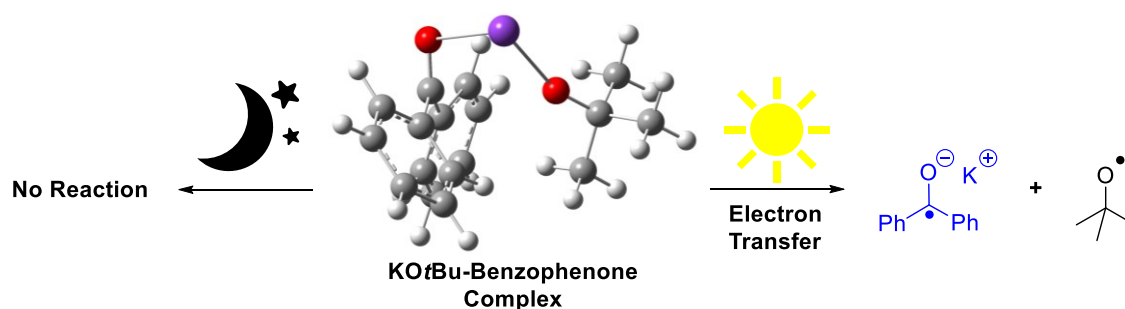
6.1 Background

The mechanism for reduction reactions between strong bases, such as alkali metal alkoxides or lithium dialkylamides, and electrophiles, such as benzophenone, has been debated for some time. Therein lies a tale of two possible mechanisms, single electron transfer or nucleophilic substitution. The 1980s saw a range of publications dedicated to research in this particular field, with the groups of Eugene Ashby and Martin Newcomb dominating the landscape.

Central to the debate was understanding the mechanism of reduction when strong bases bearing α/β-hydrogens *vs* when no α/β-hydrogens were present in the base (α-hydrogen in the case of alkoxides or β-hydrogen in the case of amides). Newcomb *et al*.[123-124] were particularly focused on the reactivity of lithium dialkylamides with benzophenone and whether reduction to benzophenone ketyl radical anion occurred *via* single electron transfer or hydride transfer pathways. In contrast, Ashby *et al*.[2, 35-36, 125] were concerned with the similar reactivity of alkali metal alkoxides with benzophenone.

The work of both groups identified that when an α-hydrogen was present in the alkoxide or a β-hydrogen in the amide base the reaction would proceed by initial hydride transfer to benzophenone (**6.1** to **6.2**). Deprotonation of **6.2** to generate dianion **6.5** would then be followed by SET to a molecule of neutral benzophenone generating two benzophenone ketyl radical anions (**6.4**). These could then yield the observed reduction product benzhydrol, **6.3**, by hydrogen atom abstraction followed by protonation.
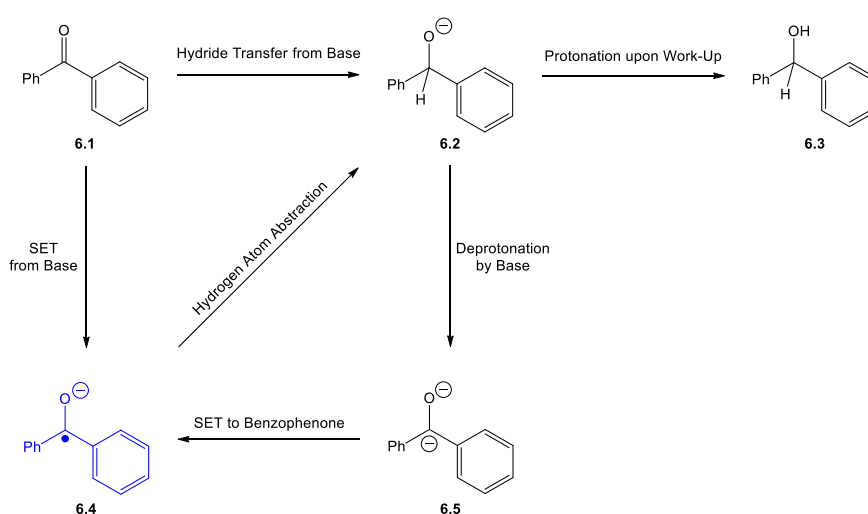
Scheme 6.1: Two proposed pathways for reduction of benzophenone by alkali metal alkoxide or amide bases, generating benzophenone ketyl radical anion *in situ*.

Newcomb *et al.*[123-124] studied the reduction of benzophenone with amide bases, in particular they used a mechanistic probe, N-lithio-N-butyl-5-methyl-1-hex-4-enamine (**6.6**), in an attempt to trap the aminyl radical formed following electron transfer from the amide. Whilst benzophenone was reduced to benzhydrol in the presence of **6.6**, no cyclised products of the amide base were observed; instead imines **6.7** and **6.8** were detected. These observations provided good evidence in favour of the hydride transfer mechanism.
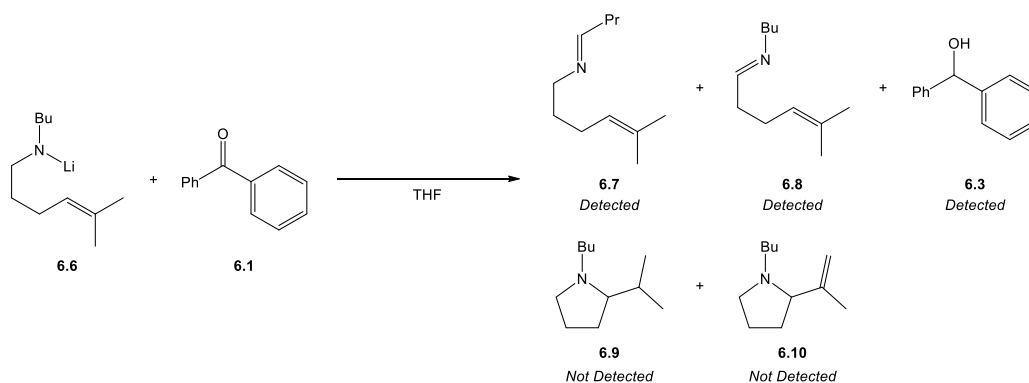
Scheme 6.2: Reaction of Newcomb *et al.*[123] between amide (**6.6**, a probe to test for electron transfer) and benzophenone.

In a further investigation, Newcomb *et al.*[124] sought to understand the formation of benzophenone ketyl radical anion in reactions of lithium dialkylamide bases (containing β-hydrogens) with benzophenone. Having previously shown that lithium dialkylamide bases do not transfer electrons to benzophenone, but can transfer β-hydrides, they moved to studying the subsequent step of the mechanism – deprotonation of lithium benzhydrolate. Upon reaction of lithium benzhydrolate with LDA Newcomb *et al.* noted the reaction mixture turning deep red, the previously reported colour for benzophenone dianion.[126] The reaction was also followed by NMR, with ^{1}H NMR showing a decrease in intensity for the methine proton of lithium benzhydrolate relative to the aromatic protons as the reaction progressed. These results supported the proposed mechanism of dianion formation, then electron transfer from dianion to neutral benzophenone to yield two molecules of benzophenone ketyl radical anion.

However, this cannot explain the mechanism for benzophenone ketyl radical anion formation when alkoxides bearing no α-hydrogen are used, *i.e.*, KO^tBu. To this end, Ashby *et al.*[2, 35, 125] proposed that in fact, alkoxides were able to act as single electron donors towards benzophenone to yield the benzophenone radical anion. In the case of alkoxides bearing an α-hydrogen, the ketyl would abstract this from another molecule of

alkoxide, ultimately forming benzhydrol. However, direct electron transfer is highly unlikely due to the mismatched electrochemical potentials of KO^{t}Bu (+0.1 V vs SCE in DMF)[40] and benzophenone (cited values vary between -1.31 V vs SCE to -2.2 V in DMF).[127-129]

Alternatively, based on our group's previous interests in organic electron donor formation discussed earlier - we proposed that organic electron donors may be formed by addition of *tert*-butoxide to a phenyl moiety of benzophenone followed by deprotonation to yield a dianion. This could then act as a single electron donor towards benzophenone, generating the ketyl radical anion. We therefore utilised DFT calculations to compare the formation of electron donor species with the direct electron transfer from KO^{t}Bu to benzophenone.
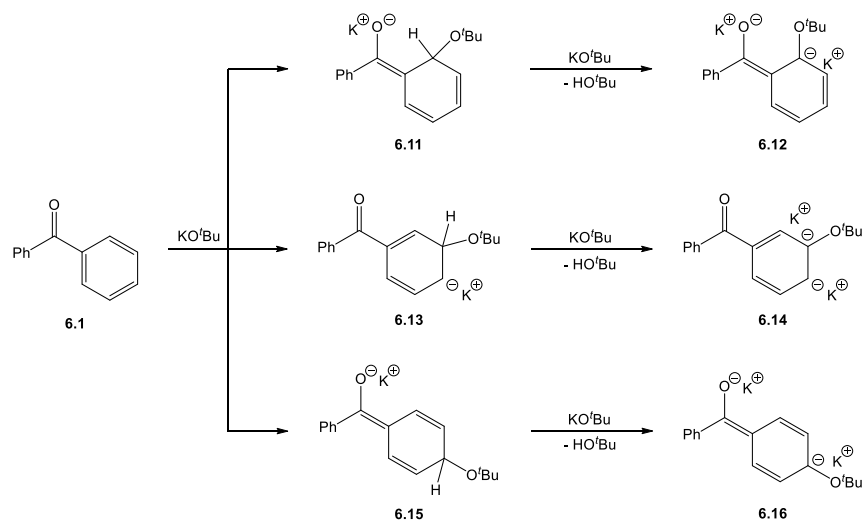
Scheme 6.3: Proposed formation of organic electron donors by reaction of KO^{t}Bu with benzophenone.

6.2 Computational Methods

DFT calculations in this chapter were run using the M06-2X functional[71-72] and 6-31++G(d,p)[74-75, 104-110] basis set on all atoms. Solvation was modelled implicitly using the CPCM model[84] with parameters for tetrahydrofuran as solvent. Time-dependent DFT (TDDFT)[130] calculations were performed on the M06-2X/6-31++G(d,p) optimised geometries, with the CAM-B3LYP functional,[131] due to its good performance with intermolecular charge transfer (CT) excitations,[132] 6-31++G(d,p) basis set and CPCM solvent model with tetrahydrofuran as solvent. All calculations were carried out in Gaussian09.[111]

Calculated ΔG_{rel} and $\Delta G^{\ddagger}$ are relative to the reactants for each step and include the formation of reactant complexes and dissociation of product complexes where appropriate.

In order to model single electron transfer reactions computationally, Marcus-Hush Theory[87] was employed with the 4-point method of Nelsen *et al.*[92] or the complexation method of Tuttle, Murphy and co-workers[93] allowing calculation of the reorganisation energy (λ), ΔG_{rel} and ΔG^*. The Nelsen 4-point method requires optimisation of the individual electron donor and acceptor species, before and after single electron transfer. Single point energy calculations must then be performed on these optimised geometries using the charge and multiplicity of their other state in the electron transfer reaction. The complexation method requires optimisation of the electron donor and acceptor as a complex in both the reactant and product electronic states. Single point energy calculations must then be performed on these optimized geometries with the alternative electronic configuration.

6.3 Investigating the Possible Formation of Organic Electron Donors

Applying the previous knowledge and experience of the Murphy and Tuttle groups, the starting point for investigating the formation of the blue coloured benzophenone ketyl radical anion, from the reaction between benzophenone and KO^tBu, focused on the possible formation of organic electron donors. This led to the proposed mechanism depicted in Scheme 6.3, where first, addition of *tert*-butoxide to the *ortho*, *meta,* or *para* position of a phenyl ring in benzophenone forms anions **6.11**, **6.13** and **6.15**, respectively. A subsequent deprotonation by another molecule of *tert*-butoxide would lead to dianions **6.12**, **6.14** and **6.16**, which would likely be very potent organic electron donors.

The addition of *tert*-butoxide to the *ortho, meta* and *para* positions was calculated both in the presence and absence of the potassium counter ion. Reactant complexes for addition reactions, which were obtained via optimisation of the final IRC structures, can be seen in Figure 6.1. Examining the results for tert-butoxide first, Figure 6.2, addition to the *meta* position (*blue line*) was endergonic by 26.3 kcal/mol, with an associated free energy barrier of 28.8 kcal/mol. Similarly, KO^tBu addition to the *meta* position (Figure 6.3, *blue line*) was endergonic by 27.5 kcal/mol whilst having a free energy barrier of 30.1 kcal/mol. The barrier for both reactions was around 2-3 kcal/mol higher than the relative free energies, showing that these reactions would be rapidly reversible. Addition at the *ortho* position exhibited a higher free energy barrier for KO^tBu (Figure 6.3, *green line*, 26.2 kcal/mol) than naked *tert*-butoxide (Figure 6.2, *green line*, 23.2 kcal/mol), whilst also being significantly more endergonic, 19.3 kcal/mol compared to 13.4 kcal/mol. *Para* addition showed a similar free energy barrier (~23 kcal/mol) for both *tert*-butoxide and KO^tBu, whilst the relative free energy was more endergonic for KO^tBu (Figure 6.3, *red line*, 17.5 kcal/mol) than naked *tert*-butoxide (Figure 6.2, *red line*, 13.0 kcal/mol).

At this stage *meta* addition was ruled out as the equilibrium for such a reaction at the experimental conditions (70 °C) would lie almost exclusively toward reactants. Meanwhile, the *ortho* and *para* additions show an equilibrium which lies in favour of the reactants by several orders of magnitude. Despite this, the subsequent deprotonation of the *ortho* and *para* adducts by *tert*-butoxide to yield dianionic candidate electron donors was calculated, Figure 6.2 & Figure 6.3. Deprotonation in the *ortho* position (*green line*) had a very different free energy barrier when either naked *tert*-butoxide (34.9 kcal/mol) or KO^tBu (20.3 kcal/mol) was utilised, similarly the relative free energy for naked *tert*-butoxide (26.3 kcal/mol) was 9.8 kcal/mol more endergonic than with KO^tBu

(16.5 kcal/mol). It can therefore be seen that formation of **6.12** would not be accessible under the reaction conditions for either *tert*-butoxide or KO^tBu since the energy spans were found to be 48.3 kcal/mol and 39.6 kcal/mol in order to afford the deprotonation.

The free energy barrier for deprotonation in the *para* position (*red line*) was found to be higher for *tert*-butoxide (34.2 kcal/mol) than KO^tBu (29.4 kcal/mol), and similarly the overall free energy difference was found to be more endergonic for *tert*-butoxide (18.9 kcal/mol) than KO^tBu (3.4 kcal/mol). *Para* addition and subsequent deprotonation to form **6.16** would therefore be inaccessible since the overall energy span for *tert*-butoxide was 47.2 kcal/mol and for KO^tBu was 46.9 kcal/mol.

a)   **b)**

c)   **d)**

e)   **f)**
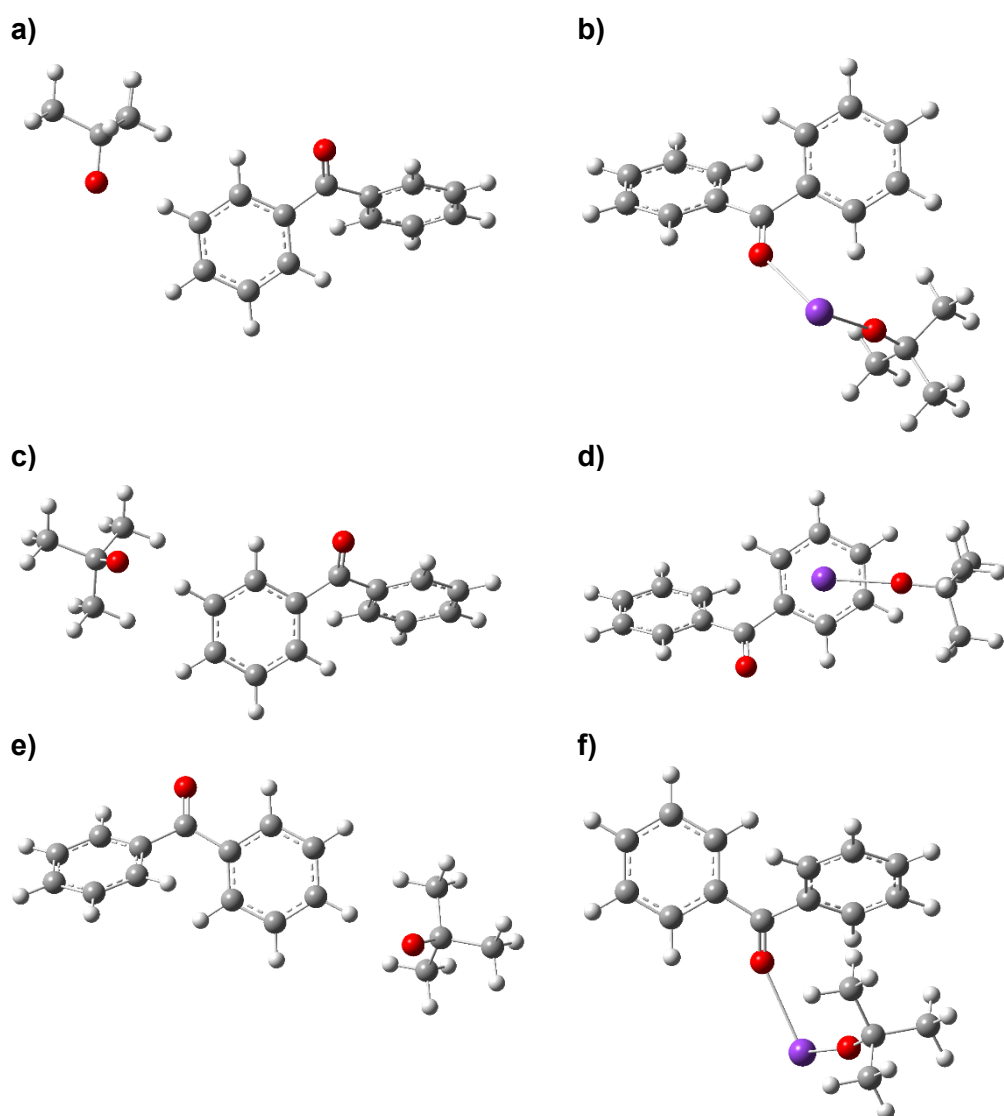
Figure 6.1: Reactant complexes obtained following optimisation of the final structure from intrinsic reaction coordinate (IRC) calculations which were run from the transition states for *tert*-butoxide addition in the *ortho, meta* and *para* positions of benzophenone for naked *tert*-butoxide (left) and KO^tBu (right).
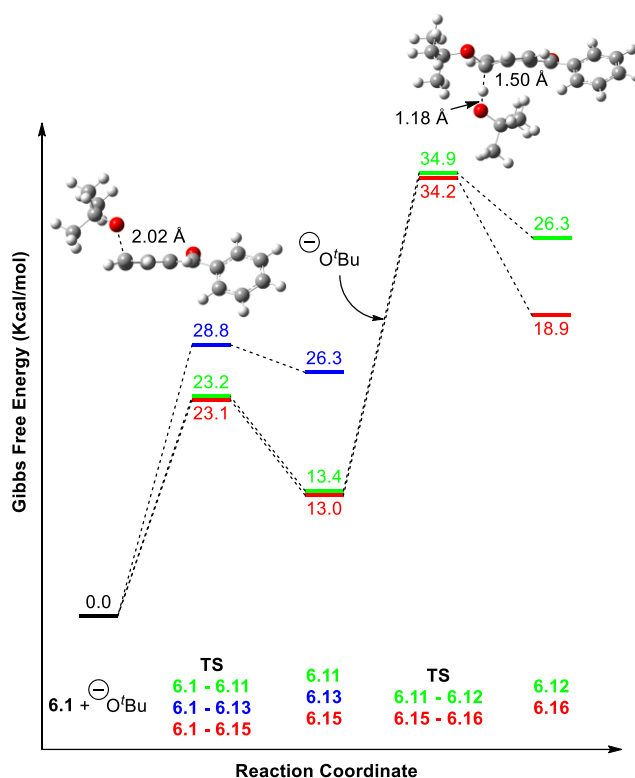
Figure 6.2: Potential energy surface for addition of *tert*-butoxide anion to benzophenone and subsequent deprotonation. (Optimised geometries for para adducts displayed)
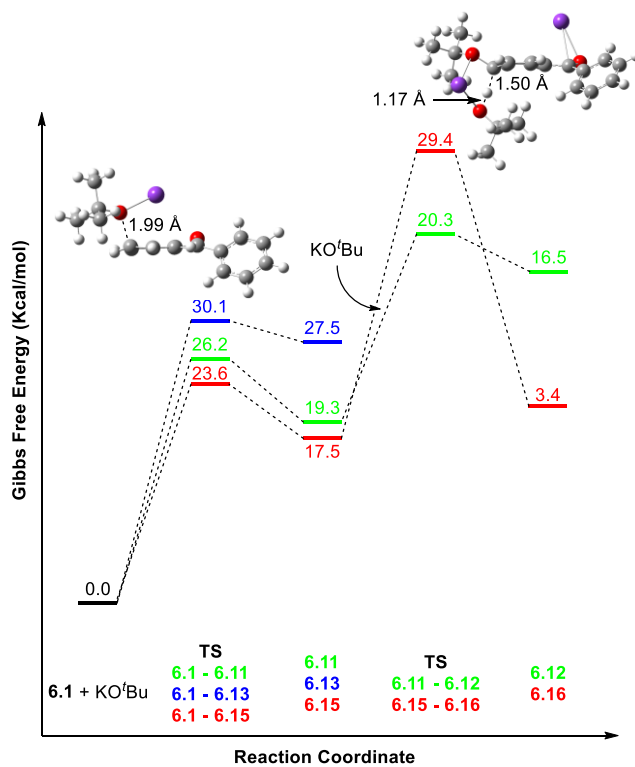
Figure 6.3: Potential energy surface for addition of KO^{t}Bu to benzophenone and subsequent deprotonation. (Optimised geometries for para adducts displayed)

Since the formation of dianionic candidate electron donors was inaccessible and endergonic, we sought to assess an alternative to the deprotonation which may prove too be more accessible and exergonic. Hydride transfer to a molecule of benzophenone, generating **6.18** which could undergo deprotonation to afford another possible strong organic electron donor, **6.21**, seemed plausible (see Scheme 6.4). Dianion **6.21** should have the ability to donate an electron to neutral benzophenone thus generating two molecules of benzophenone ketyl radical anion, **6.22**.
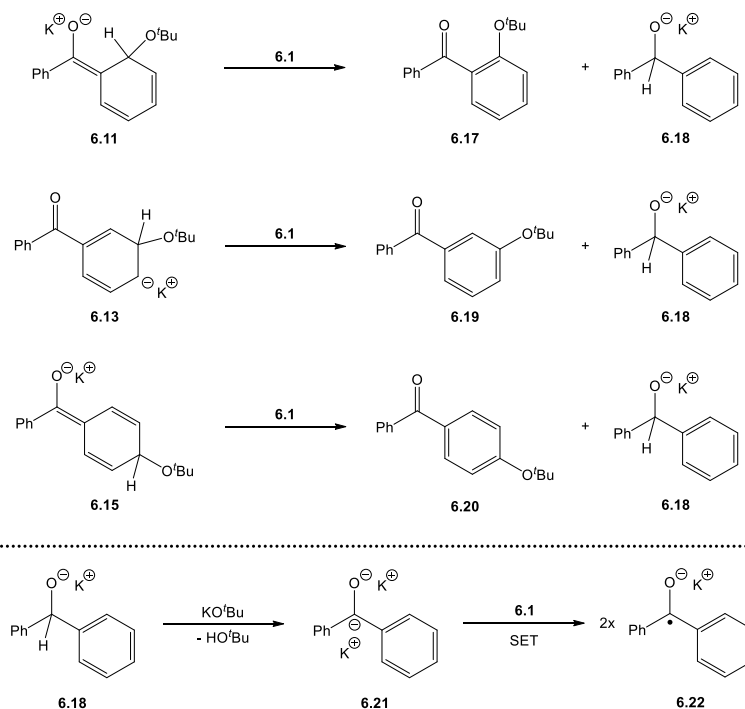
Scheme 6.4: Hydride transfer to neutral benzophenone from *ortho, meta* and *para tert*-butoxide adducts of benzophenone, and subsequent deprotonation to form benzophenone dianion.

Upon calculation of the relative free energies for hydride transfer from **6.11** or **6.15**, they were found to be slightly exergonic (-3.0 kcal/mol and -6.2 kcal/mol, respectively). The free energy barrier for hydride transfer was much larger for **6.11** (40.0 kcal/mol) compared with **6.15** (27.5 kcal/mol), however both steps have significantly large enough energy spans, when coupled with initial *tert*-butoxide addition, to conclude that they would be inaccessible (53.4 kcal/mol and 40.5 kcal/mol, respectively).

Table 6.1: Calculated relative Gibbs free energies and Gibbs energies of activation for hydride transfer from **6.11** and **6.15** to benzophenone (note: no potassium counter ions were included).

Hydride Donor	$\Delta G^{\ddagger}$ (kcal/mol)	ΔG_{rel} (kcal/mol)
6.11	40.0	-3.0
6.15	27.5	-6.2

Deprotonation of hydride adduct **6.18** by naked *tert*-butoxide had a calculated Gibbs free energy barrier of 38.2 kcal/mol and was endergonic by 23.6 kcal/mol. This offers further evidence that this pathway would not be productive in the formation of *in-situ* electron donor species.

6.4 Reduction of Benzophenone by Potassium *tert*-Butoxide

Having ruled out the possible formation of organic electron donor species in the reaction between KO^tBu and benzophenone, an alternative mechanistic proposal was required. The alternative mechanism also had to be able to account for the variation observed in time taken for the blue colour to develop when this reaction was performed on different days in the lab.

Direct electron transfer from *tert*-butoxide to benzophenone has been postulated by Ashby *et al*., therefore this warranted investigation. Utilising both the Nelsen 4-point[92] method and the method of Tuttle, Murphy and co-workers (complexation method),[93] the reorganisation energy, relative free energy and free energy of activation for SET from *tert*-butoxide and KO^tBu to benzophenone were calculated. As expected from the mismatched electrochemical potentials discussed earlier, single electron transfer from *tert*-butoxide or KO^tBu to benzophenone was found to be highly endergonic, Table 6.2.

Table 6.2: Results of Marcus theory calculations for SET from *tert*-butoxide/KO^tBu to benzophenone.

System	Method	λ (kcal/mol)	ΔG_{rel} (kcal/mol)	ΔG^* (kcal/mol)
^tBuO^− + Benzophenone	Nelsen 4-Point	10.0	38.4	58.5
	Complexation	16.9	38.1	44.7
KO^tBu + Benzophenone	Nelsen 4-Point	13.2	59.5	100.0
	Complexation	27.4	43.1	45.3

Here, serendipity struck! Whilst the reaction was being carried out in the Murphy group, a rare sunny day in Glasgow occurred and development of blue colouration in the reaction was accelerated. This provided a clue, which was followed up by controlled experiments using 400nm light emitting diodes (LEDs) alongside blank reactions where the reaction vessel was covered by foil to exclude light. Reactions in the absence of light led to no formation of blue coloured species in the reaction mixture, whereas exposure to visible light (400 nm LEDs) led to rapid formation of blue colouration in the reaction mixture, Figure 6.4. This therefore prompted a new literature search for benzophenone excitation under visible light irradiation.

Figure 6.4: Reactions of benzophenone with KO^{t}Bu in benzene, *left* - exposed to 400 nm LEDs, *right* - not exposed to light.

Benzophenone is well known for undergoing photochemical reactions under ultra-violet irradiation, however we were surprised to find that visible light promoted reactions of benzophenone had been reported.[133-136] In the work of Chen *et al.*[133] diarylketones were utilised as photocatalysts for benzylic mono- or di-fluorination. The authors tested a few diarylketones, Scheme 6.5, notably they utilised benzophenone alongside Selectfluor for the successful visible light-promoted benzylic fluorination of ethylbenzene. The Chen group have also utilised diarylketones (including benzophenone) for visible light-promoted C(sp^3)–H fluorination[136] and chlorination.[135] A mechanism involving n-π* excitation of benzophenone by visible light to ultimately produce triplet benzophenone was proposed. However, triplet benzophenone has to date only been observed following irradiation of benzophenone with UV light (see reviews by Kokotos *et al.*[137] and Nicewicz *et al.*[138] for organic photoredox reactions involving benzophenone and derivatives).
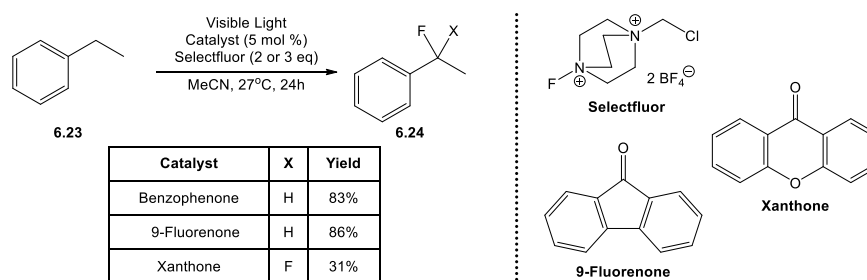
Scheme 6.5: Benzylic mono- or di-fluorination using diarylketone visible light photocatalysts by Chen *et al*.[133] (Light source: 11 W IKEA E26 Compact Fluorescent Lamp (CFL) Bulb)

As part of their investigations, Chen *et al*. measured the UV-vis spectra of benzophenone as well as the reaction mixture of the fluorination reaction with benzophenone as photocatalyst. These spectra displayed no shift of absorbance or emergence of new absorption maxima, thus suggesting that no species were present to absorb visible light when benzophenone was used as photocatalyst. In the group's second publication on C(sp^3)–H fluorination,[136] they utilised a different CFL (19W *vs.* 11W) and measured its emission spectrum, Figure 6.5. It is possible that the emission recorded in the UV region at around 360 – 365 nm, would be suitable to photoexcite benzophenone through its n-π* transition (λ_{max} = ~330 nm) since this is typically broad (310 – 370 nm).
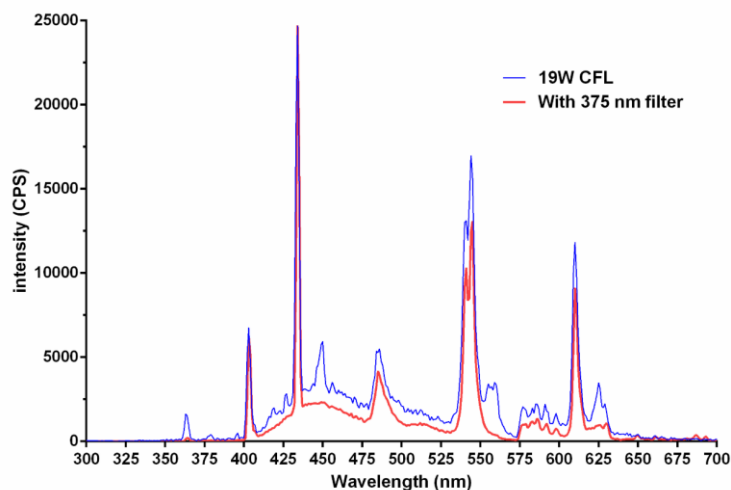
Figure 6.5: Emission spectra of the 19 W CFL used by Chen *et al*.[136] with and without a 375 nm filter. (Reproduced in accordance with RSC permissions)

Another example of visible light photocatalysis with benzophenone has been reported by Singh *et al*.[134] for radical thiol-ene reactions, of the type shown in Scheme 6.6. They utilised an 18 W CFL and stated the use of a 400 nm long-pass filter ensured the use of only visible light wavelengths. However, they did not publish an emission spectrum with and without the long-pass filter to show the wavelength range emitted.

Benzophenone	Yield
5 mol %	58 %
10 mol %	87 %
15 mol %	87 %
10 mol % (in darkness)	n.d.
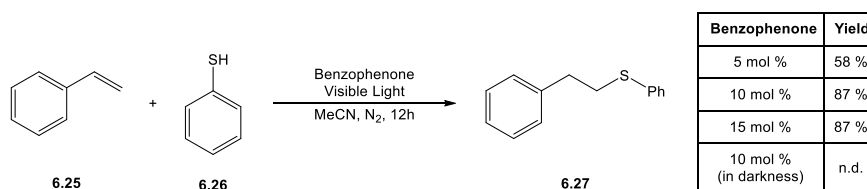
Scheme 6.6: Radical thiol-ene reaction photocatalysed by benzophenone under visible light irradiation.[134]

Since the evidence presented in these publications does not provide a convincing argument for the visible light excitation of benzophenone, further experimental work in the Murphy group was conducted. The mixture of benzophenone and KO^{t}Bu at room temperature was followed by UV-vis spectroscopy in order to assess whether any change in the spectrum of benzophenone was observed upon mixing with KO^{t}Bu. Indeed, over time the spectrum showed significant changes with the appearance at 2 hours of a peak in the visible region around 405 nm. When the analogous reaction between NaO^{t}Bu and benzophenone was monitored by UV-vis spectroscopy, no new peaks developed in the spectrum even after 24 hours.
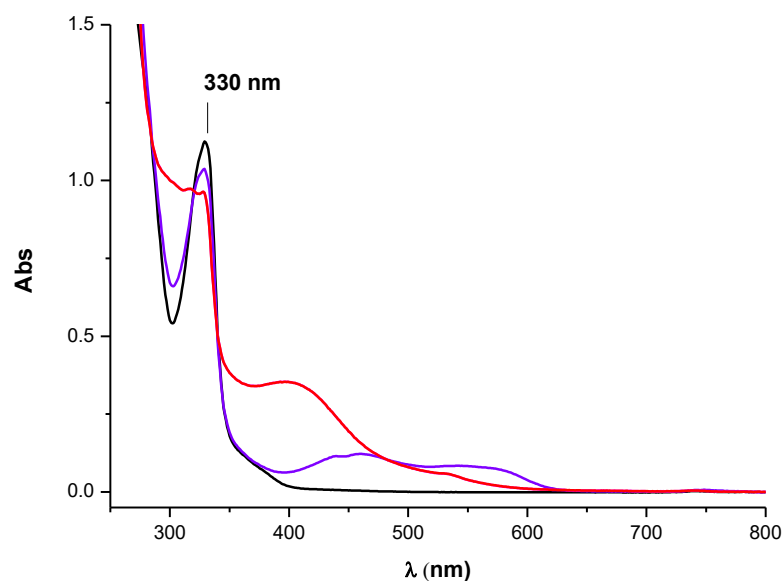
Figure 6.6: Overlaid UV-vis spectra for benzophenone (black), benzophenone plus KO^{t}Bu after 10 mins (blue) and benzophenone plus KO^{t}Bu after 2 h (red).

In order to understand the differences between the KO^{t}Bu and NaO^{t}Bu reactions with benzophenone, the binding energy for formation of a complex between the two reactants was first determined by DFT calculations.

Table 6.3: DFT-calculated Gibbs free energies for formation of *tert*-butoxide - benzophenone complexes.

	ΔG_{bind} (kcal/mol)
$^tBuO^-$	6.2
NaO^tBu	8.0
KO^tBu	6.6

These binding energies show that formation of a reactant complex between any of the *tert*-butoxides is unfavourable, albeit KO^tBu is slightly more favoured than NaO^tBu. However, we know from the UV-vis spectroscopy experiments that new absorbing species form when benzophenone and KO^tBu are mixed for 2 hours. We therefore proceeded to further study the *tert*-butoxide - benzophenone complexes using TDDFT methods which enabled the prediction of their UV-vis spectra.
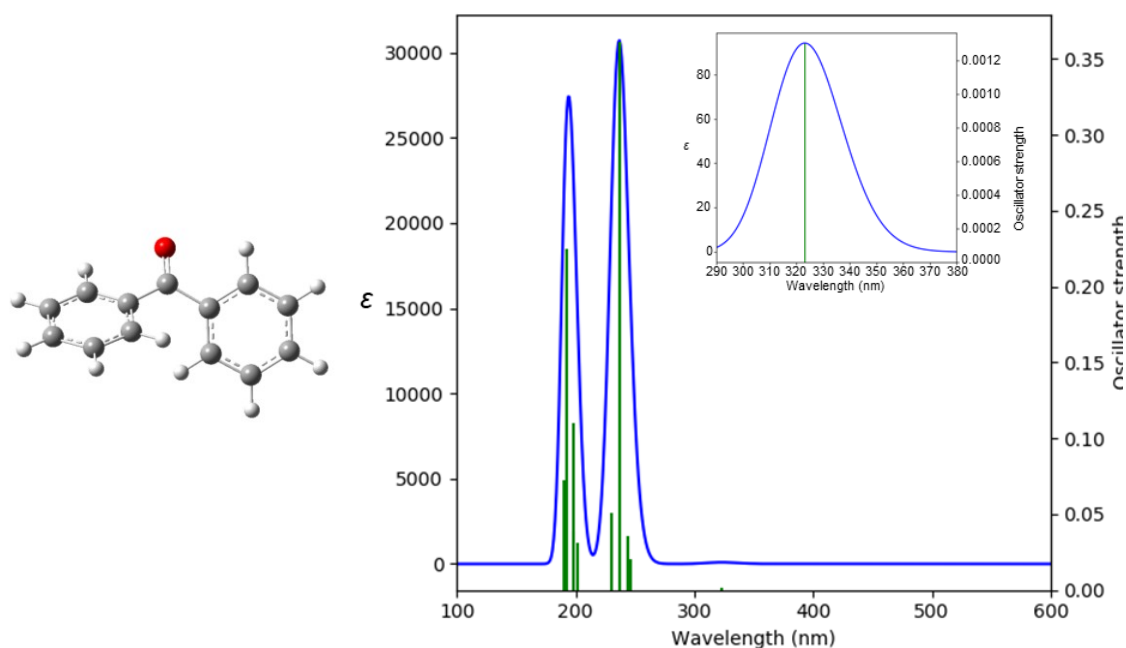
Figure 6.7: Optimised geometry of benzophenone (*left*) and TD-DFT predicted UV-vis spectrum for benzophenone (*right*).

First, the spectrum of benzophenone was calculated to determine how well the experimental spectrum could be reproduced by calculation. The calculated spectrum was in good agreement with previous experimental UV-vis spectra, therefore the spectra the *tert*-butoxide - benzophenone complexes were calculated.
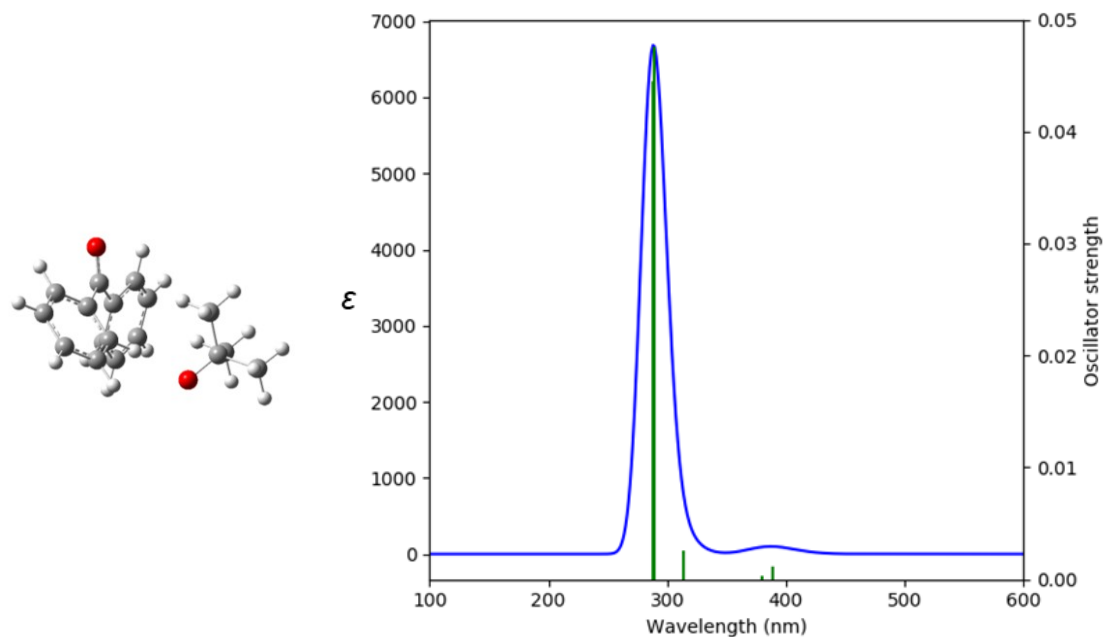
Figure 6.8: Optimised geometry for complex between naked *tert*-butoxide and benzophenone (*left*), and TD-DFT predicted UV-vis spectrum (*right*). Carbonyl carbon to alkoxide oxygen distance, 4.5 Å.
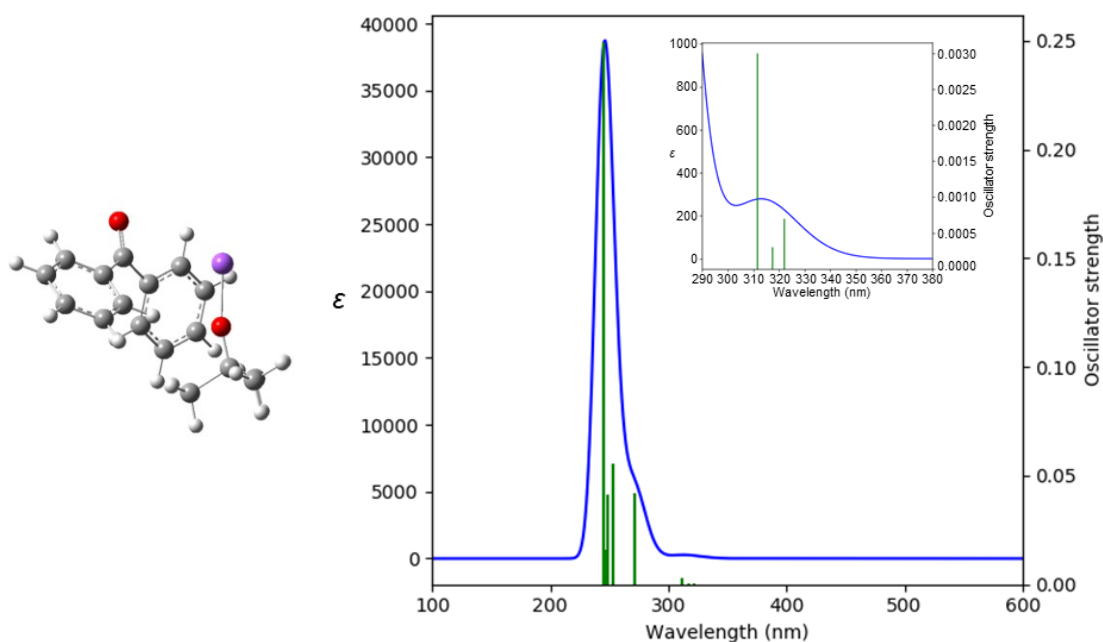
Figure 6.9: Optimised geometry for complex between NaO^tBu and benzophenone (*left*), and TD-DFT predicted UV-vis spectrum (*right*). Carbonyl carbon to alkoxide oxygen distance, 4.4 Å. (This geometry was based on the optimised geometry for KO^tBu - benzophenone complex, and no alternative geometries were explored).

117
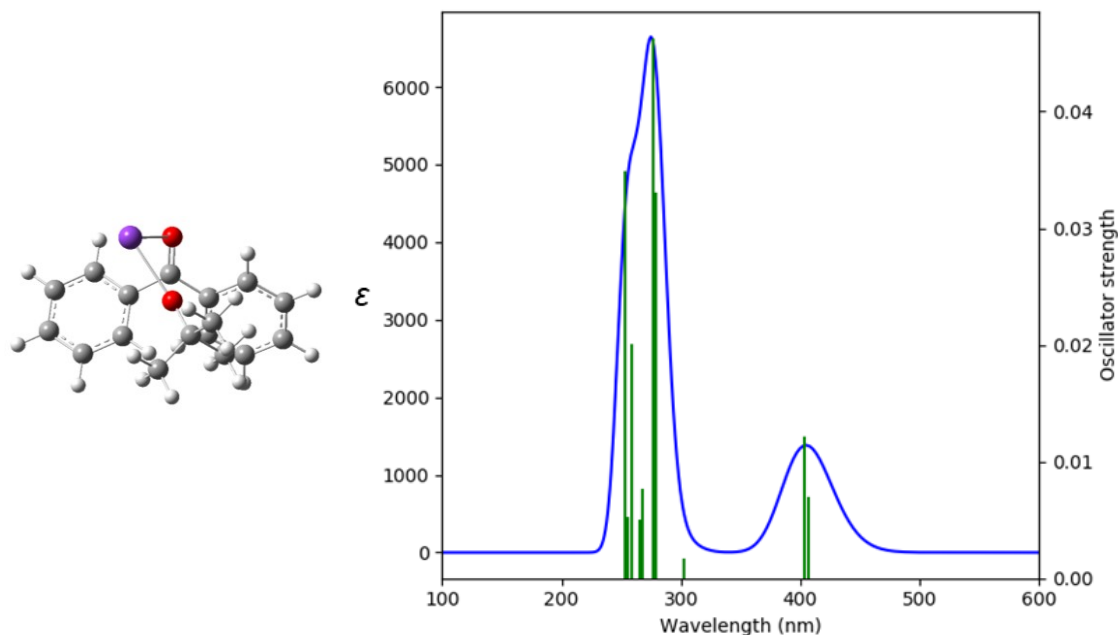
Figure 6.10: Optimised geometry for complex between KO*^t*Bu and benzophenone (*left*), and TD-DFT predicted UV-vis spectrum (*right*). Carbonyl carbon to alkoxide oxygen distance, 3.1 Å.

For the complex of naked *tert*-butoxide with benzophenone, a new absorption composed of two excitations at 380 and 389 nm is predicted. These excitations relate to charge transfer from the HOMO-1 and HOMO which correspond to *tert*-butoxide lone pairs, to the LUMO which corresponds to the benzophenone π*. Interestingly, the predicted spectrum for the NaO*^t*Bu - benzophenone complex (Figure 6.9) showed no absorption around 400 nm. However, it did show a small peak around 320 nm in keeping with the experimental observation of the n-π* transition for benzophenone alone, which remained unchanged after 24 hours reacting with NaO*^t*Bu. For the KO*^t*Bu - benzophenone complex the predicted spectrum contained two excitations at 404 and 406 nm both corresponding to charge transfer excitations from lone pairs on KO*^t*Bu to the π* of benzophenone. The KO*^t*Bu - benzophenone complex had the shortest carbonyl carbon to alkoxide oxygen distance at 3.1 Å, whilst both other complexes were over 4 Å. The potassium cation allowed this closer complexation, whereas sodium was unable to bridge at such close proximity to both reactants. This new predicted absorption peak agrees very well with the experimental UV-vis spectrum measured by the Murphy group and provides key evidence for the species responsible for the absorption. Whilst the equilibrium concentration of this species would be predicted to be very low, we know that only small concentrations of benzophenone ketyl radical anion were measured by Ashby *et al*. and such small percentages would be sufficient to form visible blue colouration.

Following on from this key piece of evidence for the KO^{t}Bu - benzophenone complex undergoing charge transfer upon visible light irradiation, the Murphy group sought further experimental proof of this. Single electron transfer from KO^{t}Bu would result in formation of *tert*-butoxyl radical, which is known to undergo rapid fragmentation to yield acetone and methyl radicals.[139-140] Under the experimental conditions methyl radicals could abstract hydrogen atoms from the solvent, THF, or alternatively add to benzophenone to form methylbenzophenone. Whilst the electron transfer reaction occurs in daylight or using 400 nm LEDs, it occurred fastest under 365 nm light irradiation. Analysis (gas chromatography - mass spectrometry, GCMS) of the products formed by irradiation of KO^{t}Bu and benzophenone in THF at 365 nm, showed methylbenzophenone had indeed been formed. To further validate this result, the Murphy group used KOEt$_3$ in place of KO^{t}Bu (KOMe$_3$) and identified monoethylated benzophenone by GCMS.

6.5 Conclusions

The search for mechanistic insights can often be a long one, in this chapter one such search has been concluded having been open since the 1980s. Initially looking upon the reduction of benzophenone by KO^{t}Bu with a new lens, the possible formation of organic electron donor species (Figure 6.11) *in situ* was investigated. However, by use of DFT calculations it was determined that such species would not be formed upon reaction of KO^{t}Bu with benzophenone.
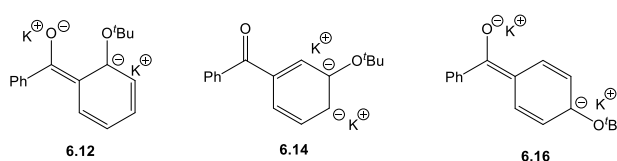
Figure 6.11: Potential organic electron donor species formed *in situ* by reaction of KO^{t}Bu with benzophenone.

The search therefore returned to the original proposal by Ashby *et al.*[2, 35] that KO^{t}Bu was acting directly as an electron donor towards benzophenone. Here, Marcus theory was utilised with DFT calculations to allow the prediction of the relative Gibbs free energy and Gibbs free energy of activation for the electron transfer reaction. Energies were determined for both naked *tert*-butoxide and KO^{t}Bu as electron donors, however it was demonstrated that neither would be able to reduce benzophenone. Reduction by naked *tert*-butoxide exhibited a relative Gibbs free energy of 38.1 kcal/mol with a predicted Gibbs free energy of activation of 44.7 kcal/mol. Meanwhile, KO^{t}Bu was shown to exhibit poorer reducing ability towards benzophenone (ΔG_{rel} = 43.1 kcal/mol and ΔG^* = 45.3 kcal/mol).

In some cases, the search for mechanistic insights must benefit from serendipity, and this work was no different. A rare sunny day in Glasgow altered the rate of blue colour development within a reaction carried out by experimental colleagues in the Murphy Group, thus providing a valuable hint that light may be a key factor. Through UV-vis experiments a visible light (~400 nm) absorbing species was shown to form after 2 hours of reacting benzophenone with KO^{t}Bu. Through TDDFT calculations, the species responsible for this absorption was shown to be a complex between KO^{t}Bu and benzophenone, with the absorption at ~400 nm assigned to a charge transfer between the butoxide lone pairs and the π^* system of benzophenone.

Around 35 years on from Ashby *et al*. proposing that KO^tBu could act as an electron donor towards benzophenone, a mechanistic insight has been revealed - KOtBu can indeed donate an electron to benzophenone, however this can only occur under light irradiation. It is highly likely therefore that the reactions carried out by Ashby were also being photoactivated by sunlight or the lab lighting.

6.6 Future Work

Having shown that KO^tBu can indeed act as an electron donor, under light irradiation, towards benzophenone, the next step would be to investigate whether other substrates would be susceptible to formation of a donor-acceptor complex with KO^tBu. The simplest extension would be to other aryl ketones such as benzaldehyde, acetophenone, fluorenone and xanthone (Figure 6.12).
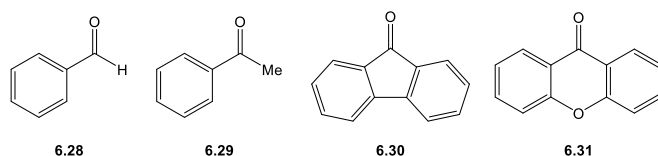
Figure 6.12: Examples of aryl ketones which could be used to probe the scope of light irradiated electron transfer from KO^tBu.

Initially, these substrates could be studied computationally in order to assess whether charge transfer complexes are formed with KO^tBu, this would provide knowledge to the experimental chemist about which wavelength of light to irradiate their reaction with, to maximise the formation of the ketyl products.

Further to investigating the scope of substrates able to form a donor-acceptor complex, it would be important to investigate whether other salts can form donor-acceptor complexes with benzophenone and undergo electron transfer following light irradiation. Salts which have previously been reported to act as electron donors would serve as a promising start point, therefore sodium iodide would be a perfect candidate, having been reported to act as an electron donor towards aryldiazonium salts.[141] By extension potassium iodide could also be a good candidate.

7. The Curious Case of Potassium
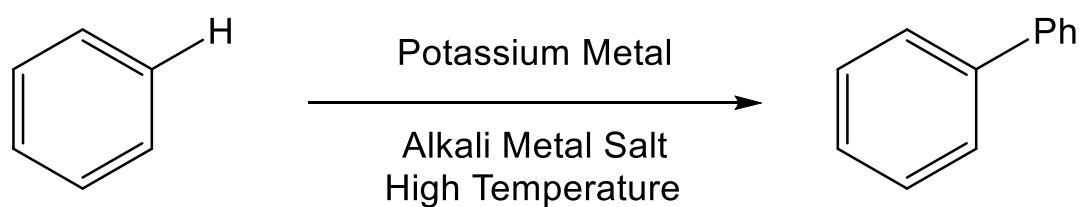
7.1 Introduction

The potassium cation presents some curious results, it has been shown already that whilst KO^{t}Bu is applicable in transition metal-free cross coupling reactions operating *via* a BHAS mechanism, NaO^{t}Bu has been limited to but a handful of reactions. Indeed, within Chapter 6 KO^{t}Bu was again shown to function, this time in the visible light photoreduction of benzophenone, whilst NaO^{t}Bu did not.

Recently, Murphy, Tuttle and co-workers have shown that this is not limited to sodium or potassium *tert*-butoxide, but also holds true for potassium hydride (KH) versus sodium hydride (NaH).[142] They found that haloarene reduction occurred in the presence of KH whilst use of NaH resulted in no reaction, Scheme 7.1.
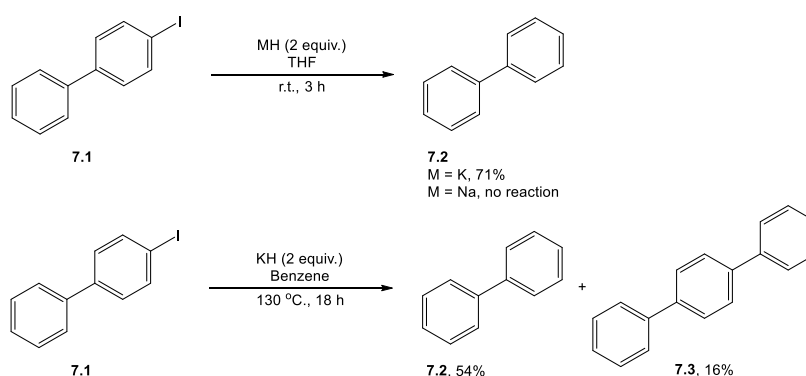
Scheme 7.1: Haloarene reduction carried out by Murphy, Tuttle and co-workers which demonstrated that KH but not NaH could afford the transformation, and also that coupling reactions occurred alongside hydrodehalogenation in benzene.

When the solvent of these reactions was switched to benzene, a mixture of coupled product **7.3** and hydrodehalogenated product **7.2** was formed. Since previous work had shown that benzyne formation was highly likely in substrates such as **7.1** little mechanistic evidence could be gained from this substrate. Murphy, Tuttle and co-workers therefore turned to hindered substrate **7.4** where benzyne formation is not possible due to the positions *ortho* to the bromide being blocked. When this substrate was treated with KH, 28% of the expected hydrodehalogenated product **7.5** was formed. Alongside the expected product, **7.6** and **7.7** were also formed, and these could only be explained by the formation of radicals. Whilst **7.5** could be formed by a Pierre-type concerted nucleophilic aromatic substitution (CS$_N$Ar) reaction,[143] it is also possible to form this *via* a radical mechanism.
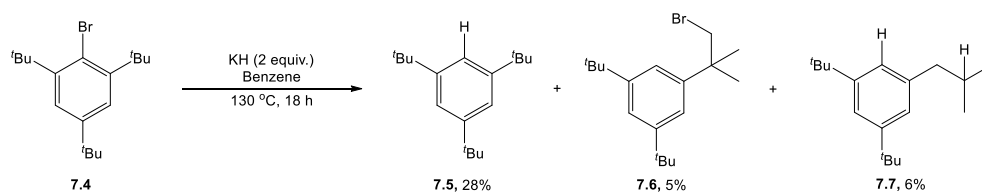
Scheme 7.2: Reduction of hindered substrate **7.4**, forming expected hydrodehalogentation product **7.5** and rearranged products **7.6** and **7.7**.

In order to understand the origins of the radical initiation, Murphy, Tuttle and co-workers conducted reactions with potassium metal and KH to test whether presence of residual potassium metal in the base reagents could have been responsible for the electron transfer required to initiate the reaction (as shown in Scheme 7.2). These results did not support this hypothesis, with similar yields of radical-type products being achieved in the presence or absence of 0.2 equiv. of potassium metal. Utilisation of potassium metal alone, or in the presence of 0.2 equiv. of KH, led to no rearranged products and formation of hydrodehalogenated product and biphenyl only, this intriguing formation of biphenyl under the action of potassium metal on benzene had never been reported before in the literature.

However, metalation of benzene and substituted benzenes by an alkali metal plus alkali metal alkyls[144-147] or alkali metal oxides[148] has been published previously, as has the reaction of alkali metals and metal hydrides on deuterated alkyl aromatics in 1956 by Hart,[149] however he only observed reaction *via* the side chains of the substrates.
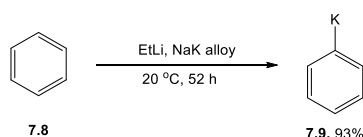
Scheme 7.3: Metalation of benzene by ethyl lithium and sodium - potassium alloy.

The Murphy and Tuttle groups therefore chose to examine this interesting homocoupling of benzene in the presence of potassium metal and KH. This started with experimental studies to determine whether this reaction was also possible using sodium metal, and the role of KH was probed by carrying out the reaction with various alkali metal salts, alkoxides and hydrides.

First the reaction of benzene (large excess, 5 mL) with potassium metal (1.5 mmol) and KH (1.5 mmol) was carried out at 150 °C in the absence of other substrates, this yielded 51 mg (0.33 mmol) of the expected product biphenyl (**7.2**). As well as biphenyl, two

cyclohexadiene products, **7.10** and **7.11** were also formed. This reaction was then repeated with potassium metal, KH, KO^{t}Bu and potassium metal plus KO^{t}Bu, Table 7.1. The reaction utilising KO^{t}Bu alongside potassium metal yielded the largest amount of biphenyl product (0.88 mmol) with only traces of the reduced products **7.10** and **7.11** observed.

Table 7.1: Homocoupling of benzene carried out by the Murphy group.
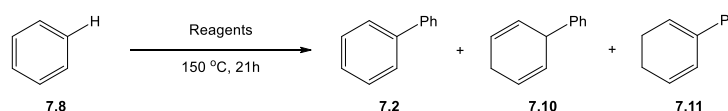
Reagents (1.5 mmol)	Yield of 7.2 (mg)	Yield of 7.10 (mg)	Yield of 7.11 (mg)
K	-	-	-
KH	Traces	-	-
KO^{t}Bu	-	-	-
K + KH	51	12	16
K + KO^{t}Bu	135	traces	traces

Further to these initial experiments, an assessment of the stoichiometry of potassium metal to KO^{t}Bu was carried out, since the latter was found to be the most successful additive. Reacting 2 mL of benzene with 0.5 mmol of both potassium metal and KO^{t}Bu resulted in a proportionate decrease in yield to 32 mg of biphenyl. Further decreasing the amount of KO^{t}Bu to 0.1 mmol had no significant effect on the yield of biphenyl (30 mg). However, when the amount of potassium metal was decreased to 0.1 mmol whilst having 1.5 mmol of KO^{t}Bu the yield of biphenyl was only 1 mg. This combination of reactions could indicate that reduction by potassium metal is an important process occurring within the homo-coupling of benzene.

The scope of the added salt was then extensively screened by the Murphy group, Table 7.2. Sodium metal, with the most successful additive KO^{t}Bu, yielded no coupled products, demonstrating that the stronger reducing power of potassium metal was required for this reaction to proceed. Variation of the cation in the salt was carried out for the series of alkali metal iodide salts, with LiI found to be ineffective whilst the remaining salts were found to be effective in the reaction. Of note was the increased formation of the phenylcyclohexadiene products for these non-basic salts, suggesting that the base may play a key role in the formation of biphenyl only. Switching from KO^{t}Bu to NaO^{t}Bu led to formation of no coupled products, with a similar outcome observed

between KBF_4 and $NaBF_4$ (no biphenyl was observed, however a small amount of phenylcyclohexadiene was formed). The potassium cation can therefore be seen as key for the reaction to proceed effectively.

Table 7.2: Screening of salts for the homocoupling of benzene carried out by the Murphy group.
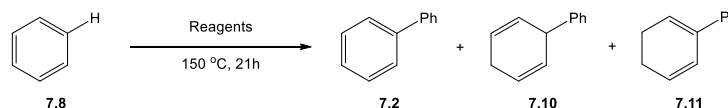
Reagents (1.5 mmol)	Yield of 7.2 (mg)	Yield of 7.10 (mg)	Yield of 7.11 (mg)
K + LiI	-	-	-
K + NaI	15	6	-
K + KI	54	traces	traces
K + RbI	42	41	-
K + CsI	18	43	25
K + KO^{t}Bu	135	traces	traces
K + NaO^{t}Bu	-	-	-
K + KBF$_4$	96	11	5
K + NaBF$_4$	-	5	-
K + KI	54	traces	traces
K + KBr	47	17	5
K + KF	14	11	traces
K + Me$_4$NCl	-	-	-
Na + KO^{t}Bu (0.5 mmol)	-	-	-

The effect of the anionic component of the salts was also investigated, with KI and KBr both effecting the reaction to about half the amount that KO^{t}Bu did. The comparison of KBF_4 and KF demonstrated that the freedom of the potassium cation was also important, with the potassium strongly bound by fluoride (lattice energy 198.3 kcal/mol)[150] resulting in a lower yield when compared to the loosely bound potassium cation in KBF_4 (lattice energy 152 kcal/mol).[151] Further emphasis on the importance of the cation was provided by no reaction being observed when Me_4NCl was utilised.

Based on the experimental screening the Murphy and Tuttle groups hypothesised two possible mechanisms for the homo-coupling of benzene reaction, a radical mechanism

initiated by a SET or an ionic mechanism initiated by the deprotonation of benzene (only additives such as KH or KO*t*Bu).

a) Radical Mechanism
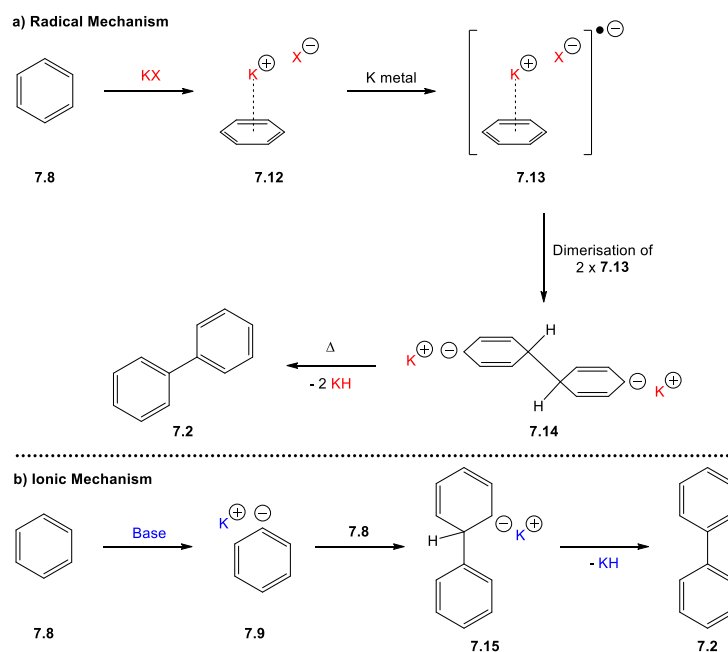
Scheme 7.4: Mechanistic proposals to be investigated for the homocoupling of benzene in the presence of potassium metal and a salt additive.

In order to more fully understand the likelihood of either mechanism, DFT calculations were to be utilised to probe the individual reaction steps to understand whether they were kinetically and thermodynamically accessible.

7.2 Computational Methods

DFT calculations in this chapter were run using the M06-2X functional[71-72] and 6-31++G(d,p)[74-75, 104-110] basis set on all atoms. Solvation was modelled implicitly using the CPCM model[84] with parameters for benzene as solvent. All calculations were carried out in Gaussian09.[111]

Calculated ΔG_{rel} and $\Delta G^{\ddagger}$ are relative to the reactants for each step and include the formation of reactant complexes and dissociation of product complexes where appropriate.

In order to model single electron transfer reactions computationally, Marcus-Hush Theory[87] was employed with the 4-point method of Nelsen *et al.*[92] or the complexation method of Tuttle, Murphy and co-workers[93] allowing calculation of the reorganisation energy (λ), ΔG_{rel} and ΔG^{*}. The Nelsen 4-point method requires optimisation of the individual electron donor and acceptor species, before and after single electron transfer. Single point energy calculations must then be performed on these optimised geometries using the charge and multiplicity of their other state in the electron transfer reaction. The complexation method requires optimisation of the electron donor and acceptor as a complex in both the reactant and product electronic states. Single point energy calculations must then be performed on these optimized geometries with the alternative electronic configuration.

Constrained DFT calculations were carried out in NWChem 6.8, utilising the M06-2X functional and aug-cc-pVDZ basis set[152] for hydrogen and carbon, and 6-31+G(d) basis set for potassium. The Löwdin[153] population scheme was utilised for the results presented.

Constrained DFT is a technique which adapts calculations carried out with density functionals in order to overcome known shortcomings with standard DFT. Many different constraints can be applied within constrained DFT, with the original formalism presented by Dederichs *et al.*[154] seeking to determine the electronic ground state of a system with the constraint that N electrons are found in a volume Ω. Other possible constraints include constraining the local *d* or *f* charge variation in transition or rare-earth metals, and constraining the magnetisation in a system.[155] The constrained DFT equation has the following general form:

$$E(N) = \min_{\rho} \max_{V} \left[E[\rho] + V \left(\sum_{\sigma} \int w^{\sigma}(\boldsymbol{r})\, \rho^{\sigma}(\boldsymbol{r})\, dr - N \right) \right]$$

Equation 7.1

Where $E[\rho]$ is the traditional DFT energy functional and the second term is a single Lagrange multiplier term which effects the constrained optimisation (constraining potential). Terms within the Lagrange multiplier term are as follows: $w^{\sigma}(\boldsymbol{r})$ is a weight function that defines the property of interest (magnetisation, charge density *etc*.) and $\rho^{\sigma}(\boldsymbol{r})$ is the electron density.

If the property to be constrained is the charge density then the weight function could be determined by a number of common methods for determining the charge on a specific atom or group of atoms, such as the Becke[156] or Löwdin[153] population schemes.

7.3 Preliminary Results

The ionic mechanism, utilising KH as base, was investigated initially. Deprotonation of benzene by KH was found to be an endergonic reaction (9.7 kcal/mol) but with an easily accessible barrier at the elevated reaction temperatures. Since this reaction affords hydrogen gas as a product it would be an irreversible reaction, therefore despite the reaction being endergonic, phenyl potassium concentrations would continue to increase with time. Addition of phenyl potassium to benzene has already been reported in the literature[157] and the reaction was only slightly endergonic, again with an easily accessible free energy barrier. The final step of the ionic mechanism would be expulsion of KH from **7.15** to yield biphenyl, despite the gain of aromaticity afforded by expelling KH this reaction was almost thermoneutral.
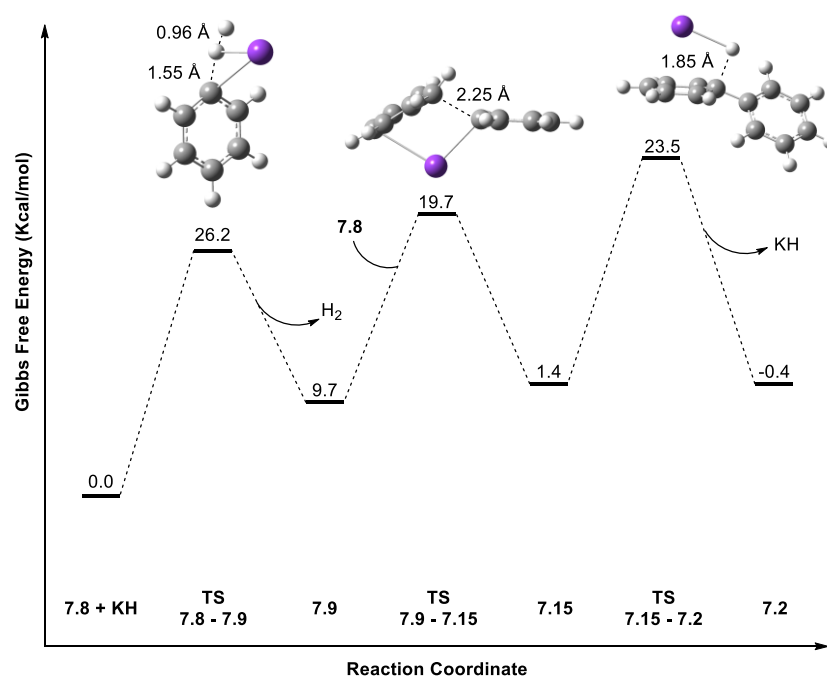
Figure 7.1: Potential energy surface for formation of biphenyl (**7.2**) from benzene (**7.8**).

An interesting alternative to KH expulsion from **7.15**, would be deprotonation to yield dianion **7.16**, likely to be a potent electron donor which could be involved in initiation of the radical mechanism when potassium metal is used alongside a base. This reaction was found to have an activation free energy of 13.4 kcal/mol whilst being exergonic by 17.8 kcal/mol, rendering this a more favourable reaction than KH expulsion from **7.15**. Indeed, these results are only relevant to the reaction of KH alone with benzene, the role of potassium metal has not been taken into account. Since the combination of KH and potassium metal affords a higher yield of biphenyl than simply KH alone, potassium metal

must enhance the basicity of KH, or an altogether different mechanism could be operating. Further experimental characterisation of the reaction between KH/KO^{t}Bu with potassium metal must be carried out in order for more in-depth computational investigations to take place.
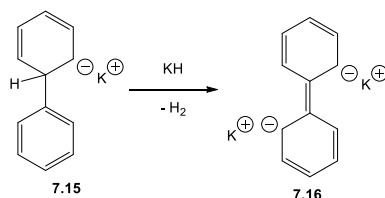
Scheme 7.5: Deprotonation of phenylcyclohexadienyl anion by KH.

The radical mechanism presented similar challenges in that composite structures formed by reaction of potassium metal with added salts such as KO^{t}Bu or KI were not known, and therefore in order to represent these accurately within calculations would be impossible. That said, taking a simplistic approach would allow qualitative assessment of the proposed reaction mechanism. A search of the literature for representations of potassium metal was carried out, and the work of Aguado[158] provided a detailed study on potassium cluster size and how representative these clusters were of bulk metal. Aguado found that cluster sizes of >60 atoms were required in order to start mimicking the HOMO-LUMO gap, ionisation potential and electron affinity of potassium metal. Running DFT calculations of such large clusters was not possible with the available computational resources, therefore the 8 - 20 atom cluster structures of Chakrabarti *et al.*[159] were turned to. The smallest of these, the 8-atom potassium cluster was chosen since it represented the simplest and least computationally expensive cluster. In addition, the 21-atom cluster structure of Aguado was also utilised to determine whether moving closer to bulk metal properties had a significant impact on the calculated electron transfer parameters.

It is worth noting at this stage some of the practicalities of utilising constrained DFT with donor-acceptor complexes. It is clear from Table 7.3 that only one result was obtained utilising this approach, however, this does not represent the number of systems where attempts to apply constrained DFT were made. Constrained DFT optimisations of triplet complexes between K$_8$, benzene and each alkali metal cation were attempted, however optimisation of the CDFT multipliers were unsuccessful for each using the Löwdin population scheme. Attempts were therefore made to achieve an improved starting geometry by first optimising utilising Mulliken populations which proved successful for

the lithium cation. Upon re-optimsation of this triplet complex with Löwdin populations the CDFT multipliers again failed to optimise. Due to the preliminary nature of this study, time constraints did not allow for further investigation of the methodology in order to improve the optimisation procedures.

Despite these difficulties with constrained DFT optimisations, the potential power of this methodology in expanding the range of systems which can be studied as electron donor-acceptor complexes remains large. As has been demonstrated throughout the other chapters in this work, there exist two conventional techniques for estimating electron transfer parameters using DFT: the Nelsen 4-point method[92] and the method of Tuttle, Murphy and co-workers.[93] The Nelsen 4-point method was shown to be less accurate for organic electron donor systems by Tuttle, Murphy and co-workers during the testing of their method. However, the latter method also has its drawbacks when applied to conventional DFT methods - in order to study an electron transfer reaction as a donor-acceptor complex, both the donor and acceptor must be in the singlet state, as such the product complex following electron transfer would be in the triplet state. This is necessary as for any other electronic configuration in the reactant state, the unpaired electrons (be this from a doublet or triplet *etc.*) would reside in the most stable electronic configuration and thus upon attempting to optimise the product complex one would be presented with the same state as that optimised in the reactant complex. This is rooted in the application of conventional DFT to study these electron transfer complexes; for a DFT optimisation one cannot specify where particular electrons should reside, they will simply reside in the most stable electronic configuration. Here, the power of constrained DFT shines through; one can specify that a certain volume should equate to a particular spin or charge and as such the method of Tuttle, Murphy and co-workers could in theory be extended to study any and all electron donor-acceptor complexes.

Table 7.3: Results of single electron transfer calculations from potassium clusters to benzene and benzene-cation complexes.

System	Method	λ (kcal/mol)	ΔG$_{rel}$ (kcal/mol)	ΔG* (kcal/mol)
K$_8$ + Benzene	Nelsen 4-Point	16.2	48.2	64.0
K$_8$ + Benzene-K$^+$	Nelsen 4-Point	16.6	-2.2	3.1
	Complexation (Constrained DFT, Gas Phase)	18.7	-5.1	2.5
K$_8$ + Benzene-Na$^+$	Nelsen 4-Point	19.5	-5.9	2.4
K$_8$ + Benzene-Li$^+$	Nelsen 4-Point	16.6	-13.8	0.1
K$_{21}$ + Benzene	Nelsen 4-Point	14.8	41.3	53.2
K$_{21}$ + Benzene-K$^+$	Nelsen 4-Point	15.1	-9.2	0.6
K$_8$ + Benzene-K$^+$-Benzene	Nelsen 4-Point	10.8	-1.9	1.8

Returning to the results obtained here, the Nelsen 4-point method was utilised to gain a quick and qualitative understanding of the energetics involved with electron transfer between a K$_8$ cluster and benzene or benzene plus an alkali metal cation (Lithium, Sodium or Potassium). As anticipated the calculated electron transfer parameters for reduction of benzene by K$_8$ alone were found to be prohibitive, being highly endergonic (ΔG$_{rel}$ = 48.2 kcal/mol) and exhibiting a large calculated activation free energy (ΔG* = 64.0 kcal/mol). Upon moving to the larger K$_{21}$ cluster, with properties closer to bulk potassium, the reduction is still predicted to be inaccessible. Such a reduction typically requires dissolving metal conditions i.e. potassium in liquid ammonia.[160] The reorganisation energy (λ) for these electron transfers was found to be dominated by the contribution from benzene which was 26.6 kcal/mol, meanwhile reorganisation of the K$_8$ and K$_{21}$ clusters was found to be 5.8 kcal/mol and 2.9 kcal/mol, respectively. The small reorganisation energy associated with the clusters can be also be noticed in the optimised structures (Figure 7.2), where it can be seen that minimal geometrical changes occur upon loss of an electron. On the other hand, the reorganisation of benzene to benzene radical anion results in loss of planarity and loss of aromaticity, explaining the larger reorganisation energy.

Upon complexation of an alkali metal cation (lithium, sodium or potassium) the electron transfer parameters become favourable with each electron transfer calculated to be exergonic and have a small activation free energy (3.1 kcal/mol for potassium cation, 2.4 kcal/mol for sodium cation and 0.1 kcal/mol for lithium cation). A further calculation of the electron transfer parameters for SET from K_8 to benzene and potassium cation was carried out using constrained DFT. This resulted in very similar results as those obtained by the Nelsen 4-point method; unfortunately, as already mentioned above, the use of constrained DFT for lithium and sodium cation systems was not possible.

Complexation of a further benzene molecule to the potassium cation to form a sandwich complex (Figure 7.3d) was also investigated, this however made no significant change to the calculated electron transfer parameters.

Figure 7.2: Optimised geometries of **a)** K_8 cluster, **b)** K_8 radical cation, **c)** K_{21} cluster, **d)** K_{21} cation, **e)** benzene and **f)** benzene radical anion.
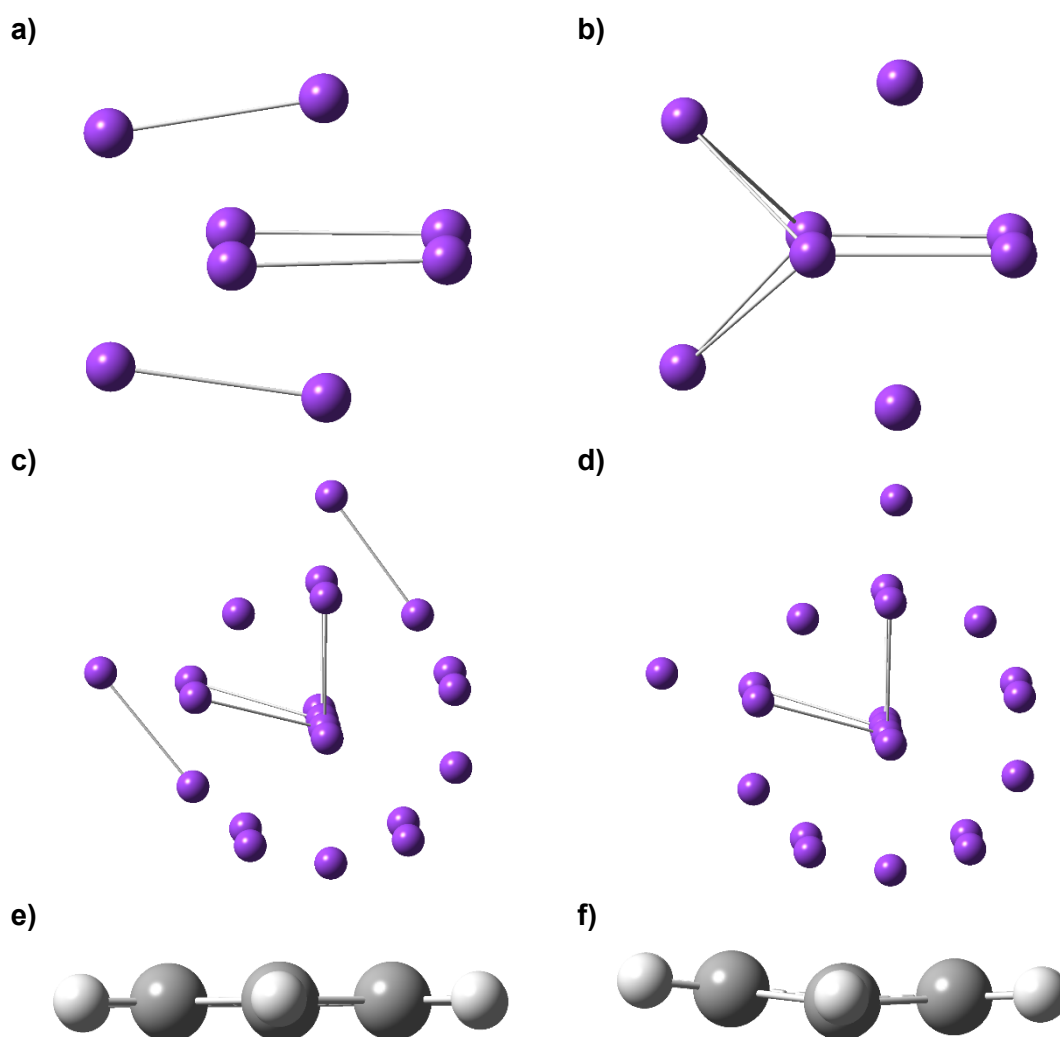
Experimental work has demonstrated that the cation of the salt is key to the reaction performance, therefore comparison between potassium, sodium and lithium cations was important to carry out. For all three cations the reaction was predicted to be exergonic and have a small activation free energy. These results do not follow the experimentally observed trend of no reaction or low conversion for lithium and sodium salts respectively when compared to the higher yielding potassium salts. In order to further understand why the calculations conducted have not been able to differentiate between the alkali metal cations as per the experimental results, the suitability of the potassium cluster and also the representation of the salt additive must be interrogated.

Figure 7.3: Spin density maps for benzene radical anion with **a)** lithium cation, **b)** sodium cation and **c)** potassium cation. The spin density map for benzene radical anion - potassium cation - benzene sandwich complex is depicted in **d)**.
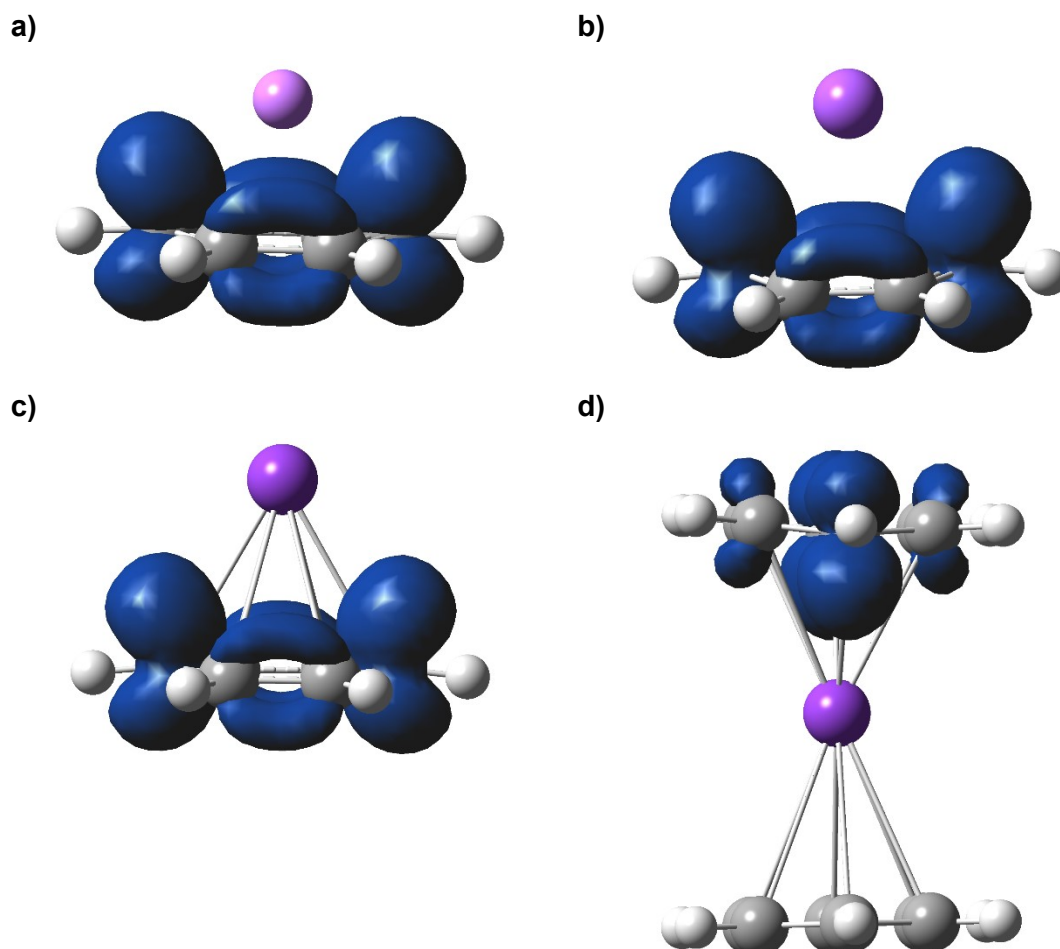
First, the suitability of the potassium cluster will be discussed. The vertical ionisation potential (VIP) for potassium clusters of size K_2 to K_{20} has been calculated by Banerjee *et al.*[159] whilst it has also been calculated for K_{13} to K_{80} clusters by Aguado.[158] These

studies have shown that the VIP decreases upon increasing the size of the cluster; at clusters above K_{70} the variation in the VIP was small and the HOMO-LUMO gap was small. This suggested clusters of size K_{70} or greater were approaching the properties expected of the metallic state. Upon consideration of this data it would therefore seem logical to suggest the application of a cluster of size K_{70} or greater would improve the electron transfer calculations carried out above. However, upon moving to larger clusters the VIP was found to be decreasing and as such would suggest that electron transfer reactions would become more favoured since less energy is required to ionise the potassium cluster. As has been shown in Table 7.3, the electron transfer parameters have been predicted to be favourable, meaning that improving the electron donor (potassium cluster) properties would not lead to a differentiation in the alkali metal cation effects.

In order to differentiate the effect of the alkali metal salts in the benzene homocoupling reaction, it would therefore require a better representation of the alkali metal salt than simply one single cation. Experimental work has indeed shown that the anion from the salt can lead to differences in yield, however these effects were not dominant when compared to the effects of changing the alkali metal cation. Another factor to be considered would be the potential for formation of a composite structure upon the reaction of potassium metal with the added alkali metal salt. For example, composite structures have been observed by Chiba *et al.*[161] in their use of sodium hydride with lithium iodide. However, such a composite structure would have to be determined by experimental methods before further DFT calculations could be carried out taking this approach.

The remaining steps of the proposed radical mechanism also warranted investigation by DFT calculations in order to determine whether they were possible in terms of Gibbs free energy.
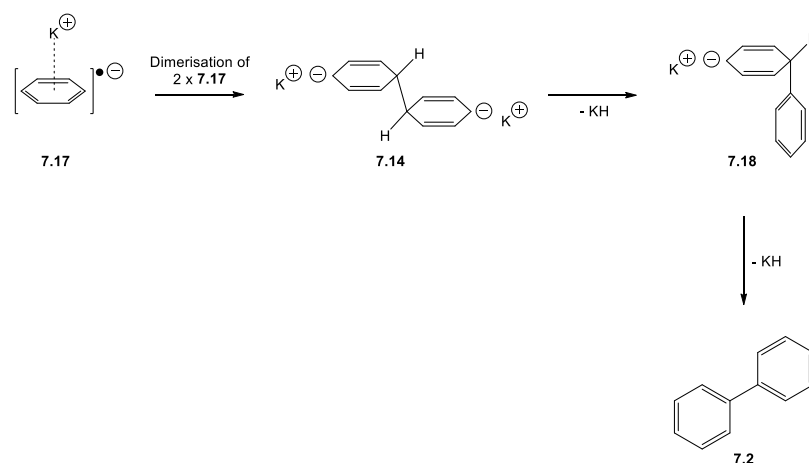
Scheme 7.6: Remaining steps in the proposed radical mechanism following the initial single electron transfer to benzene.

Following single electron transfer to generate benzene radical anions, two would be required to dimerise to yield **7.14**. A transition state for this dimerisation was unable to be located, due to the multireference nature of the reaction (multireference methods were not attempted in the search for this transition state). However, the relative energy for this reaction was found to be endergonic by only 1.2 kcal/mol. Following dimerisation, dianion **7.14** must undergo expulsion of two molecules of KH. The first KH expulsion had an accessible free energy barrier of 23.3 kcal/mol and was slightly exergonic, meanwhile the second KH expulsion was found to be thermoneutral and have an accessible barrier.

Table 7.4: Results of DFT calculations for the remaining steps of the proposed radical mechanism for the homocoupling of benzene.

Reaction Step	$\Delta G^{\ddagger}$ (kcal/mol)	ΔG_{rel} (kcal/mol)
7.17 - 7.14	Unable to optimise	1.2
7.14 - 7.18	23.3	-3.2
7.18 - 7.2	21.8	0.0

These results suggest that indeed the initial single electron transfer step would be the key to this mechanism, it therefore adds further weight to the importance of furthering the study of the single electron transfer.

7.4 Conclusions

The discovery of the benzene homocoupling reaction under the action of potassium metal plus an alkali metal salt additive on benzene by experimental colleagues in the Murphy Group has allowed this preliminary study into the proposed reaction mechanisms. Two proposals have been made, one occurring through an ionic mechanism and involving a strong base (potassium hydride or *tert*-butoxide) whilst the second was a radical mechanism initiated by an electron transfer to benzene. The second mechanism was proposed as a necessary alternative for the cases where no strong base was utilised within the reaction, i.e. potassium iodide was the additive alongside potassium metal.

The ionic mechanism was studied with potassium hydride as the base, the addition of phenyl potassium to benzene would be the rate-determining step with an energy span of 29.4 kcal/mol. Further to this, an alternative to the final KH expulsion to yield the biphenyl product was investigated: the deprotonation of phenylcyclohexadienyl anion to yield dianion **7.16**. This was found to have a lower free energy barrier and be more exergonic than the KH expulsion. These results suggest that this ionic mechanism would only be suitable for the initiation of a radical chain reaction, and not be responsible for the yields of biphenyl observed experimentally. It should be noted however that the effects of potassium metal upon the base were unable to be incorporated into the calculations conducted here. This is due to the unknown nature of the reaction which occurs between potassium metal and a base such as KH or KO^{t}Bu.

Through investigations of the proposed radical mechanism, it was found that the dimerisation of benzene radical anions was only slightly endergonic and that expulsion of two molecules of KH would be accessible and favourable in terms of free energy. This therefore left the key to this mechanism to be the initial single electron transfer reaction. Attempts to study the single electron transfer from K_8 and K_{21} clusters to benzene or benzene plus a complexed alkali metal cation (lithium, sodium or potassium) were made utilising the Nelsen 4-point method for studying electron transfer reactions. No significant difference was observed for the electron transfer from K_8 or K_{21} clusters to the alkali metal cation complexed benzene, with all found to be exergonic and possess small predicted activation energies. More accurate calculations were attempted through use of constrained DFT and the method of Tuttle, Murphy and co-workers for studying electron transfers. These calculations were only able to furnish one result for the potassium cation complexed benzene receiving an electron from the K_8 cluster. For all

other alkali metal cations, the constrained DFT optimisations were not able to be converged due to the constrained DFT multipliers being unable to be optimised for these systems. Despite the calculated energetics for SET being very accessible we have not been able to understand the observed differences for the alkali metal salts, the subsequent steps after SET were also found to be accessible and we therefore conclude that the SET reaction required more detailed study in order to fully understand the energetics.

Similarly to the ionic mechanism, the effects of potassium metal upon the added salt (i.e. potassium iodide) were not incorporated into these calculations. Simply, the salt was represented as one alkali metal cation complexed to benzene. The results presented herein suggest that the effects of potassium metal on the alkali metal salt require further investigation in order to allow calculations to better represent the system being studied.

This chapter sought to unearth mechanistic insights into the newly discovered benzene homocoupling reaction, an ionic mechanism has been shown to only be productive enough to furnish initiator levels of electron donor **7.16**. Further insights surrounding the radical mechanism have thus far been out of reach, however, it has been shown that it will be important to understand the effects potassium metal and the alkali metal salt have upon each other in order to progress in the search for mechanistic insights.

7.5 Future Work

The preliminary nature of this study (conducted over 3 months) has demonstrated the difficulties in studying such a complex system where potassium metal and an additive together enable a reaction to occur. Whilst studying the small potassium clusters in this study it has been noted that the optimisations of the K_{21} system take on the order of 7 days to fully converge, whilst running on 40 cores of the ARCHIE-WEST supercomputer. Should future studies look to reach the >60 atom potassium clusters, shown to better represent bulk metal, the computational costs involved will be high.

To further develop these results, it would be extremely valuable to experimentally determine the reactions taking place between potassium metal and the added salts such as potassium iodide. Understanding whether these reagents are forming a composite structure such as that observed by Chiba *et al*.[161] upon reaction of sodium hydride with sodium iodide, would allow a more detailed computational investigation to take place. With further knowledge of the product formed by reaction of potassium metal with the

added salt, it would be possible to perform DFT calculations to determine whether the reaction was proceeding *via* an electron transfer or deprotonation mechanism.

Optimisation of the reaction conditions would also be an important piece of future work, since carrying out the reaction in sealed tubes at 150 °C could be prohibitive for others looking to utilise the reaction. By optimising the reaction conditions, it would then be possible to begin investigating further substrates to determine whether they could undergo similar homocoupling reactions. Other aromatic substrates such as naphthalene and anthracene would be interesting in the fact that they could afford a number of isomers of coupled products. If indeed the reaction proceeds by an electron transfer mechanism; attempting to carry out Birch alkylation reactions of benzene could also be a possibility by introducing an alkyl halide electrophile. Such developments would further the synthetic utility of the potassium metal plus salt conditions.

8. Conclusions

The research presented in this thesis has demonstrated the power of computational methods to gain mechanistic insights into reactions. These mechanistic insights gained from calculations often guided experimental colleagues to design new reactions in order to delve deeper into the mechanistic details.

Chapter 4 saw an investigation into the proposed reaction mechanism of Ghorai *et al.*[1] for the formation of 1,2,4-triarylbenzenes from 1,3-diarylpropan-1-ones or 1,3-diaryl-2-propen-1-ols. This mechanism was shown to have one key energetically unfavourable step; loss of phenyl anion from an intermediate with an insufficient driving force (formation of an α,β-unsaturated ketone) to enable such a bad leaving group to be eliminated ($\Delta G^{\ddagger}$ = 48.8 kcal/mol and ΔG_{rel} = 30.7 kcal/mol). An alternative mechanism was then demonstrated to be far more favourable, with the elimination of the phenyl anion identified to occur from a 1,3-cyclohexadiene intermediate ($\Delta G^{\ddagger}$ = 30.8 kcal/mol and ΔG_{rel} = -108.7 kcal/mol). Understanding the loss of the aryl/phenyl anion in this reaction allows the concept of leaving groups discussed at the beginning of Chapter 4 to be revisited. Here it has been shown that the nature of the leaving group (hydride or phenyl anion) could not be *a priori* determined by the pK_a of the conjugate acid, as is typical in organic chemistry. Had the leaving group been predicted utilising the pK_a of the conjugate acids, hydride would have been predicted to act as the leaving group since the pK_a of hydrogen is ~36 compared to benzene whose pK_a is 43. This result opens the possibility for further exploration of so called 'bad leaving groups' such as the phenyl anion.

Chapter 5 saw the search for mechanistic insights move to the miraculous Stoltz-Grubbs reducing system of KO^{t}Bu plus triethysilane (or hydrosilane), which has been shown to perform a wide range of reactions experimentally; from silylation of indoles to desulfurisation of sulfur containing heterocycles. Despite wide ranging experimental and computational studies by Grubbs *et al.*[58-60] the mechanism for all of the transformations performed by this system were not clear. Here, the number of complex reaction pathways available to interrogate using DFT were vast, however of interest were the ability of the reagents to perform the reduction of polyaromatic hydrocarbons and N-benzylindole. Further to this, the mechanism of N-phenylindole rearrangement to 9,10-dihydroacridine also warranted investigation to understand the roles of KO^{t}Bu and Et$_3$SiH. Initial calculations probed the formation of proposed electron donor Me$_3$SiO^{t}Bu radical anion from *tert*-butoxide and trimethylsilyl radical, and found that formation of this proposed electron donor was favoured (note: trimethylsilane was used in place of

triethylsilane in calculations). The formation of pentavalent silicate anion [Me$_3$Si(H)O^{t}Bu] was also probed and found to reside in an equilibrium slightly favouring the reactants (ΔG_{rel} = 1.4 kcal/mol).

DFT calculations allowed the comparison of single electron transfer and hydride transfer mechanisms for a range of substrates. A surprising result was encountered for SET from Me$_3$SiO^{t}Bu radical anion to the polycyclic aromatic hydrocarbon's naphthalene, anthracene and phenanthrene: the Marcus inverse region. Each of polycyclic aromatic hydrocarbons had a similar reorganisation energy, however from naphthalene to phenanthrene to anthracene the relative Gibbs free energy become more favourable. This resulted in the predicted free energy of activation increasing in the same order, thus displaying behaviour associated with the Marcus inverse region. On the other hand, SET to N-benzylindole and N-methyl-N-phenylaniline was found to be favoured. Conversely, hydride transfer (from [Me$_3$Si(H)O^{t}Bu] anion) to N-benzylindole and N-methyl-N-phenylaniline was ruled out due to large free energy barriers ($\Delta G^{\ddagger}$ = 36.9 and 40.7 kcal/mol respectively). Hydride reduction of the PAHs was demonstrated to be operative, with free energy barriers found to be lower than the predicted activation energies for SET. These results provide mechanistic insights for two strands of the complex reaction pathways involved with the Stoltz-Grubbs reducing system.

In order to investigate a further possible strand of the complex Stoltz-Grubbs reducing system, the rearrangement of N-phenylindole to 9,10-dihydroacridine was investigated. A SET initiated mechanism was studied first, but despite SET to N-phenylindole being favoured, the subsequent ring opening of the N-phenylindole radical anion was disfavoured (ΔG_{rel} = 28.2 kcal/mol). Inspiration was then taken from the work of Jeon *et al.*[121] to study the possible hydrogen atom transfer to N-phenylindole from the [Me$_3$Si(H)O^{t}Bu] anion, previously shown to be capable of hydride transfer. Whilst the multireference nature of such a transition state was not able to be probed by the computational methods available, a simplified hydrogen atom addition was. This was found to be exergonic and have an accessible free energy barrier, however the subsequent ring opening step was again found to be unfavourable. Despite mechanistic insights associated with this latter aspect of the complex Stoltz-Grubbs reducing system remaining elusive, insights underpinning the reducing abilities of this system have been uncovered. These insights were only accessible after first considering the complex ways in which the two reagents could react to yield other more reactive intermediates.

Furthering the study of KO^{t}Bu in the single electron transfer arena, Chapter 6 delved into the somewhat historic debate of Ashby *et al.*[2, 125] and Newcomb *et al.*[123-124] surrounding the ability of alkoxides to serve directly as electron donors. Whilst experimental colleagues struggled to find mechanistic understanding through experiment, DFT calculations allowed the *in situ* formation of organic electron donor species to be ruled out. A serendipitous reaction carried out in the lab adjusted our mechanistic compass towards the sun (light), and here TDDFT excelled in reaching mechanistic understanding. Prediction of UV-vis spectra for a range of *tert*-butoxide - benzophenone complexes (naked, with Na$^+$ and with K$^+$) showed the formation of a key charge transfer occurring around 410 nm, for the KO^{t}Bu complex only. Experimental measurements aligned with predicted spectra, therefore allowing the structure of the KO^{t}Bu - benzophenone complex to be interrogated, highlighting the ability of the potassium cation to hold the alkoxide and benzophenone in close proximity (3.1 Å). This proving the difference for NaO^{t}Bu which could not form such a close interaction instead holding the alkoxide 4.5 Å away from benzophenone, resulting in no formation of a visible light induced charge transfer complex.

Here, the search for mechanistic insights relied heavily upon the computational results, without these the understanding of the KO^{t}Bu - benzophenone complex would not have been possible. Nor would the differences between the reaction of benzophenone with NaO^{t}Bu and KO^{t}Bu have been rationalised.

The unique abilities of potassium were again the focus of Chapter 7, however here it was the turn of potassium metal. The never before reported homocoupling of benzene to biphenyl was discovered by experimental colleagues in the Murphy group, by reacting benzene with potassium metal in the presence of an alkali metal salt (KO^{t}Bu was shown to be the most effective). Here computational investigations were focused upon the potential competitive mechanisms of single electron transfer to benzene *vs* its deprotonation. The latter however being impossible in the presence of non-basic salts such as KI, meaning that understanding the SET mechanism was key.

The deprotonation of benzene was studied with KH as the base, whilst the presence of potassium metal was not considered due to a lack of understanding of how this reacts with KH to form composite structures. DFT calculations revealed that the deprotonation mechanism would yield the dianion of biphenyl, however this would only be in quantities capable of initiating further radical mechanisms and alone would not lead to the quantities of biphenyl observed experimentally.

The conventional Nelsen 4-point method[92] for studying SET reactions computationally was then applied to the radical mechanism. However, no significant differences were observed for the simplified systems studied, K_8 as the electron donor and the alkali metal cations lithium, sodium or potassium complexed to benzene as the electron acceptor. The more accurate method of Tuttle, Murphy and co-workers[93] was not suitable for studying these systems due to the optimisation of triplet product complexes resulting in triplet states residing on potassium clusters. Preliminary tests of constrained DFT applied to the Tuttle, Murphy and co-worker's complexation method were therefore carried out, however due to time and technical constraints these were only conducted for the potassium cation system in the gas phase. The result of this calculation was in agreement with the result obtained by the Nelsen 4-point method.

The search for mechanistic insights from the complex reactions taking place in the mixture of potassium metal, alkali metal salt and benzene must therefore continue. In order for the search to be fruitful, the complex nature of the reaction between potassium metal and the added alkali metal salts must first be understood to determine what, if any, composite structures are being formed. Such composite structures may lead to surface reactions or enhanced electron donor properties towards benzene.

This research sought to provide mechanistic insights in a landscape of complex reaction pathways, and it has shown how computational methods can be utilised to reach this destination in many cases. The ability of computational methods to access insights into reaction mechanisms which are far from the reaches of experiment have been key to the successes presented throughout. However, it has also shown that in some instances being restricted to solely computational methods can leave mechanistic insights out of reach.

9. References

1. Rehan, M.; Maity, S.; Morya, L. K.; Pal, K.; Ghorai, P., *Angew. Chem. Int. Ed.* **2016**, *55* (27), 7728-7732.

2. Ashby, E. C.; Argyropoulos, J. N., *J. Org. Chem.* **1986**, *51* (19), 3593-3597.

3. Sun, C.-L.; Shi, Z.-J., *Chem. Rev.* **2014**, *114* (18), 9219-9280.

4. Leadbeater, N. E.; Marco, M., *Angew. Chem. Int. Ed.* **2003**, *42* (12), 1407-1409.

5. Leadbeater, N. E.; Marco, M., *J. Org. Chem.* **2003**, *68* (14), 5660-5667.

6. Yanagisawa, S.; Ueda, K.; Taniguchi, T.; Itami, K., *Org. Lett.* **2008**, *10* (20), 4673-4676.

7. Liu, W.; Cao, H.; Zhang, H.; Zhang, H.; Chung, K. H.; He, C.; Wang, H.; Kwong, F. Y.; Lei, A., *J. Am. Chem. Soc.* **2010**, *132* (47), 16737-16740.

8. Wotiz, J. H.; Kleopfer, R. D.; Barelski, P. M.; Hinckley, C. C.; Koster, D. F., *J. Org. Chem.* **1972**, *37* (11), 1758-1763.

9. Shirakawa, E.; Itoh, K.-i.; Higashino, T.; Hayashi, T., *J. Am. Chem. Soc.* **2010**, *132* (44), 15537-15539.

10. Sun, C.-L.; Li, H.; Yu, D.-G.; Yu, M.; Zhou, X.; Lu, X.-Y.; Huang, K.; Zheng, S.-F.; Li, B.-J.; Shi, Z.-J., *Nat. Chem.* **2010**, *2* (12), 1044-1049.

11. Studer, A.; Curran, D. P., *Angew. Chem. Int. Ed.* **2011**, *50* (22), 5018-5022.

12. Curran, D. P.; Keller, A. I., *J. Am. Chem. Soc.* **2006**, *128* (42), 13706-13707.

13. Todres, Z. V., *Ion-radical organic chemistry : principles and applications, CRC Press* **2009**.

14. Tanimoro, K.; Ueno, M.; Takeda, K.; Kirihata, M.; Tanimori, S., *J. Org. Chem.* **2012**, *77* (18), 7844-7849.

15. Liu, W.; Tian, F.; Wang, X.; Yu, H.; Bi, Y., *Chem. Comm.* **2013**, *49* (29), 2983-2985.

16. Wu, Y.; Wong, S. M.; Mao, F.; Chan, T. L.; Kwong, F. Y., *Org. Lett.* **2012**, *14* (20), 5306-5309.

17. Sun, C.-L.; Gu, Y.-F.; Wang, B.; Shi, Z.-J., *Chem. Eur. J.* **2011**, *17* (39), 10844-10847.

18. De, S.; Ghosh, S.; Bhunia, S.; Sheikh, J. A.; Bisai, A., *Org. Lett.* **2012**, *14* (17), 4466-4469.

19. Zhou, S.-Z.; Doni, E.; Anderson, G. M.; Kane, R. G.; MacDougall, S. W.; Ironmonger, V. M.; Tuttle, T.; Murphy, J. A., *J. Am. Chem. Soc.* **2014**, *136* (51), 17818-17826.

20. Zhou, S.-Z.; Anderson, G. M.; Mondal, B.; Doni, E.; Ironmonger, V.; Kranz, M.; Tuttle, T.; Murphy, J. A., *Chem. Sci.* **2014**, *5* (2), 476-482.

21. Murphy, J. A., *J. Org. Chem.* **2014**, *79* (9), 3731-3746.

22. Doni, E.; Murphy, J. A., *Chem. Comm.* **2014**, *50* (46), 6073-6087.

23. Woodward, R. B.; Wendler, N. L.; Brutschy, F. J., *J. Am. Chem. Soc.* **1945**, *67* (9), 1425-1429.

24. Barham, J. P.; Coulthard, G.; Kane, R. G.; Delgado, N.; John, M. P.; Murphy, J. A., *Angew. Chem. Int. Ed.* **2016**, *55* (14), 4492-4496.

25. Zhang, L.; Yang, H.; Jiao, L., *J. Am. Chem. Soc.* **2016**, *138* (22), 7151-7160.

26. Zhu, Y.-W.; Shi, Y.-X., *J. Fluorine Chem.* **2016**, *188*, 10-13.

27. De, S.; Mishra, S.; Kakde, B. N.; Dey, D.; Bisai, A., *J. Org. Chem.* **2013**, *78* (16), 7823-7844.

28. Campbell, R.; Cannon, D.; García-Álvarez, P.; Kennedy, A. R.; Mulvey, R. E.; Robertson, S. D.; Saßmannshausen, J.; Tuttle, T., *J. Am. Chem. Soc.* **2011**, *133* (34), 13706-13717.

29. Dewanji, A.; Mück-Lichtenfeld, C.; Studer, A., *Angew. Chem. Int. Ed.* **2016**, *55* (23), 6749-6752.

30. Murphy, J. A.; Garnier, J.; Park, S. R.; Schoenebeck, F.; Zhou, S.-Z.; Turner, A. T., *Org. Lett.* **2008**, *10* (6), 1227-1230.

31. Schoenebeck, F.; Murphy, J. A.; Zhou, S.-Z.; Uenoyama, Y.; Miclo, Y.; Tuttle, T., *J. Am. Chem. Soc.* **2007**, *129* (44), 13368-13369.

32. Murphy, J. A.; Khan, T. A.; Zhou, S.-Z.; Thomson, D. W.; Mahesh, M., *Angew. Chem. Int. Ed.* **2005**, *44* (9), 1356-1360.

33. Cuthbertson, J.; Gray, V. J.; Wilden, J. D., *Chem. Commun.* **2014**, *50* (20), 2575-2578.

34. Bajracharya, G. B.; Daugulis, O., *Org. Lett.* **2008**, *10* (20), 4625-4628.

35. Ashby, E. C.; Goel, A. B.; Argyropoulos, J. N., *Tetrahedron Lett.* **1982**, *23* (22), 2273-2276.

36. Ashby, E. C., *Acc. Chem. Res.* **1988**, *21* (11), 414-421.

37. Fyfe, C. A.; Foster, R., *Chemical Communications (London)* **1967**, (23), 1219-1219.

38. Foster, R.; Mackie, R. K., *Tetrahedron* **1962**, *18* (10), 1131-1135.

39. Pollitt, R. J.; Saunders, B. C., *J. Chem. Soc.* **1965**, (0), 4615-4628.

40. Yi, H.; Jutand, A.; Lei, A., *Chem. Comm.* **2015**, *51* (3), 545-548.

41. Barham, J. P.; Coulthard, G.; Emery, K. J.; Doni, E.; Cumine, F.; Nocera, G.; John, M. P.; Berlouis, L. E. A.; McGuire, T.; Tuttle, T.; Murphy, J. A., *J. Am. Chem. Soc.* **2016**, *138* (23), 7402-7410.

42. Patil, M., *J. Org. Chem.* **2016**, *81* (2), 632-639.

43. Pichette Drapeau, M.; Fabre, I.; Grimaud, L.; Ciofini, I.; Ollevier, T.; Taillefer, M., *Angew. Chem. Int. Ed.* **2015**, *54* (36), 10587-10591.

44. Wei, W.-t.; Dong, X.-j.; Nie, S.-z.; Chen, Y.-y.; Zhang, X.-j.; Yan, M., *Org. Lett.* **2013**, *15* (23), 6018-6021.

45. Chen, Y.-y.; Zhang, N.-n.; Ye, L.-m.; Chen, J.-h.; Sun, X.; Zhang, X.-j.; Yan, M., *RSC Adv.* **2015**, *5* (59), 48046-48049.

46. Oksdath-Mansilla, G.; Argüello, J. E.; Peñéñory, A. B., *Tetrahedron Lett.* **2013**, *54* (12), 1515-1518.

47. Budén, M. E.; Bardagí, J. I.; Puiatti, M.; Rossi, R. A., *J. Org. Chem.* **2017**, *82* (16), 8325-8333.

48. Chatgilialoglu, C., *Acc. Chem. Res.* **1992**, *25* (4), 188-194.

49. Kursanov, D. N.; Parnes, Z. N.; Loim, N. M., *Synthesis* **1974**, *1974* (09), 633-651.

50. Yang, D.; Tanner, D. D., *J. Org. Chem.* **1986**, *51* (12), 2267-2270.

51. Corriu, R.; Guérin, C.; Henner, B.; Wang, Q., *J. Organomet. Chem.* **1989**, *365* (3), C7-C10.

52. Corriu, R. J. P.; Guerin, C.; Henner, B. J. L.; Wang, Q., *J. Organomet. Chem.* **1992**, *439* (1), C1-C5.

53. Corriu, R. J. P., *J. Organomet. Chem.* **1990**, *400* (1), 81-106.

54. Becker, B.; Corriu, R. J. P.; Guérin, C.; Henner, B.; Wang, Q., *J. Organomet. Chem.* **1989**, *368* (2), C25-C28.

55. Becker, B.; Corriu, R.; Guerin, C.; Henner, B.; Wang, Q., *J. Organomet. Chem.* **1989**, *359* (2), C33-C35.

56. Fedorov, A.; Toutov, A. A.; Swisher, N. A.; Grubbs, R. H., *Chem. Sci.* **2013**, *4* (4), 1640-1645.

57. Toutov, A. A.; Liu, W.-B.; Betz, K. N.; Fedorov, A.; Stoltz, B. M.; Grubbs, R. H., *Nature* **2015**, *518* (7537), 80-84.

58. Banerjee, S.; Yang, Y.-F.; Jenkins, I. D.; Liang, Y.; Toutov, A. A.; Liu, W.-B.; Schuman, D. P.; Grubbs, R. H.; Stoltz, B. M.; Krenske, E. H., *J. Am. Chem. Soc.* **2017**, *139* (20), 6880-6887.

59. Liu, W. B.; Schuman, D. P.; Yang, Y. F.; Toutov, A. A.; Liang, Y.; Klare, H. F. T.; Nesnas, N.; Oestreich, M.; Blackmond, D. G.; Virgil, S. C.; Banerjee, S.; Zare, R. N.; Grubbs, R. H.; Houk, K. N.; Stoltz, B. M., *J. Am. Chem. Soc.* **2017**, *139* (20), 6867-6879.

60. Toutov, A. A.; Salata, M.; Fedorov, A.; Yang, Y.-F.; Liang, Y.; Cariou, R.; Betz, K. N.; Couzijn, E. P. A.; Shabaker, J. W.; Houk, K. N.; Grubbs, R. H., *Nature Energy* **2017**, *2*, 17008.

61. Harvey, J., *Computational Chemistry*, Oxford University Press, 2018.

62. Cramer, C. J., *Essentials of Computational Chemistry: Theories and Models*, John Wiley and Sons Ltd, 2002.

63. Wolfram Koch, M. C. H., *A Chemist's Guide to Density Functional Theory*, 2nd Edition, 2001.

64. Hohenberg, P.; Kohn, W., *Phys. Rev.* **1964**, *136* (3B), B864-B871.

65. Kohn, W.; Sham, L. J., *Phys. Rev.* **1965**, *140* (4A), A1133-A1138.

66. Vosko, S. H.; Wilk, L.; Nusair, M., *Can. J. Phys.* **1980**, *58* (8), 1200-1211.

67. Vega, L.; Ruvireta, J.; Viñes, F.; Illas, F., *J. Chem. Theory Comput.* **2018**, *14* (1), 395-403.

68. Stephens, P. J.; Devlin, F. J.; Chabalowski, C. F.; Frisch, M. J., *J. Phys. Chem.* **1994**, *98* (45), 11623-11627.

69. Becke, A. D., *Phys. Rev. A* **1988**, *38* (6), 3098-3100.

70. Lee, C.; Yang, W.; Parr, R. G., *Phys. Rev. B* **1988**, *37* (2), 785-789.

71. Zhao, Y.; Truhlar, D. G., *Theor. Chem. Acc.* **2007**, *120* (1), 215-241.

72. Zhao, Y.; Truhlar, D. G., *Acc. Chem. Res.* **2008**, *41* (2), 157-167.

73. Peverati, R.; Truhlar, D. G., *Phil. Trans. R. Soc. A* **2014**, *372* (2011), 1-52.

74. Hehre, W. J.; Ditchfield, R.; Pople, J. A., *J. Chem. Phys.* **1972**, *56* (5), 2257-2261.

75. Hariharan, P. C.; Pople, J. A., *Theoretica chimica acta* **1973**, *28* (3), 213-222.

76. Frisch, M. J.; Pople, J. A.; Binkley, J. S., *J. Chem. Phys.* **1984**, *80* (7), 3265-3269.

77. Barone, V.; Cossi, M.; Tomasi, J., *J. Chem. Phys.* **1997**, *107* (8), 3210-3221.

78. Pierotti, R. A., *Chem. Rev.* **1976**, *76* (6), 717-726.

79. Jorgensen, W. L.; Madura, J. D.; Swenson, C. J., *J. Am. Chem. Soc.* **1984**, *106* (22), 6638-6646.

80. Floris, F.; Tomasi, J., *J. Comput. Chem.* **1989**, *10* (5), 616-627.

81. del Valle, F. J. O.; Aguilar, M. A., *THEOCHEM* **1993**, *280* (1), 25-47.

82. Marenich, A. V.; Cramer, C. J.; Truhlar, D. G., *J. Phys. Chem., B* **2009**, *113* (18), 6378-6396.

83. Miertuš, S.; Scrocco, E.; Tomasi, J., *Chem. Phys.* **1981**, *55* (1), 117-129.

84. Cossi, M.; Rega, N.; Scalmani, G.; Barone, V., *J. Comput. Chem.* **2003**, *24* (6), 669-681.

85. Eyring, H., *J. Chem. Phys.* **1935**, *3* (2), 107-115.

86. Marcus, R. A., *Angew. Chem. Int. Ed.* **1993**, *32* (8), 1111-1121.

87. Marcus, R. A., *J. Chem. Phys.* **1965**, *43* (2), 679-701.

88. Rosokha, S. V.; Newton, M. D.; Head-Gordon, M.; Kochi, J. K., *Chem. Phys.* **2006**, *324* (1), 117-128.

89. Rosokha, S. V.; Dibrov, S. M.; Rosokha, T. Y.; Kochi, J. K., *Photochem. Photobiol. Sci.* **2006**, *5* (10), 914-924.

90. Rosokha, S. V.; Lu, J. M.; Newton, M. D.; Kochi, J. K., *J. Am. Chem. Soc.* **2005**, *127* (20), 7411-7420.

91. Kazemiabnavi, S.; Dutta, P.; Banerjee, S., *J. Phys. Chem. C* **2014**, *118* (47), 27183-27192.

92. Nelsen, S. F.; Blackstock, S. C.; Kim, Y., *J. Am. Chem. Soc.* **1987**, *109* (3), 677-682.

93. Anderson, G. M.; Cameron, I.; Murphy, J. A.; Tuttle, T., *RSC Adv.* **2016**, *6* (14), 11335-11343.

94. Schmid, G. A.; Borschberg, H.-J., *Helv. Chim. Acta* **2001**, *84* (2), 401-415.

95. Zheng, H.-X.; Xiao, Z.-F.; Yao, C.-Z.; Li, Q.-Q.; Ning, X.-S.; Kang, Y.-B.; Tang, Y., *Org. Lett.* **2015**, *17* (24), 6102-6105.

96. Suchand, B.; Satyanarayana, G., *Eur. J. Org. Chem.* **2017**, *2017* (26), 3886-3895.

97. Johnston, A. J. S.; McLaughlin, M. G.; Reid, J. P.; Cook, M. J., *Org. Biomol. Chem.* **2013**, *11* (44), 7662-7666.

98. Hofmann, J. E.; Argabright, P. A.; Schriesheim, A., *Tetrahedron Lett.* **1964**, *5* (17), 1005-1008.

99. Venkatasubramanian, N.; Siegel, S., *J. Org. Chem.* **1988**, *53* (25), 5972-5974.

100. Staley, S. W.; Erdman, J. P., *J. Am. Chem. Soc.* **1970**, *92* (12), 3832-3833.

101. Collins, C. J.; Hombach, H. P.; Maxwell, B. E.; Benjamin, B. M.; McKamey, D., *J. Am. Chem. Soc.* **1981**, *103* (5), 1213-1214.

102. Schmidt, E. Y.; Tatarinova, I. V.; Ushakov, I. A.; Trofimov, B. A., *Mendeleev Commun.* **2016**, *26* (5), 378-379.

103. Castanedo, R.; Covarrubias-Zúñiga, A.; Maldonado, L. A., *Tetrahedron Lett.* **2006**, *47* (6), 973-976.

104. Rassolov, V. A.; Ratner, M. A.; Pople, J. A.; Redfern, P. C.; Curtiss, L. A., *J. Comput. Chem.* **2001**, *22* (9), 976-984.

105. Rassolov, V. A.; Pople, J. A.; Ratner, M. A.; Windus, T. L., *J. Chem. Phys.* **1998**, *109* (4), 1223-1229.

106. Francl, M. M.; Pietro, W. J.; Hehre, W. J.; Binkley, J. S.; Gordon, M. S.; DeFrees, D. J.; Pople, J. A., *J. Chem. Phys.* **1982**, *77* (7), 3654-3665.

107. Hariharan, P. C.; Pople, J. A., *Mol. Phys.* **1974**, *27* (1), 209-214.

108. Ditchfield, R.; Hehre, W. J.; Pople, J. A., *J. Chem. Phys.* **1971**, *54* (2), 724-728.

109. C., B. R.; A., C. L., *J. Comput. Chem.* **1990**, *11* (10), 1206-1216.

110. Blaudeau, J.-P.; McGrath, M. P.; Curtiss, L. A.; Radom, L., *J. Chem. Phys.* **1997**, *107* (13), 5016-5021.

111. Frisch, M. J.; Trucks, G. W.; Schlegel, H. B.; Scuseria, G. E.; Robb, M. A.; Cheeseman, J. R.; Scalmani, G.; Barone, V.; Mennucci, B.; Petersson, G. A.; Nakatsuji, H.; Caricato, M.; Li, X.; Hratchian, H. P.; Izmaylov, A. F.; Bloino, J.; Zheng, G.; Sonnenberg, J. L.; Hada, M.; Ehara, M.; Toyota, K.; Fukuda, R.; Hasegawa, J.; Ishida, M.; Nakajima, T.; Honda, Y.; Kitao, O.; Nakai, H.; Vreven, T.; Montgomery, J. A., Jr.;; Peralta, J. E.; Ogliaro, F.; Bearpark, M.; Heyd, J. J.; Brothers, E.; Kudin, K. N.; Staroverov, V. N.; Kobayashi, R.; Normand, J.; Raghavachari, K.; Rendell, A.; Burant, J. C.; Iyengar, S. S.; Tomasi, J.; Cossi, M.; Rega, N.; Millam, J. M.; Klene, M.; Knox, J. E.; Cross, J. B.; Bakken, V.; Adamo, C.; Jaramillo, J.; Gomperts, R.; Stratmann, R. E.; Yazyev, O.; Austin, A. J.; Cammi, R.; Pomelli, C.; Ochterski, J. W.; Martin, R. L.;

Morokuma, K.; Zakrzewski, V. G.; Voth, G. A.; Salvador, P.; Dannenberg, J. J.; Dapprich, S.; Daniels, A. D.; Farkas, Ö.; Foresman, J. B.; Ortiz, J. V.; Cioslowski, J.; Fox, D. J. *Gaussian 09, Revision A.02*, Gaussian, Inc., Wallingford CT: 2009.

112. Besora, M.; Vidossich, P.; Lledós, A.; Ujaque, G.; Maseras, F., *J. Phys. Chem., A* **2018**, *122* (5), 1392-1399.

113. Fujiwara, J.; Fukutani, Y.; Sano, H.; Maruoka, K.; Yamamoto, H., *J. Am. Chem. Soc.* **1983**, *105* (24), 7177-7179.

114. Talukdar, S.; Nayak, S. K.; Banerji, A., *J. Org. Chem.* **1998**, *63* (15), 4925-4929.

115. Doni, E.; O'Sullivan, S.; Murphy, J. A., *Angew. Chem. Int. Ed.* **2013**, *52* (8), 2239-2242.

116. Xu, P.; Würthwein, E.-U.; Daniliuc, C. G.; Studer, A., *Angew. Chem. Int. Ed.* **2017**, *56* (44), 13872-13875.

117. Altshuller, A. P.; Rosenblum, L., *J. Am. Chem. Soc.* **1955**, *77* (2), 272-274.

118. Smith, A. J.; Young, A.; Rohrbach, S.; O'Connor, E. F.; Allison, M.; Wang, H.-S.; Poole, D. L.; Tuttle, T.; Murphy, J. A., *Angew. Chem. Int. Ed.* **2017**, *56* (44), 13747-13751.

119. Marcus, R. A., *Discussions of the Faraday Society* **1960**, *29* (0), 21-31.

120. Walton, J. C., *J. Phys. Chem., A* **2018**, *122* (5), 1422-1431.

121. Asgari, P.; Hua, Y.; Bokka, A.; Thiamsiri, C.; Prasitwatcharakorn, W.; Karedath, A.; Chen, X.; Sardar, S.; Yum, K.; Leem, G.; Pierce, B. S.; Nam, K.; Gao, J.; Jeon, J., *Nature Catalysis* **2019**, *2* (2), 164-173.

122. Miller, J. R.; Calcaterra, L. T.; Closs, G. L., *J. Am. Chem. Soc.* **1984**, *106* (10), 3047-3049.

123. Newcomb, M.; Burchill, M. T., *J. Am. Chem. Soc.* **1984**, *106* (8), 2450-2451.

124. Newcomb, M.; Burchill, M. T., *J. Am. Chem. Soc.* **1984**, *106* (26), 8276-8282.

125. Ashby, E. C.; Argyropoulos, J. N., *Tetrahedron Lett.* **1986**, *27* (4), 465-468.

126. Trzupek, L. S.; Newirth, T. L.; Kelly, E. G.; Sbarbati, N. E.; Whitesides, G. M., *J. Am. Chem. Soc.* **1973**, *95* (24), 8118-8133.

127. Tsierkezos, N. G., *J. Solution Chem.* **2007**, *36* (10), 1301-1310.

128. Connelly, N. G.; Geiger, W. E., *Chem. Rev.* **1996**, *96* (2), 877-910.

129. Jensen, B. S.; Parker, V. D., *J. Chem. Soc., Chem. Comm.* **1974**, (10), 367-368.

130. Scalmani, G.; Frisch, M. J.; Mennucci, B.; Tomasi, J.; Cammi, R.; Barone, V., *J. Chem. Phys.* **2006**, *124* (9), 094107.

131. Yanai, T.; Tew, D. P.; Handy, N. C., *Chem. Phys. Lett.* **2004**, *393* (1), 51-57.

132. Peach, M. J. G.; Benfield, P.; Helgaker, T.; Tozer, D. J., *J. Chem. Phys.* **2008**, *128* (4), 044118.

133. Xia, J.-B.; Zhu, C.; Chen, C., *J. Am. Chem. Soc.* **2013**, *135* (46), 17494-17500.

134. Singh, M.; Yadav, A. K.; Yadav, L. D. S.; Singh, R. K. P., *Tetrahedron Lett.* **2017**, *58* (23), 2206-2208.

135. Han, L.; Xia, J.-B.; You, L.; Chen, C., *Tetrahedron* **2017**, *73* (26), 3696-3701.

136. Xia, J.-B.; Zhu, C.; Chen, C., *Chem. Comm.* **2014**, *50* (79), 11701-11704.

137. Sideri, I. K.; Voutyritsa, E.; Kokotos, C. G., *Org. Biomol. Chem.* **2018**.

138. Romero, N. A.; Nicewicz, D. A., *Chem. Rev.* **2016**, *116* (17), 10075-10166.

139. Walling, C.; Jacknow, B. B., *J. Am. Chem. Soc.* **1960**, *82* (23), 6108-6112.

140. Griller, D.; Ingold, K. U., *Acc. Chem. Res.* **1980**, *13* (9), 317-323.

141. Kosynkin, D.; Bockman, T. M.; Kochi, J. K., *J. Am. Chem. Soc.* **1997**, *119* (21), 4846-4855.

142. Barham, J. P.; Dalton, S. E.; Allison, M.; Nocera, G.; Young, A.; John, M. P.; McGuire, T.; Campos, S.; Tuttle, T.; Murphy, J. A., *J. Am. Chem. Soc.* **2018**, *140* (36), 11510-11518.

143. Handel, H.; Pasquini, M. A.; Pierre, J. L., *Tetrahedron* **1980**, *36* (22), 3205-3208.

144. Bryce-Smith, D.; Turner, E. E., *J. Chem. Soc.* **1953**, (0), 861-867.

145. Claff, C. E.; Morton, A. A., *J. Org. Chem.* **1955**, *20* (4), 440-442.

146. Morton, A. A.; Claff, C. E.; Collins, F. W., *J. Org. Chem.* **1955**, *20* (4), 428-439.

147. Morton, A. A.; Claff, C. E., *J. Am. Chem. Soc.* **1954**, *76* (19), 4935-4938.

148. Kijeński, J.; Radomski, P.; Fedoryńska, E., *J. Catal.* **2001**, *203* (2), 407-425.

149. Hart, H., *J. Am. Chem. Soc.* **1956**, *78* (11), 2619-2622.

150. Weast, R. C., *CRC handbook of chemistry and physics Sixty-seventh edition*, CRC Press Inc, United States, 1986.

151. Altshuller, A. P., *J. Am. Chem. Soc.* **1955**, *77* (23), 6187-6188.

152. Kendall, R. A.; Jr., T. H. D.; Harrison, R. J., *J. Chem. Phys.* **1992**, *96* (9), 6796-6806.

153. Löwdin, P. O., *J. Chem. Phys.* **1950**, *18* (3), 365-375.

154. Dederichs, P. H.; Blügel, S.; Zeller, R.; Akai, H., *Phys. Rev. Lett.* **1984**, *53* (26), 2512-2515.

155. Kaduk, B.; Kowalczyk, T.; Van Voorhis, T., *Chem. Rev.* **2012**, *112* (1), 321-370.

156. Becke, A. D., *J. Chem. Phys.* **1988**, *88* (4), 2547-2553.

157. Morton, A. A.; Lanpher, E. J., *J. Org. Chem.* **1958**, *23* (11), 1639-1642.

158. Aguado, A., *Computational and Theoretical Chemistry* **2013**, *1021*, 135-143.

159. Banerjee, A.; Ghanty, T. K.; Chakrabarti, A., *J. Phys. Chem., A* **2008**, *112* (48), 12303-12311.

160. Slaugh, L. H.; Raley, J. H., *J. Org. Chem.* **1967**, *32* (2), 369-371.

161. Hong, Z.; Ong, D. Y.; Muduli, S. K.; Too, P. C.; Chan, G. H.; Tnay, Y. L.; Chiba, S.; Nishiyama, Y.; Hirao, H.; Soo, H. S., *Chem. Eur. J.* **2016**, *22* (21), 7108-7114.